2005

Ductile crack growth emanating from Sharp Notes in a low Alloy Steel

Aladdin I. Abu-Assi

United Arab Emirates University

Deanship of Graduate Studies

DUCTILE CRACK GROWTH EMANATING FROM SHARP NOTCHES IN A LOW ALLOY STEEL

By

Aladdin I. Abu-Assi

Supervised by:

Dr. Abdel-Hamid I. Mourad

Mechanical Engineering Dept.

UAE University

A Thesis Submitted to the Deanship of Graduate Studies

in Partial Fulfilment of the

Requirements for Degree of Masters of Science in

Materials Science and Engineering

United Arab Emirates University

2004- 2005

ES/F11

United Arab Emirates University
Graduate Studies
M.S.c. Program in Materials Science and Engineering

THESIS EXAMINATION REPORT

Student ID : 200250408
Student Name : Aladdin Ihsan Abu-Assi

Title of The Thesis : Ductile Crack Growth Emanating From Sharp Notches in A Low Alloy Steel.

The Thesis Examination as A Partial Fulfillment of M. Sc. Degree in Materilas Science and Engineering Was conducted on ..... Based on Examining the Thesis and the Students Presentation and the Subsequent Discussion, The Committee Recommends:

☑ Thesis is Satisfactory as is.

☐ Thesis is Satisfactory After Minor Modifications.

☐ Thesis should be Re-Evaluated After Major Modifications.

☐ Thesis is Rejected.

Examining Committee Members:

Thesis Supervisor: Name: Abdel-Hamid I. Mourad Signature: ..... Date:

Thesis Co-Advisor: Name: ..... Signature: ..... Date: Jan, 12, 2005

Member : Name: Y. J. CHAO Signature: Yuh J. Chao Date: 1-12-05

Name: Khaled El-Sawy Signature: ..... Date: Jan. 12, 200

Approval of Program Coordinator:

Dr. Yousef Haik ..... Date : 12/1/05

Materials Science & Engineering Program
Dean of Graduate Studies
United Arab Emirates University

APPROVAL:
Dean of Graduate Studies ..... Date :.....

Dean of Graduate Studies
U. A. E. UNIVERSITY

ACKNOWLEDGMENT

I wish to thank the Lord of the worlds for offering me life, sanity and faith. Indeed He has favoured me in many ways over many fellow humans. Therefore, it can only be appropriate that I offer my perpetual and sincerest gratitude, praise and humility to Him Alone.

I wish next, to express my deepest gratitude to my mum and dad. They have spared no effort or resource in my well upbringing to the person I am. Without them....

I wish also to thank UAE University for offering me such an exclusive opportunity to do read for my Masters and undertake my research, through the Graduate Scholarship Programme. I do not think any university can be as generous to scholarship as UAE University. I pray to God that such an opportunity does remain for many others after my colleagues and myself.

I wish to express my gratitude to Dr. Abdel-Hamid I. Mourad for his supervision and mentoring. I have certainly learned a lot from him. I wish to admit that his tact and diplomacy, on many occasions, surpasses anything I have seen so far.

I wish also to thank Interplast Staff: Mr. Harjoot Singh and his staff Abdel-Majed, Gurprit and Yograj for their courteous cooperation and help with the machining, which has been key to this research.

I wish also to thank workshop staff; Mr. Abdel-Rahman, Mr. Abdel-Tawab and Mr. Hussein. I wish also to thank university staff members; specifically Eng. Abdel-Sattar Nour-Eldin, Mr. Reda Sabir and Mr. Yasser El-Basha.

And last, but not least, my family, my friends and colleagues, and my outer fraternal sphere: Your prayers, support and well wishes have been very inspiring and strengthening indeed.

ABSTRACT

Stable crack growth behaviour emanating from a sharp notch is investigated. Material chosen for tests was EN 34NiCrMo6 low alloy steel (akin to 4340/4330). Tests were carried out on CT specimens for various loading angles and a_0/W ratios to obtain load vs. load-line displacement, P-Δ_{LL}, curves. Experimental results were analysed. A normalisation approach of P-Δ_{LL} curves has been attempted and all experimental curves were represented as a single characteristic curve. Such approach has been also applied on experimental data available from other experimental investigations and results were encouraging, as it may address transferability issue. Fracture surfaces were also examined; crack-front tunnelling was obtained using dye penetrant technique to determine extent of stable crack growth. Tests on various notch sizes were also carried out and show that despite more than ten folds increase in notch radius, the maximum load increase recorded for CT was not more than 15%.

TABLE OF CONTENTS

List Of Tables

List Of Figures

CHAPTER 1

INTRODUCTION

1.1 MOTIVATION

Long gone the days when design engineers relied on magic safety factors to account for the devil's work when assessing strengths of components and structures. Safety factors were often employed to account for uncertainties that may lead to unexpected failures in service. Today, engineers are more enlightened and understand that cracks are the silent and hidden devils that, in numerous cases, have caused fatalities and not just material cost.

Modern fracture mechanics has evolved to allow the understanding of how cracks affect the integrity and strength of a structure. It has allowed for what is now known as damage tolerant design, where engineers can reliably predict strength and life of a component or structure despite the presence of cracks.

Notches are common features in a component or structure that is known for being sources of initiation and growth of cracks. This is so because notches are stress concentrators, increasing stresses within their vicinity. Moreover, when servicing structures or components, it has become common practice for technicians and repairmen deal with sharp cracks when detected. One of the ways a cracked structure may be repaired is by

blunting the crack-tips, usually by drilling off the tips. This is very so the case especially if material was tough such as steels or aluminium alloys. In effect, the sharp crack has become a sharp notch.

Traditional notch design is based on notch-tip yielding. A classical yielding criterion would be usually used with a geometric concentration factor. This may be suitable for blunt notches, but for sharply notched bodies, the loading capacity is much larger than that load that causes yielding at the crack tip. When notch-tip "fails", a crack is formed at the tip, and thus one can apply fracture mechanics tools for strength assessment, by predicting the material response to the presence of a crack. Classical fracture mechanics assumes instant failure if for a given load, a critical size is reached, or if a critical load is exceeded for a given crack size.

Plastic yielding that occurs at the crack-tip complicates material response by causing stable crack growth, even though it does add to material toughness. Evaluating a critical crack size for a given load, or a critical load for a given crack size in the classical sense is not straightforward. Numerous researches have been carried out to understand material response under stable crack growth, but straightforward resistance assessment is yet pending.

Therefore the motivation in this current investigation is to investigate the stable crack growth behaviour of specimens with sharp notches with various notch sizes and loading angles. Material chosen was low-alloy steel, EN 34NiCrMo6, which is a typically "tough" material common to numerous engineering applications.

1.2 OUTLINE

This thesis is presented in 3 parts. The first part, in chapter 2, would present a literature review on stable crack growth behaviour and recent attempts at characterisation and modelling. The second part would present the material and experimental set-up used in chapter 3, and then will present results with discussion in chapter 4. In the final part, an interesting finding during experimentation, regarding the effect of machining on stable crack growth, would be presented in chapter 5, followed by a summary of the findings and recommendations for future work, in chapter 6.

CHAPTER 2

LITERATURE SURVEY

2.1 CLASSICAL LINEAR ELASTIC FRACTURE MECHANICS

The basis of Linear Elastic Fracture Mechanics (LEFM) is stress-field characterisation within a cracked elastic body, in terms of a stress field intensity parameter, *K*. The material's toughness is then evaluated as the limit of stress-field strengths that it can withstand. Using traditional linear elasticity theory, the approach was developed during the late half of the 20^{th} century. LEFM approach forms the foundations of modern fracture mechanics, although there are problems with the theory and thus its application is limited as would be seen later.

2.1.1 Stress Intensity, K, and Crack-Tip Stress Fields

The overall stress field of a cracked elastic body can be determined by summing contributions from three idealised modes of crack loading: opening tensile mode (mode I), in-plane shear mode (mode II) and out-of plane shear mode (mode III) as shown in **Fig. 2.1**. Using linear elasticity, solutions to the resulting boundary value problem can be obtained, depending on geometry and crack-loading mode.

Various researchers have indeed derived solutions for the crack-vicinity stress fields. The general form of the stress field in a cracked elastic body, can be expressed as an asymptotic expansion series **[1]**:

$$\sigma_{ij} = \frac{k}{\sqrt{r}} f_{ij}(\theta) + A_0\, g_{ij}(\theta) + A_1 r^{\frac{1}{2}}\, g_{ij}^{(1)}(\theta) + A_2\, r\, g_{ij}^{(2)}(\theta) + A_3 r^{\frac{3}{2}}\, g_{ij}^{(3)}(\theta) + \ldots \tag{2.1}$$

where r, and θ are defined as in **Fig 2.2**, A_0, A_1, A_2 .. are constants, $f_{ij}(\theta)$, $g_{ij}^{(1)}(\theta)$, $g_{ij}^{(2)}(\theta)$, $g_{ij}^{(3)}(\theta)$ are known functions of θ, and k is a stress-field intensity parameter, more commonly defined as K, such that:

$$k = \frac{K}{\sqrt{2\pi}} \tag{2.2}$$

Now taking the limit of the stress field to near the crack-tip (i.e. crack-tip vicinity), the stress field becomes dominated by the first "singular" term and hence higher order terms become insignificant, i.e. **[1-4]**:

For mode I: $$\lim_{r\to 0} \sigma_{ij}^{(I)} = \frac{K_I}{\sqrt{2\pi r}} f_{ij}^{(I)}(\theta) \tag{2.3.a}$$

For mode II: $$\lim_{r\to 0} \sigma_{ij}^{(II)} = \frac{K_{II}}{\sqrt{2\pi r}} f_{ij}^{(II)}(\theta) \tag{2.3.b}$$

For mode III: $$\lim_{r\to 0} \sigma_{ij}^{(III)} = \frac{K_{III}}{\sqrt{2\pi r}} f_{ij}^{(III)}(\theta) \tag{2.3.c}$$

where K_I, K_{II} and K_{III} are the stress intensities for mode-I, mode-II and mode-III respectively.

Now, considering pure Mode-I loading of crack, the normal stress, σ_{yy}, at $\theta = 0^o$, **Eq(2.3.a)** becomes simply:

$$\sigma_{yy} = \frac{K_I}{\sqrt{2\pi r}} \tag{2.4}$$

Various solutions for K can be found in stress intensity handbooks such as Murakami's Stress Intensity Factors Handbook [5]. Generally, K for mode-I loading, K_I, has the form:

$$K_I = Y\sigma_\infty \sqrt{\pi a} \tag{2.5}$$

where Y is a configuration factor, σ_∞ is far-field stress and a is crack size.

Fracture behaviour, in the context of LEFM, presumes that a crack would grow unstably to cause catastrophic failure once a critical value of stress intensity, K_C, is reached. Such K_C can be corresponded to a critical load value, P_Q, which can be determined experimentally. When critical load is applied, it causes the formation of finite crack growth. The initiation of such finite crack growth causes release of stored potential elastic-strain energy, which in turn causes formation of additional crack growth with additional release of potential strain energy; in effect causing a positive-feedback loop leading to unstable state of crack growth. The critical stress intensity factor, K_C (K_{IC} for mode-I), is therefore regarded as the fracture toughness of the component or structure in question.

2.1.2 Limitations of Linear Elastic Fracture Mechanics

Generally, the various stress fields presented in **Eq(2.3.a-c)** are inversely proportional to the square root of distance from crack-tip, r: i.e.

$$\sigma_{ij} \propto \frac{1}{\sqrt{r}} \tag{2.6}$$

This implies that, as r gets closer to the crack tip, the stresses would be unrealistically high; i.e. stresses would be much beyond any material's ultimate strength. Indeed

theoretically, the stress is singular (tentatively infinite) at crack-tip (when $r = 0$). If the material is ductile, yielding is supposed to occur at much lower stresses, and as a result, associated load relief, and stress redistribution occur within the vicinity of the crack-tip. Real stresses are therefore far from the proportionality presented at Eq.(2.6) and puts the applicability of K into question. The extent of yielding at the crack-tip, known as crack-tip plasticity, is strongly related to the material's ability to deform at that region.

2.1.3 Effect of Stress State at Crack Tip: Stress Triaxiality and Constraint

One fundamental factor affecting plasticity at the crack tip is state of stress (stress triaxiality). The state of stress at the vicinity of a crack tip in ductile materials affect significantly its plasticity; plane-stress tends to promote crack-tip plasticity while plane-strain inhibits (constrains) such process. Specimen geometry, and more specifically the thickness, has the strongest influence on the state of stress, which is also known in the trade as "constraint". Generally, specimen thickness affects out-of plane constraint while specimen width (planar size) affects in-plane constraint [6]. Constraint is quantified in terms of the stress triaxiality ratio, h, defined as the ratio of hydrostatic stress, σ_h, to effective (Von-Mises) stress, σ_e [7]:

$$h = \frac{\sigma_h}{\sigma_e} = \frac{\sigma_1 + \sigma_2 + \sigma_3}{3\sqrt{\sigma_1^{\,2} + \sigma_2^{\,2} + \sigma_1\sigma_2}} \qquad (2.7)$$

Plane-strain state of stress has highest triaxiality ratio (constraint), while plane-stress has lowest triaxiality ratio (constraint). This is illustrated in Fig. 2.3 where thickness effect on mode-I fracture toughness (K_I) is shown. Other common factors that affect stress triaxiality are shown in Fig. 2.4.

2.1.4 Plastic Zone Sizes

Various researchers have carried out analyses to evaluate the extent of yielding ahead of a crack-tip, also known as plastic zone size. As reported in refs. **[1-4]** Barenblatt and Dugdale conducted a simple elastic analysis for plane stress condition and their analysis suggested that plastic zone size, r_p can be expressed in terms of stress intensity, K_I and yield strength, σ_{YS}:

$$r_p \leq \frac{\pi}{8}\left(\frac{K_I}{\sigma_{YS}}\right)^2 \qquad (2.8.a)$$

while Irwin, as reported in ref. **[1]**, also conducted a similar analyses and suggested that for plane stress:

$$r_p \leq \frac{1}{\pi}\left(\frac{K_I}{\sigma_{YS}}\right)^2 \qquad (2.8.b)$$

This is relatively bigger than r_p for the case of plane strain, where:

$$r_p \leq \frac{1}{3\pi}\left(\frac{K_I}{\sigma_{YS}}\right)^2 \qquad (2.8.c)$$

Note that **Eq.(2.8.a)** and **Eq.(2.8.b)** differ by about 20%, which shows the approximate nature of analyses used. More other detailed (and more accurate) analyses were conducted by other researchers and can be found in **[1, 2, 4]**.

2.1.5 Small Scale Yielding

Complexities of crack tip plasticity and associated stress fields and the dependence on constraint have prompted early research to consider the case of least yielding, i.e. plane-strain fracture, as a material property characterising the material's resistance to crack growth. In plane-strain fracture behaviour, high constraint condition implies limited

crack-tip yielding. Crack-tip stress fields, derived with the use of Linear Elastic Fracture Mechanics (LEFM) analyses, can be applied provided that crack-tip yielding is very limited. Such condition of limited crack tip yielding is known as small scale yielding condition, i.e. the size of plastic deformation or plastic zone at the crack tip is limited to allow linear elasticity assumption (and hence LEFM) to be valid. Note that in **Fig. 2.3**, the K_I value becomes minimum and insensitive to thickness dimension, B, at plane-strain fracture. This has been experimentally shown to occur when the following condition is satisfied **[1-4, 8]**:

$$B \geq 2.5\left(\frac{K_I}{\sigma_{YS}}\right)^2 \tag{2.9}$$

Eq.(2.9) describes the geometry restriction in ASTM E399 [8] for plane-strain fracture toughness. Other restrictions related to small scale yielding conditions also exist for K_{IC} measurement: most noteworthy is ratio of critical load, P_Q (95% secant), to maximum load, P_{max}, **[1,8]**, which can be written as:

$$P_{\max} \leq 1.10\, P_Q \tag{2.10}$$

As mentioned before, P_Q is regarded as critical load causing initiation of unstable crack growth and is therefore used to determine K_{IC}.

2.2 THE PHENOMENON OF STABLE CRACK GROWTH

Many tough materials do not exhibit unstable crack growth and catastrophic failure once crack growth has initiated, rather they exhibit an apparent increase in toughness, i.e. stable crack growth behaviour. In stable crack growth, the critical load required to produce a finite crack extension increases with crack growth.

Stable crack growth is attributed to irreversible processes, like plastic deformation, viscoelastic flow, martensitic transformation, microcracking etc., that have accrued within the vicinity of the crack-tip. The very high stresses that exist at the vicinity of a crack-tip have promoted such irreversible processes. **Fig. 2.5** shows examples of various irreversible processes for different types of materials. For metals, the main irreversible process leading to stable crack growth is plastic deformation (yielding). Such irreversible processes have been dissipating some (released) potential strain energy during crack growth and hence any further crack growth would require reimbursement of this "spent" potential strain energy which requires load on the cracked member/component to be increased.

Stable crack growth behaviour can be observed through mechanical response of a fracture specimen in a fracture test. Typical fracture specimens are shown in **Fig. 2.6**. Preparation of fracture specimen usually involves fatigue pre-cracking to obtain a relatively sharp and a straight-through crack front. In most fracture tests, load (P) vs. load-line displacement (Δ_{LL}) (or crack-mouth opening Δ_{CMO}) and/or load vs. crack growth (Δa) data are recorded. **Figs. 2.7** and **2.8** show typical plots of stable crack growth behaviour.

Typical load response of a cracked specimen may be characterised into three distinct behaviours, as shown in **Fig. 2.7**: linear elastic response, initiation /stable crack growth and unstable crack growth/failure.

In the first phase of linear elastic response, no crack initiation/growth is observed and the P-Δ of the cracked specimen can be predicted using the constitutive linear elasticity laws.

Although no macroscopic crack initiation/growth has been observed at this phase, irreversible processes have been occurring within the vicinity of the crack tip, though limited and negligible - as these processes have not accrued enough to affect behaviour. If loading-unloading cycles were to occur in this linear elastic region, accumulation of such processes would eventually lead to fatigue crack initiation, fatigue crack growth and eventual failure. However, for quasi-static loading, one can fairly claim that *nearly* all of the work done on the specimen, in deforming the specimen at this linear elastic phase, is stored as potential elastic-strain energy that is recoverable upon unloading.

In the second phase, these irreversible processes have accrued enough to cause crack growth initiation, at initiation load, P_i, and stable crack growth. Note that prior initiation, the specimen has departed from a linear elastic response and, provided the material can yield, the crack-tip would blunt. In this phase, the crack would grow intermittently (in spurts) with increased loading until a maximum load, P_{max}, is reached. During this phase stored potential strain energy is released. This released strain energy is insufficient for a sustained crack growth due to the irreversibilities mentioned earlier – and hence leading to finite and intermittent growth behaviour. At maximum load, the potential strain energy released in a crack growth increment would just suffice the formation of new crack surfaces as well as the associated irreversibilities.

Further crack growth increments would weaken the specimen and lead to the third phase, where excess potential strain energy is released and maximum load can no longer be supported. In the case of load-controlled loading, uninterruptible (unstable) crack growth and catastrophic failure would occur at maximum load. In the case of displacement-controlled loading, further crack growth is accompanied by load shedding (load relief).

2.2.1 Sources of Stable Crack Growth

Generally, stable crack growth behaviour can be attributed to two main sources that affect yielding process; state of stress and material yielding (plastic) behaviour: i.e. constraint and material plasticity.

Issues regarding constraint, and its characterisation by a triaxiality ratio, have been discussed earlier, but worth to mention here is that many materials that do exhibit small scale yielding under plane-strain (i.e. full constraint) conditions can and do show stable crack growth at lower constraint conditions, when plastic yielding is more significant.

A material that shows high plasticity can exhibit stable crack growth behaviour at plane-strain (high constraint) conditions. This is the case in metals exhibiting high ductility/toughness, where small scale yielding would only be satisfied at prohibitively thick specimens. However, such materials may not necessarily exhibit stable crack behaviour at plane-stress condition. In such cases continuous crack blunting and global yielding may dominate with very limited crack growth occurs.

2.2.2 Theories of Plastic Behaviour

The plastic stress-strain behaviour of a material can be described in terms of Ramberg-Osgood Relationship [1] where:

$$\frac{\varepsilon}{\varepsilon_0} = \frac{\sigma}{\sigma_0} + \alpha\left(\frac{\sigma}{\sigma_0}\right)^n \qquad (2.11)$$

where ε_0 and σ_0 are yield strain and strength, n is known as a plastic-hardening exponent and α is a constant.

It may be useful here to recall two general theories of plasticity: deformation theory and incremental theory of plasticity. In deformation theory of plasticity, a unique (plastic) stress-strain relationship based on effective stresses and strain is presumed to exist, which is independent of the state of stress [9]:

$$\varepsilon' = \frac{\sigma'}{E} + \varepsilon'_P \tag{2.12}$$

where ε' and σ' are effective (Von-Mises) strain and strength, and ε_P' is effective plastic strain.

Here, there is no indication of "incidence" of plastic strains, plastic strains would occur uniquely at a specific applied stress (beyond yielding): i.e. no discrimination between loading and unloading behaviour. Therefore, deformation theory of plasticity is said to imply loading path independence. In incremental theory of plasticity, the differential of plastic strains and stresses are considered. Therefore, loading/unloading (stress differential) does affect the resulting plastic strains and loading path dependence does therefore exist [9].

2.2.3 Features of Stable Crack Growth

There are distinct features on a fractured specimen surface that do indicate stable crack growth behaviour. Generally, such features are related to plastic yielding in some form or other and are shown in **Figs. 2.9-12** and are as follows

1- Stretched Zone, **Fig. 2.9**: When a fatigue pre-cracked specimen is loaded, crack-tip blunts before any crack growth occurs. When crack growth does occur, the

history of the initial crack blunt can be seen on the fracture surface and is termed the stretch-zone width (SZW). Usually stretched zone can be seen from Scanning Electron Microscope (SEM) fractographs.

2- Crack Front Tunnelling, **Fig. 2.10**: As mentioned before, plastic yielding is dependent on state of stress, as well as yielding behaviour. The state of stress however is not constant throughout the thickness of specimen; at the surface exists a purely plane stress state of stress, while at the core (mid-thickness) higher triaxiality exists. This implies that plastic zone development is relatively limited at the core-thickness of the specimen and therefore crack growth would occur at the core prior to crack growth at the surface, leading to a progressively curved crack-front growth.

3- Slant Fracture, **Fig. 2.11**: Slant fracture is typical for stable crack growth behaviour involving significant low constraint i.e. dominance of plane stress condition. In such cases orientation of the plane of maximum shear, at 45^{o} transverse to the crack front, causes the crack to progressively grow into that plane. Note that, as mentioned before, when the material exhibits high yield capacity, stable crack growth can occur even at plane strain (high constraint) conditions. However, in that case, crack slant does not occur and flat (but tunnelled) crack growth does occur.

4- Microvoid Coalescence, **Fig. 2.12**: The micro-mechanics of yielding involves formation, growth and coalescence of voids around secondary phases and impurities. Macroscopically, this appears as a dimpled surface. If a fractured

specimen examined under Scanning Electron Microscope (SEM), such features would be visible indeed.

2.3 CHARACTERISATION/MODELLING OF STABLE CRACK GROWTH BEHAVIOUR

Characterisation and prediction of stable crack growth has been a topic that attracted numerous researchers in the past two decades. However, many of these attempts were successful only at geometry/configuration specific characterisation of stable crack growth. Others demanded extensive FE modelling and analysis; a more general characterisation of a material's intrinsic behaviour is still pending.

Generally, there have been various methodologies to characterising stable crack growth behaviour:

1- Extension of LEFM (R-curve approach).

2- Elastic-Plastic Fracture Mechanics (EPFM), which includes a varied mix of theoretical, experimental and heuristic approaches.

3- Local Criterion Approach; basically micro-mechanical (damage) modelling of ductile fracture at crack-tip vicinity.

2.3.1 R-curve Characterisation, K_R

The R-curve method to characterise stable crack growth is an extension of classical LEFM. The rationale is that if critical stress intensity, K_C, were to increase with crack growth, then plotting toughness, K vs. crack growth, Δa, would be a reasonable analysis

of stable crack growth. The obtained plot is known as K_R curve. R-curve testing has been standardised and covered by ASTM E561 [10]. The resistance curve can also be represented by energy release rate, G, vs. Δa:

$$G = \frac{K_I^{\,2}}{E'} \tag{2.13}$$

where E' is effective Young's modulus depending on state of stress; it is equal to uni-axial Young's modulus, E, for the case of plane stress and equal to $E/(1-\nu^2)$.

Typical R-curve is shown in **Fig. 2.13**. There is no specific geometry restriction for E561. However, there is requirement for geometry with dominantly elastic response (contained yielding). Moreover, K_R curves can be size/geometry dependent and generally does characterise the performance of specific thickness rather than material performance. There are also issues with measurements of effective crack size; should physical sizes be used or derived values? Derived values may involve indirect measurements, using unloading compliance, or using corrections to physical cracks based on plastic zone size. Generally, R-curve method, as per E561, is increasingly regarded as obsolete [11, 12].

2.3.2 Elastic-Plastic Fracture Mechanics

Limitations of classical LEFM have prompted researchers to look for ways to characterise and model crack growth and fracture behaviour for materials showing considerable yield capacity. The primary objective is prediction of onset (propagation) of crack growth. Two approaches have been developed: energy approach -via J-integral concept and its variants - and crack-tip deformation characterisation (crack-opening displacement/angle). Both approaches have been shown to be compatible [1].

2.3.2.1 Energy Approach: J-integral (J_{IC} and J_R Curve)

A conceptual path independent line-integral, termed *J*-integral, has been originally derived for a non-linear elastic cracked body based on conservation of potential strain energy. The analogy was then proposed that since loading behaviour of a non-linear elastic material is identical to an elasto-plastic material (according to deformation plasticity theory) then the mechanical response at the vicinity of a crack in an elastic-plastic material would be identical too. For a cracked linearly elastic body, it was found that there is compatibility of *J*, in LEFM context, with energy release rate term, *G*, such that [1-4]:

$$J_{elastic} = G = \frac{K^2}{E'} \tag{2.14}$$

J-integral has therefore evolved to indicate an energy-rate parameter for the case of elasto-plastic materials, rather than the original path-independent integral parameter [3]:

$$J = -\frac{\partial(U/B)}{\partial a} \tag{2.15}$$

J-integral has been used successfully to characterise initiation of stable crack growth, in terms of J_{IC}. Recent updated testing standard exists as ASTM E-1737 [13] and covers the measurement of several of *J* parameters; J_c for brittle fracture, J_{IC} for initiation of stable crack growth, and J_m for *J* at maximum load for stable crack growth behaviour. Conventionally, *J* is measured from P-Δ_{LL} plot of a fracture test. The net area-under a loading-unloading curve, A_{pl} as shown in **Fig. 2.14**, which represents dissipated potential energy, is used to measure *J*.

$$J = J_{elastic} + J_{pl} \tag{2.16.a}$$

where

$$J_{pl} = \frac{\eta_{pl} A_{pl}}{Bb} \tag{2.16.b}$$

and η_{pl} is a geometry factor.

J has also been regarded as characterising stress fields within a cracked elastoplastic material, through Hutchinson, Rice and Rosengren (HRR) singularity relationship [1], which can be represented as:

$$\frac{\sigma_{ij}}{\sigma_0} = \left(\frac{\Gamma}{\bar{r}}\right)^{\frac{1}{n+1}} S_{ij}(n,\theta) \qquad (2.17.a)$$

where $$\Gamma = \frac{E}{\alpha . I_n . \sigma_0} = \frac{1}{\alpha . I_n . \varepsilon_0} \qquad (2.17.b)$$

and $$\bar{r} = r . \frac{\sigma_0}{J} \qquad (2.17.c)$$

and I_n is an integration constant and $S_{ij}(n, \theta)$ are known functions of n and θ.

However, issues regarding extending J to elastoplastic materials do exist due to fundamental difference between unloading behaviour of a non-linear elastic material and unloading of an elastoplastic material (according to incremental plasticity theory). This may not be applicable for a stationary (non-growing crack) but is especially true when crack growth occurs and unloading does result at the plastic wake. Therefore, validity of J-integral is limited and the notion of path independence is challenged; not to mention the ambiguity about what would J actually mean for the case of an elastoplastic material.

It was generally accepted according to findings by Shih [14] that if Δa is within 6% of ligament stable crack growth, J is regarded as path independent; i.e. $\Delta a \leq 0.06\, b$. Brocks and Yuan [14], however, conducted plane-stress and plane-strain studies and found that J is path dependent, even at crack growth amounts smaller than that of 6% of b. This does place doubts on the validity of J when characterising stable crack growth.

To bypass the problem of effect of crack growth on validity of J, it has been common practice to plot J against crack extension, Δa, and in effect obtaining a crack-resistance curve termed of J_R curve. J_R curve has been indeed used commonly to characterise and model stable crack growth behaviour. Some researchers have extended the use of J_R curves to define a tearing modulus, T_R.

$$T_R = \frac{E}{\sigma_0^{\,2}} \cdot \frac{dJ_R}{da} \tag{2.18}$$

Hence, unstable crack growth would occur if applied T_R exceeds a measured critical T_R [1].

One should note here that other issues, that have been a concern in K_R testing, do still remain. Neimitz et al. [15] reports on the issues regarding J_R testing as well as geometry dependence. According to Neimitz et al. [15], various equations that exist for J_R, to account for crack growth, do give varying results. Also, experimental measurement of Δa may still differ depending on technique used; common techniques like optical/visual surface measurement, unloading compliance and electric-potential drop techniques do not necessarily give similar results. Also, one should not underestimate the complication of crack-tunnelling common during stable crack growth behaviour. Neimitz et al. have therefore adopted two techniques simultaneously for reliable Δa measurement [15, 16].

Size and geometry sensitivities do exist too with J_R testing, especially when substantial deformation (plastic strains), termed large scale yielding, occurs at the crack-tip. This invalidates small strain assumption used in derivation of J. Large scale yielding is very relevant for the case of testing specimens of relatively lower constraint; when crack-tip

plastic deformations are comparable to thickness [1, 2]. Size limitations, according to ASTM E 1737 [13], do exist on specimen dimensions to ensure that values obtained are material specific, or in more accurate terms, insensitive to size provided limit is not exceeded:

$$B, b \geq 20 \frac{J_{max}}{\sigma_Y} \tag{2.19}$$

This has been obtained from extensive FE models on geometry dependence of J. Even though E 1737 allows testing of thinner specimens than that of E399 (for K_{IC}), it still does form a limitation on size and is therefore restrictive for low constraint, when plane-stress testing is concerned.

Kolednik [17] has carried out an investigation on the effect of in-plane constraint (ligament size) on J_R curves and found that such effects can be characterised into three distinct patterns: Wider-higher, wider lower and wider no-effect patterns. Wider higher pattern was attributed to the case of large scale yielding under plane-stress conditions. Wider no-effect pattern was attributed to also large scale yielding, but under plane-strain conditions. Wider-lower pattern was attributed to small scale yielding conditions. Shan et al. [18] has attempted to account for out-of plane constraint (effect of thickness) using a numerical "mixing" model. The fracture behaviour is arithmetically mixed via a plane-stress fraction, β, which is determined either heuristically or analytically for a particular section slenderness ration thickness, B/b.

Recently, there have been trends to use a derivative of J, termed energy dissipation rate, D, to characterise resistance to stable crack growth. According to Sumpter [12, 19]:

$$D = \frac{1}{B}\frac{dA_{pl}}{da} = \frac{b}{\eta_{pl}}\frac{dJ_{pl}}{da} \qquad (2.20.a)$$

According to Brocks and Anushewski [20], provide an alternative definition of D:

$$D = (W - a)\frac{dJ_{pl}}{da} \qquad (2.20.b)$$

Sumpter [19] and, Brocks and Anushewski [20] have both provided data and results comparison to support their proposals, of a geometry independent characterisation. However, more experiments and analyses are needed.

More successful and thorough modelling of constraint can be achieved by employing an additional constraint-related parameter to J. This will be discussed in the two-parameter approach.

2.3.2.2 Crack Tip Opening Displacement (CTOD)

The CTOD, δ, has evolved from experimental observations on crack blunting [1]. The exact definition of CTOD may differ for different researchers but are generally similar as shown in **Fig. 15**. Indeed, it was found that CTOD was compatible with LEFM for small scale yielding cases. Moreover, it was found that CTOD can be related to J-integral through the relationship [1]:

$$J = m.\sigma_{YS}.\delta \qquad (2.21)$$

where m is a dimensionless constant that is dependent on stress state and is unity for plane stress. Li et al. [21] examined the *CTOD-J* relationship through the m factor and found that m depends on toughness of material and crack size, a/W, and much less on amount of stable crack growth, Δa. It was thus argued that CTOD can be a used as a

parameter characterising stable crack growth behaviour. Even though CTOD is essentially similar to J, it has the advantage that it can be readily used in FE framework.

Since it may be difficult to directly measure CTOD in an experiment, CTOD can be inferred from measuring crack opening at distance behind crack tip. Indeed various standards cover guidelines for CTOD testing such as ASTM E-1290 **[22]**. CTOD can be obtained at initiation of stable crack growth as δ_i, or at maximum load as δ_m. There are, however, restrictions on geometries. E-1290 specifies that section dimensions, for any specimen configuration, should be:

$$B, b \geq 30\,\delta \tag{2.22}$$

Any other dimensions would be thickness specific and not a general material characteristic. This is also due to issues with constraint.

Schwalbe et al **[23, 24]** have proposed a modified CTOD definition, termed δ_5, measured not at the crack-tip, but over a gauge-length of 5 mm behind the crack-tip. δ_5 has displayed robustness for characterising resistance to stable crack extension and has been proposed as part of an engineering design procedure, known as engineering treatment model (ETM), which has shown to be valid as other fracture-design codes, R6-3 **[24]**. Moreover, preparations are in progress to standardise measurement of δ_5 **[11, 24]** as parameter characterising stable crack extension.

2.3.2.3 Crack-tip opening Angle (CTOA)

A crack-tip parameter, CTOA, Ψ, is defined in **Fig. 16**. It is very similar to CTOD, and has been shown to be very useful in characterising and modelling stable crack growth. CTOA can also be inferred from measured CTOD values:

$$\Psi = 2\tan^{-1}\left(\frac{\delta}{2d}\right) \tag{2.23}$$

CTOA as a fracture criterion has been known for some time, but problems arose with early research, when attempts to use 2D FE models, based on either plane-stress or plane-strain conditions, were not capable of matching experimental data, according to a review by Newman et al. [25]. Experimental data shows that CTOA, at initiation, to be relatively high and non-constant. CTOA becomes fairly constant only after some finite crack extension, as shown in **Fig. 2.17**. Newman et al. [25] attribute these modelling to the flawed assumption of a uniform state of stress at initiation as well as crack-tip blunting and tunnelling at the crack front. Mahmoud and Lease [26] has investigated stable crack growth for an aluminium alloy at various thicknesses and has found that transition of CTOA values decreases with increasing thickness. James and Newman [27] conducted a thorough investigation on crack tunnelling and found that the CTOA also varied along the crack front. Crack tunnelling adds to complications with regard to modelling stable crack growth for 2D FE models. Some researchers have circumvented these problems by using a hybrid approach, worthy to note is plane-strain core method proposed by Newman et al. [25, 28, 29] and hybrid scheme method proposed by Shan et al. [18]. In the plane-strain core scheme, a finite region along the crack front is presumed to be fully constraint, i.e. under plane-strain condition, while the rest of specimen is not constraint,

i.e. under plane-stress. Results have been shown to be compatible with experimental results.

The scheme proposed by Shan et al. [30] is more intuitive. First, a combined state of stress is formulated, using a mixing factor determined from geometry, then two parameters were used to simulate stable crack growth: δ_i for initiation of stable crack growth, and then CTOA for progression of crack growth. This method has been shown to emulate experimental results. Another FE modelling scheme, whereby crack growth is represented as an averaged with respect to thickness, was employed successfully by James and Newman [27], in order to account for tunnelling. Hampton and Nelson [31] using 3D crack-front model, managed to get good predictions for failure loads for space module structure.

Issues regarding measurement of a constant CTOA have been covered by Schwalbe et al. [11]. Application of CTOA in modelling of stable crack growth have been reviewed by Newman et al. [25]. Newman et al. asserts, through various experiments and simulations [11, 25, 28] that CTOA can characterise stable crack growth, especially that stable crack growth affected by low constraint. Lam et al. [32], however, found such assertion to be rather optimistic and have instead used schemes that capture initial CTOA transition using a bi-linear approximation and found that this gives better predictions using 3D FE models.

2.3.3 Two Parameter Approach: T-Stress, J-Q and J-A_2 Characterisation

Limitations of J_R curve to account for size/geometry sensitivity of stable crack growth behaviour has prompted researchers to look for additional parameters that can describe

constraint and associated stress-strain fields; most common are the T-stress, Q and A_2 constraint parameters.

2.3.3.1 T-stress:

When stress intensity parameter has been derived from the solution provided in eq.(1), the first singular term was considered as dominating at the vicinity of the crack-tip. However, several researchers have found that the second term, which is a constant, does have an influence on the development of plastic zones ahead of a crack-tip, and hence has potential to characterise constraint and stable crack growth [1]:

$$\sigma_T = A_0 . g_{ij}(\theta) \tag{2.24}$$

T-stress is more conveniently described in terms of a biaxiality ratio, β_T [1]:

$$\beta_T = \frac{T\sqrt{\pi a}}{K_I} \tag{2.25}$$

Generally, *T*-stress is considered an indicator for in-plane constraint (ligament size effect) and is normally used with *K* to describe stress-fields. One should note that *T*-stress is independent of distance from crack-tip, *r*. Even though it was derived from a purely elastic analysis, it was found to be relevant even when significant plastic deformation occurs at the vicinity of crack-tip, provided that $|\beta_T| > 0.4$ [1].

Many researchers have found *T*-stress to be very useful as a constraint parameter. It has been included in recent European initiative, Structural Integrity Assessment Procedures (SINTAP) according to Ainsworth et al. [33]. *T*-stress has also been found to be useful with elastic-plastic analyses. Thaulow et al. [35] used *T*-stress values to derive constraint correction factors, in terms of η_{pl} factors for SENB specimens for a high strength steel

alloy. Moreover, Nyhus et al. [36] have successfully normalised experimental J_R curves using T-stress values. Neimitz [16] has proposed a modified Dugdale model that accounted for T-stress contribution to geometric constraint.

2.3.3.2 Q-parameter

Q parameter has been proposed by O'Dowd et al. [1]. Q-parameter, like T-stress, is another measure of constraint, and is regarded as a triaxiality parameter. It is used in conjunction with J. It is, however, different from T-stress in two respects. First, it is derived from an HRR stress field analysis, which gives a better insight to plastic stress fields. Second, unlike T-stress, it is not a constant but is dependent mainly, among other factors, on applied load. Q is defined as follows [35]:

$$Q = \frac{(\sigma_{\theta\theta})_{HRR} - \sigma_{\theta\theta}}{\sigma_0} \tag{2.26}$$

Q was initially derived using plane-strain analysis, but Ma et al. [37] found that such assumption gives rise to inaccuracies. Neimitz et al. [16] claimed, after a thorough investigation of stable crack growth of various specimen configurations, and using both plane-strain and plane-stress analyses, that Q-parameter can only qualitatively describe the effect of constraint on J_R curves. Thaulow et al. [35], however, used an alternative definition of Q, based hydrostatic stress:

$$Q_H = \frac{(\sigma_h)_{HRR} - \sigma_h}{\sigma_0} \tag{2.27}$$

and was successful at deriving constraint corrections. Zhu and Jang [38] have also, in an earlier research, modified the definition of Q and successfully normalised J_R curves. Determination of Q, or any Q-related terms, requires extensive FE effort. Moreover, if 2-

D models are to be used, a correct assumption of state of stress is needed; which may not be possible for the case of low-constraint stable crack growth.

2.3.3.3 A_2 Parameter

Similar to T-stress, A_2 parameter is obtained through considering other "non-singular" terms of elastic-plastic asymptotic series expansion. Various researchers, according to Chao and Lam [39], have indeed obtained asymptotic elastic-plastic solutions for the case of non-linear materials and have found that the first three terms of the expansion are needed to characterise the stress field. Generally, the three-term expansion, for mode-I loading, can be expressed in terms of J (i.e. in terms of $\bar{r}$) and A_2, according to Nikishkov [40]:

$$\frac{\sigma_{ij}}{\sigma_0} = (\Gamma)^{\frac{1}{n+1}}\left[\bar{r}^{x}.S_{ij}^{(1)}(n,\theta) + A_2.\bar{r}^{y}.S_{ij}^{(2)}(n,\theta) + A_2.^2\bar{r}^{z}.S_{ij}^{(3)}(n,\theta)\right] \tag{2.28.a}$$

where $$x = -\frac{1}{1+n} \tag{2.28.b}$$

$$z = 2y - x \tag{2.28.c}$$

and y is determined numerically.

or alternatively, it can better expressed as:

$$\frac{\sigma_{ij}}{\sigma_0} = \left(\frac{\Gamma}{\bar{r}}\right)^{\frac{1}{n+1}}\left[S_{ij}^{(1)}(n,\theta) + \left(A_2.\bar{r}^{(y-x)}\right)S_{ij}^{(2)}(n,\theta) + \left(A_2.\bar{r}^{(y-x)}\right)^2.S_{ij}^{(3)}(n,\theta)\right] \tag{2.28.d}$$

A_2 parameter is usually determined by numerically fitting FE results of stress fields into the above equation [40]. Chao and Lam [39] developed a procedure to evaluate A_2 parameter experimentally, by equating and relating simulated δ_5 values to A_2. However, Chao and Lam [39] acknowledged that fitting was used to plane-strain FE analyses, which is incorrect. J-A_2 method does still more development.

Generally, the several two-parameter approaches have shown their ability to characterise the influence of constraint and hence stable crack growth behaviour, which were promising. Nevertheless, one should note the FE effort required, which were extensive indeed. A more straightforward method is yet to be developed.

2.3.4 Local Approach

Local approaches are in effect local failure criteria applied to a given stress field within a crack-tip vicinity, usually obtained from an FE model, to predict path and "instant" of crack growth. Traditionally, they were based on adaptations of common and various failure criteria. Modern local approaches are, however, based on modelling micro-mechanics (micro-damage) of ductile fracture. This is either done through modelling microvoid nucleation and coalescence mechanism or through a purely phenomenological approach called cohesive zone modelling (CZM).

One of the most popular models developed to model microvoid coalescence was that proposed by Gurson which was modified further by Tvergaard and Needleman [1]; the final model is commonly known as the GTN model. The model is a continuum model that assumes crack would grow when voids reach a critical size, i.e. when void

coalescence occurs. The void growth is described in terms of the yield-surface function, Φ, which is a function of hydrostatic and equivalent stresses, σ_m and σ_e, yield strength of the material, σ_{YS}, and effective void volume-fraction, f^*. When void coalescence occurs, $\Phi = 0$ **[1, 41]**:

$$\Phi = 0 = \left(\frac{\sigma_e}{\sigma_{ys}^{\ 2}}\right)^2 + 2.q_1.f'\cosh\left(\frac{3}{2}.q_2.\frac{\sigma_m}{\sigma_{ys}}\right) + \left(1 + q_1^{\ 2}.f'^2\right) \tag{2.29}$$

Note that q_1,q_2 are fitting parameters and can be determined along with f^* from tensile tests on smooth and notched specimens. The model is then used as a local criterion for crack growth within an FE model.

In CZM approach, a purely phenomenological model of ductile rupture is employed: failure is presumed to occur within a (cohesive) process zone - along traction interfaces of cohesive cells, where a constitutive relationship for traction stress vs. separation is assumed, e.g. linear, bilinear or exponential. Method is very potent for a variety of applications such as interface fracture and heterogeneous materials. For homogenous materials, failure occurs at interfaces of arbitrary cells akin to micro-structural grains. In a FEA framework, mesh is used as geometrical interfaces for cohesive cells, and failure along interfaces forms the local criterion for macroscopic crack growth. Cornec et al. **[42]** covered procedures for application of CZM.

Various issues and improvisations do exist with local approaches in general and it is related to its application within FEA framework, most important is that of mesh sensitivities. Mesh sensitivities do arise due to the local nature (and hence mesh reliance)

of the model. FE applications of local approaches have thus relied on "computational cells", rather than mesh elements, where the size of the computational cells have some physical significance, such as microstructure/grain size. Issues regarding computational cells and other modelling issues relating to a local approach modelling, especially when GTN scheme is employed, has been covered by Gullerud et al. [43].

Other issues are more particular to the methods used. Chabanet et al. [44] found that CZM could not account for varying triaxiality due to inherent weakness in the constitutive cohesive-separation laws used. Moreover, Li and Chandra [45] found that various cohesive-separation laws give discrepancies in crack growth predictions.

GTN modelling also suffers from some particular drawbacks. The GTN model does accounts for microvoid coalescence but does not provide for initiation of void growth. Various adaptations have been proposed, e.g. Zhang et al. [46]. However, it was still found that high initial void volume fraction, f, and void shape do affect accuracy of crack growth predictions, according to Zhang et al. [46]. Moreover, Bernauer and Brocks [47] reported on a European round-robin that has been conducted and found discrepancies between predictions of various labs as well as discrepancies with experimental results. This has been attributed on determination of fitting parameters (e.g. f^*, q_1 and q_2) which are not free from controversy and to software application of to simulate local failure development. Generally, GTN has been found to be very promising despite the discrepancies and drawbacks mentioned [46, 47]. Examples of successful numerical modelling of stable crack growth behaviour have been demonstrated by Nègre et al. [41] and Rivalin et al. [48]. One however, should not underestimate the computational effort and cost of such approaches, especially when 3D modelling is used [44].

2.4 MIXED-MODE STABLE CRACK GROWTH

Cracks in real life structures may be subjected to more than one mode of crack-loading. An understanding of stable crack growth under mixed-mode loading would therefore be key to producing reliable and efficient structural assessment procedures. The basic crack loading modes have been described earlier and are shown in **Fig.** 2.1. The combination of mode-I and II loadings would be our primary interest due to its relative practical importance to other combinations.

2.4.1 Mixed-Mode Testing

Experimental studies on stable crack growth under mixed-mode (I and II) loading are, however, not as extensive as Mode-I loading. This is mainly due to experimental complications associated with mixed-mode testing where one should consider the two-dimensional displacement field at the crack-tip. Also, no consistent behaviour could be concluded from the limited experimental results that are available to date in the literature as shown in **Fig 2.18 [50]**. Roy and Narasimhan [49] and Laukkanen [50] have reviewed varies issues which can be summarised as follows:

1-Instrumentation: Measuring the tensile and shear displacement components directly poses practical installation problems of such systems to produce accurate readings **[50]**.

2- Measurement of crack growth: There are problems with the various methods used to measure crack growth. The unloading compliance cannot be used, as it is a function of mode-mixity. Potential drop method is affected by shearing **[50]**.

3- Crack face contact: This is especially true where a mode II loading is dominant. Contact between crack faces/flanks raises issues such as effect of friction. Although friction adds resistance to crack growth, it is not easily quantitatively separable from the material's intrinsic resistance to crack-growth [50].

4- Application of shear load: Application of shear load generally leads to an increase in overall load requirement, which can be very large, especially when testing of steel alloys is involved. This may necessitate testing frames of relatively high loading capacities. Moreover, if 3PB/4PB configurations are used, deformation of support rolls may contribute to the already existing measurement difficulties [50].

5- Range of mode-mixities: Mixed-Mode experiments involve investigating various fracture characteristics against a particular mode-mixity. Plane-strain FE studies show that some specimens may not be suited for a varied range of mode-mixity, i.e. of limited mode-mixity [49].

6- *J*- Dominance: Maintaining plastic strains within small-strain assumption within crack-tip for varied mode-mixity is very desirable, mainly maintaining condition of *J*-dominance (i.e. not large scale-yielding). However, some specimens may experience a large plastic deformation at the vicinity of the crack-tip, i.e. large scale yielding, for differing mode-mixity, as shown by Roy and Narasimhan [49].

Various experimental arrangements that exist address part of these issues in different ways and have been used by researchers, although an established reliable method is yet to be formulated. **Fig. 2.19** summarises the various experimental configurations.

Mahanty and Savant [51], and Maiti and Mourad [52], for example, have used a 3PB configuration with an inclined crack, which has been originally suggested by Ahmed et al. [50, 52]. This arrangement has difficulties in pre-cracking, where special arrangements and fixtures are needed to produce pre-cracks. Also, starter notches have to be machined into the specimen depending on the mode-mix required and thus have inherent limited flexibility. Tohgo, according to Li [53], used a 3PB specimen with a straight crack, but with offset loading. A 4PB arrangement with offset loading has originally been suggested by Goa et al., and has been used by Laukkanen [50]. 3PB and 4PB specimen configuration with offset arrangements have advantages of flexible mode-mix choice, ease of implementation to current experimental set-ups and no special fatigue pre-cracking equipment is needed. However, they do suffer from the fundamental problems of non-rigidity, especially with increasing offset, and this can lead to errors with regard to measured displacements and assumed mode-mixity.

Banks-Sills and Arcan, according to Laukkanen [50], have suggested what is known now as Arcan fixture, which has the advantage of uniform mode-II shear distribution, and is much more rigid arrangement. Arcan specimen has been used by Amstutz et al., and by Sutton et al. [54, 55]. Aoki et al. [56], Roy et al. [57] and, Pirondi and Donne [58] have used a compact-tension shear (CTS) specimens, which are also rigid. Arcan and CTS arrangements do have the disadvantage of discrete (and thus inflexible) loading mixes, but their relative rigidity guarantees more reliable data.

A modified compact tension (CT) specimen is similar to the conventional CT configuration but has an additional hole to give a varied loading angle. It is also rigid and

has much simpler loading configuration. Such configuration has been originally suggested by Sakata et al., according to Roy and Narasimhan [49], and was used by Mahanty and Maiti [59], Maiti and Mourad [60], and recently by Mourad et al. [61]. Roy and Narasimhan [49], however, claim that such configuration does suffer from very limited mode-mixity range (close to Mode-I), even at high loading angles (45^{o}). This may be true, but caution is needed as such claims were based on plane-strain analysis. A modified Compact Tension specimen will be used in this current study.

2.4.2 Characterisation of mixed-mode crack growth

Characterisation of mixed-mode crack growth behaviour involves three main issues; mode-mixity, criterion for onset of crack growth and direction (path) of such crack growth.

2.4.2.1 Mode Mixity

Mode mixity defines the ratio between tensile (mode-I) and in-plane shear (mode-II) stress intensities. In LEFM context, if mode-I and mode-II stress intensities "vectors" are added, then an effective (resultant) stress intensity factor, K_e, can be defined:

$$K_e = \sqrt{K_I^{\,2} + K_{II}^{\,2}} \tag{2.30}$$

Mode mixity can thus be defined as the adjacent angle to mode-I component, termed phase angle, ψ, [62]:

$$\psi_e = \arctan\left(\frac{K_{II}}{K_I}\right) \tag{2.31}$$

Therefore, $\psi_e = 90^o$ for purely mode-II loading and $\psi_e = 0^o$ for purely mode-I. One should note that ψ_e is not to be confused with loading angle/ crack-inclination angle.

Alternatively, it can be expressed in terms of mode-mixity parameter, M_e [63]:

$$M_e = \frac{2}{\pi}\arctan\left(\frac{K_{II}}{K_I}\right) \tag{2.32}$$

So, $M_e = 1$ for the case of pure mode-II loading and $M_e = 0$ for pure mode-I loading.

One should note the M_e and ψ_e are essentially the same since $M_e = (2/\pi)\psi_e$. One should also note that some researchers do prefer an inverse definition, although with trivial difference, such that $M_e = 1$ and $\psi_e = 90^o$ for pure mode-I loading.

In EPFM, a local mode mixity can be defined as ratio of shear-to-tensile stress, which is a function of the distance from the crack-tip, r [53, 62, 64]:

$$\psi(r) = \arctan\left(\left.\frac{\sigma_{r,\theta}}{\sigma_{\theta,\theta}}\right|_{\theta=0}\right) \tag{2.33}$$

In an EPFM context, M_e and ψ_e are still relevant as far-field (or global) mode mixity [64].

Studies on elastic-plastic mode-mixity have been conducted by Bose and Castañeda [62] and Dhirendra and Narasimhan [64]. Bose and Castañeda [62] conducted an analytical study to determine asymptotic stress field solutions for mixed mode stable crack growth in a linear-hardening elastic-plastic material under plane strain conditions. They have found that stress field parameters at the crack-tip assume finite values pertaining to either mode-I (tensile) mode or mode-II (shear) mode. Dhirendra and Narasimhan [64] conducted FE studies for a power-hardening elastic-plastic material using a modified

small scale yielding model and incremental theory of plasticity. They have analysed systems with various values of n and various constraints in terms of T-stress. They have confirmed the notion that at the crack-tip, the stress-fields are very similar to that of mode-I for a wide range of remote mixity parameters, i.e. $0 < \psi_e < 60^o$.

Such results regarding local mode-mixity can be correlated to experimental observations for crack formation (initiation) and growth under mixed-mode conditions. Pirondi and Donne [58] reported in earlier studies that there exists a non-uniform damage field surrounding the crack-tip under mixed-mode conditions. This causes one side of the crack-tip to experience yielding and blunting under tensile stresses, while causing crack sharpening on the other side, under the action of shear stresses as shown in **Fig. 2.20**. Mode mixity, strain-hardening exponent and microstructure are key factors that decide which of the competing mechanisms dominate. Usually tensile stresses dominate and hence a purely local mode-I type crack growth occurs.

Generally for ductile materials, the resistance to stable crack growth increases with increasing ψ_e i.e. critical load required to reach failure increases. However, there are cases, and specifically for some steel alloys, where increasing mode-mixity decreases the resistance to crack growth i.e. the material is apparently weaker than in mode-I. It has been observed that higher ductility causes this weaker mode-II toughness [58].

2.4.2.2 Criteria for Onset of Stable Crack Growth under Mixed Mode Conditions

Criteria for onset of stable crack growth are not that different from those of mode-I, which have been mentioned earlier. Criteria that have been used successfully, some with

minor adaptations for mixed-mode condition, like J_R curve, CTOD/CTOA as well as local approach. Aoki et al. [56], for example, have used a J-integral variant, $\hat{J}$, as well as stretch zone width (SZW) measurements to characterise mixed mode stable crack growth in an Aluminium alloy using CTS specimen configuration. Mahanty and Savant [51], using 3PB with inclined notch, attempted to use crack-mouth opening displacement (CMOD) as a characterising parameter, but their results were inconclusive. Mahanty and Maiti [59] attempted to use crack-opening angle (COA) using 3PB with inclined notch and modified CT specimen configurations and their results showed the COA can be used as a characterising parameter. Maiti and Mourad [52, 60] have measured CTOA using replication technique, where crack surface details were imprinted on plasticine and have also used FE analyses. They also found that CTOA could be a viable criterion. Sutton et al. [54, 65] as well as Pirondi and Donne [58] have used an adapted CTOD criterion. Pirondi and Donne [58] have also represented their findings using J_R curve. Laukkanen [50] conducted investigations using 4PB specimen arrangement and also presented results using J_R curve.

It is worthy to mention that such characterisation attempts do still suffer from the same shortcomings that were faced for plain mode-I characterisation, mainly the issue of transferability problem as well as needing a complimentary criterion to specify crack growth direction. CTOD criterion as developed by Ma et al. [63, 65] is an exception and does show potential to overcoming such problems. The suggested CTOD criterion consist of two critical parameters, δ_{Ic} and δ_{IIc}, each correspond to $\delta_{(5)}$ criterion in mode-I and mode-II fracture. Failure would occur when either components (tensile or shear) reaches critical value first. The criterion does also predict crack growth direction, according to

Sutton et al. [65], and have shown how the criterion was used in a FE modelling framework reproduced experimental data.

2.4.2.3 Criterion for Direction of Stable Crack under Mixed Mode Conditions

Under purely mode-I loading, crack is expected to grow, after initiation, in the planar direction perpendicular to loading. However, under mixed-mode loading (I/II), there is no guarantee that the crack would maintain its original orientation to loading angle. Indeed, the crack does bifurcate, i.e. change its original orientation. Traditionally, several theories have been established for some time, mainly based on purely elastic solutions, which have been extended satisfactorily to mixed-mode ductile crack growth but some do incorporate elastic-plastic parameter J. Theories such as Maximum Tangential Stress (MTS) criterion, Maximum Circumferential Stress (MCS) criterion, Maximum Energy Release Rate criterion, Minimum Strain-Energy Density criterion are examples of known criterion in the trade. Generally such criteria are satisfactory when dominant mode-I loading is concerned [66].

However, observations by Amstutz et al., according to Sutton et al. [54, 66], regarding mixed-mode ductile crack growth, have shown that direction sharply changes after a certain specific loading angle/mode mixity. This was not captured in traditional direction theories. Such transition was attributed to competition between Tensile (T-type) and Shear (S-type) cracks, and found to be consistent with studies local mode mixity [53]. Sutton et al. [65] found that proposals by Ma et al. [63] are very adequate; crack will grow in local mode-I direction if $\delta_{(5)\text{-I}}$ reaches a critical value first; crack will grow in local mode-II direction if $\delta_{(5)\text{-II}}$ reaches its critical value first. Li et al. [53], on the other hand used a combined J-M_P criterion that also captures such transition, in terms of a

critical local mixity, M_{Pc} value. However, such criterion was based on plane-strain solutions, in calculating M_{Pc}. The method, therefore, does require further development.

2.5 STABLE CRACK GROWTH EMANATING FROM NOTCHES

Most of investigations presented have addressed the issue of stable crack growth from the perspective that it does initiate from an existing sharp crack, usually obtained in test specimens via fatigue precracking. Stable crack growth emanating from (sharp) notches are limited. Indeed, only Giovanola et al. [67], Krompholz and Kalkhof [68] and recently Mourad et al. [61] have reported experimentation that have address fracture initiation from notches. Giovanola et al. [67] and, Krompholz and Kalkhof [68] have both addressed stable crack growth of different steel alloys but for blunt notches, through various geometrically scaled 3PB specimens. Mourad et al. [61] have carried out an experimental investigation of stable crack growth in CT specimens using wire-EDM sharp notches. The investigation involved testing specimens with various loading angles.

The relevance of stable crack growth from (sharp) notches cannot be underestimated. This is so from two perspectives. First, structures and components are usually designed according a yielding criterion at notch tip. This may correspond to initiation of damage (blunting / crack initiation) at the notch-tip. If the material does exhibit stable crack growth, then such design approach may be over conservative, since safety factors are also employed. The second perspective is that a real crack, in a ductile material, is in actuality a (very) sharp notch. Despite the fact that most theoretical postulations presume a sharp crack in a continuum, most of FE schemes in fact employ a finite but sharp semi-circular

notch rather than cracks. It may be fruitful, therefore to investigate stable crack growth behaviour emanating from notches.

2.6 CLOSURE

Various issues regarding stable crack growth have been presented. The source of such behaviour has been attributed to the competing mechanisms of yielding (crack-tip blunting) and crack growth. The variations of state of stress, whether through section of material, or during crack growth is the main source of complication. Predicting onset of crack growth during stable crack growth is therefore not straightforward. Numerous attempts at characterising stable crack growth have been presented. Most of these attempts either suffer some form of geometry dependence or require extensive FE effort. Mode-mixity adds complication when shear and tensile failure modes compete.

Work on stable crack growth emanating from notches is lacking. An understanding of stable crack growth emanating from sharp notches may contribute to a better understanding of stable crack growth.

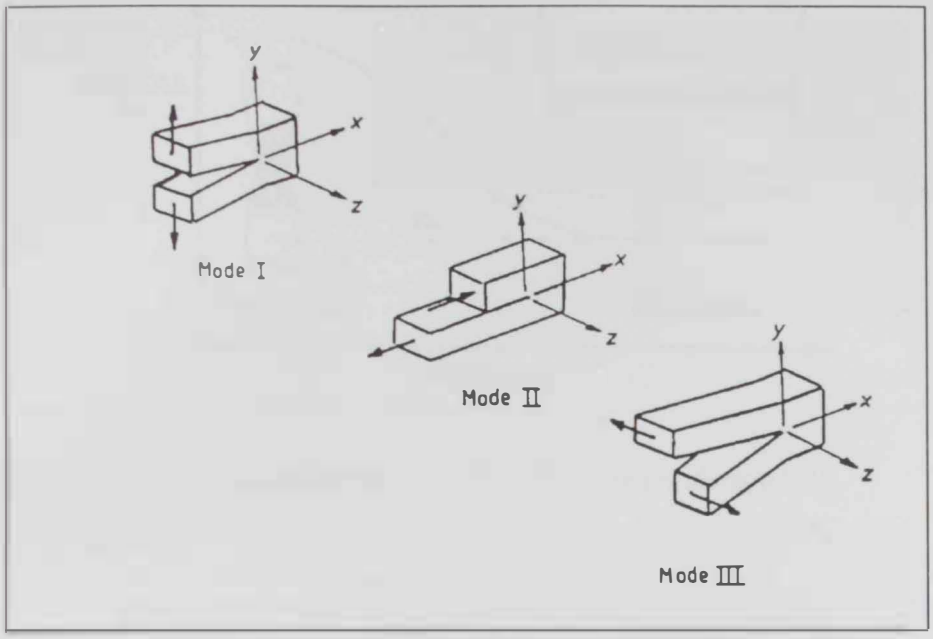

Fig. 2.1: Modes of crack loading (Parker [4]).

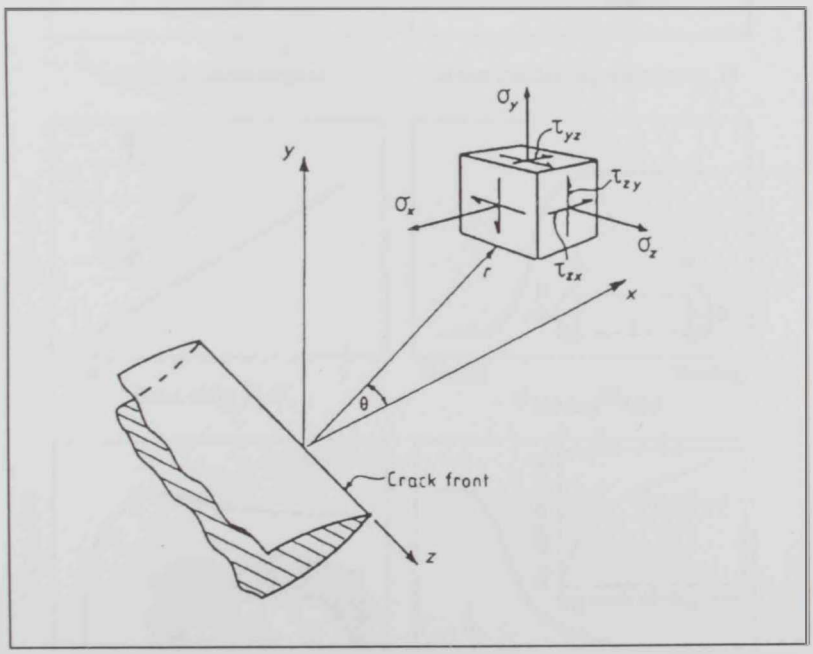

Fig. 2.2: Definition for coordinates system for crack-tip 3D stress element variables (Parker [4]).

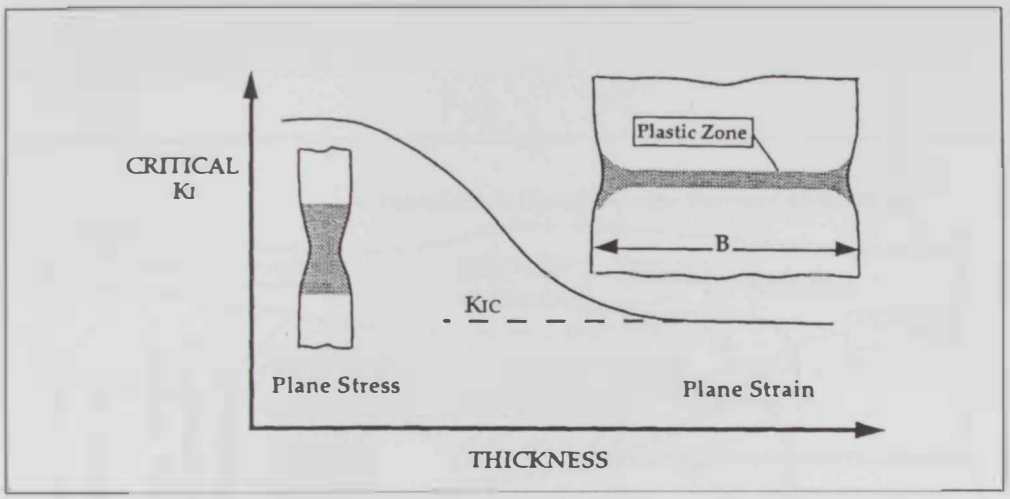

Fig. 2.3: Effect of specimen thickness on mode-I fracture (Anderson [1]).

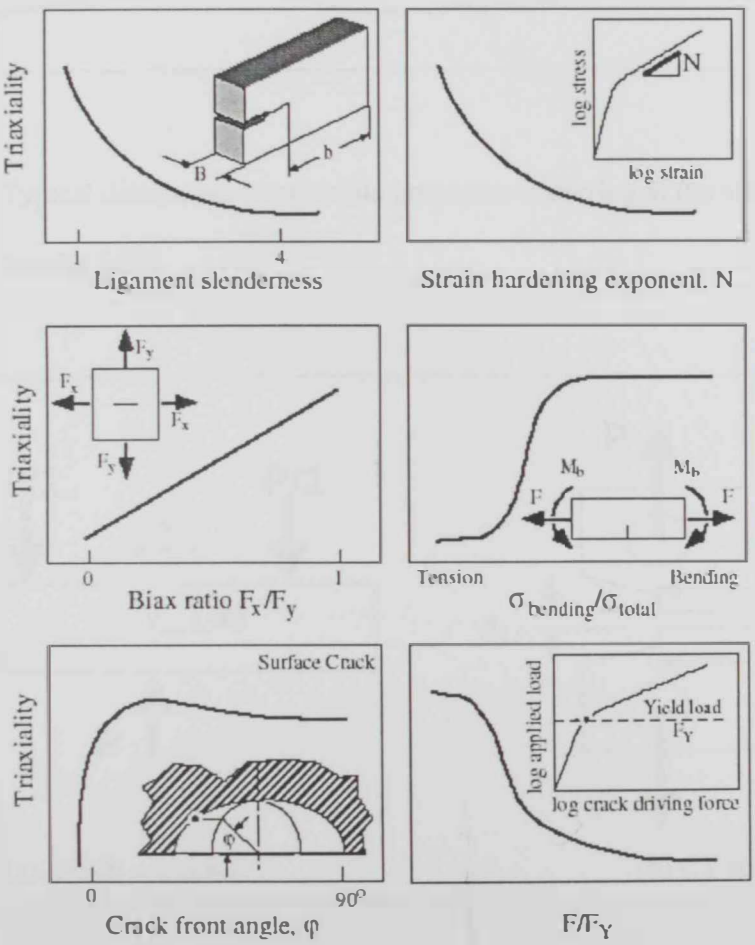

Fig. 2.4: Effect of various parameters on near-crack-tip triaxiality (Schwalbe et al. [11]).

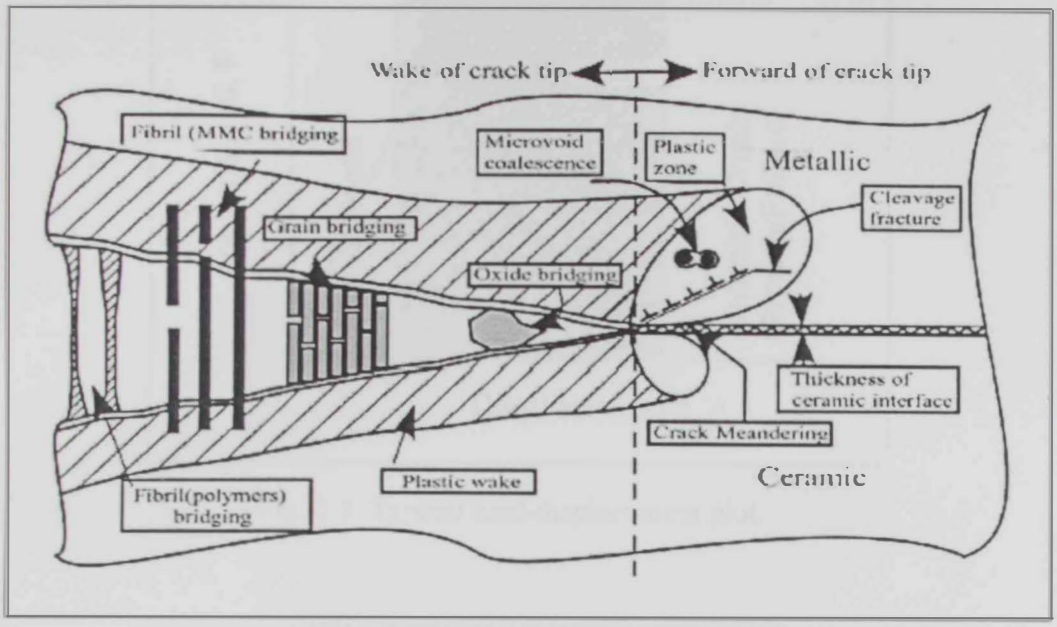

Fig. 2.5: Typical dissipative irreversible processes occurring at the vicinity of a crack tip (Li and Chandra [45]).

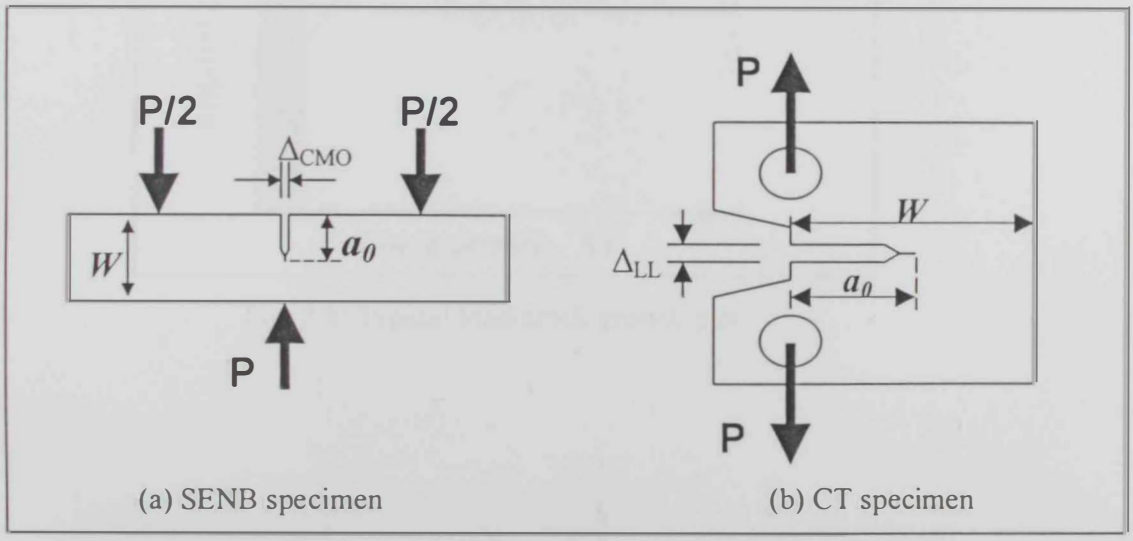

Fig. 2.6: Typical fracture specimens (a) Single Edge Notched Bending (SENB); (b) Compact-Tension (CT) Specimens.

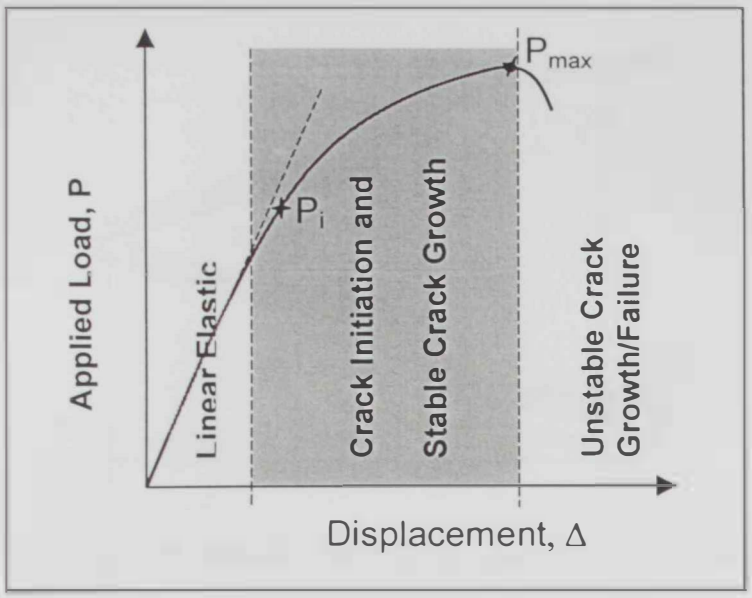

Fig. 2.7: Typical load-displacement plot.

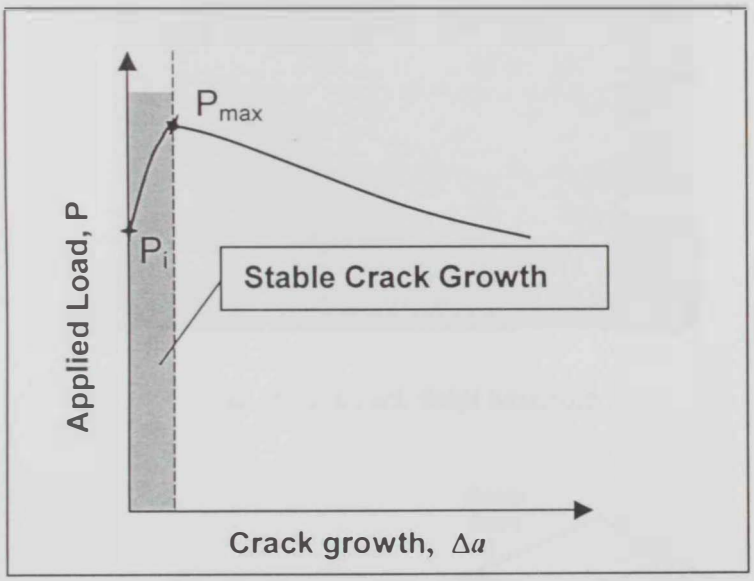

Fig. 2.8: Typical load-crack growth plot.

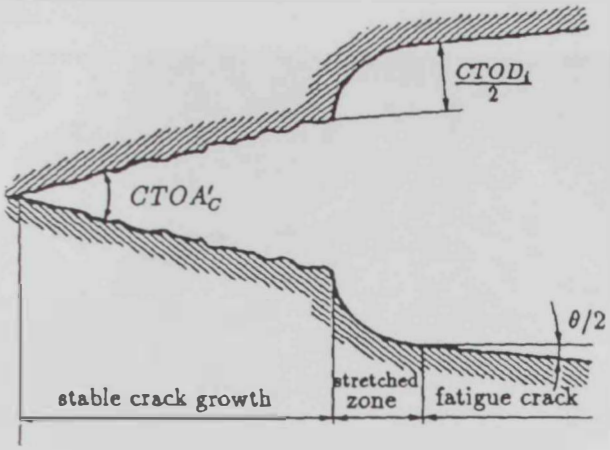

Fig. 2. 9: Stretch zone width (adapted from Shan et. al [30]).

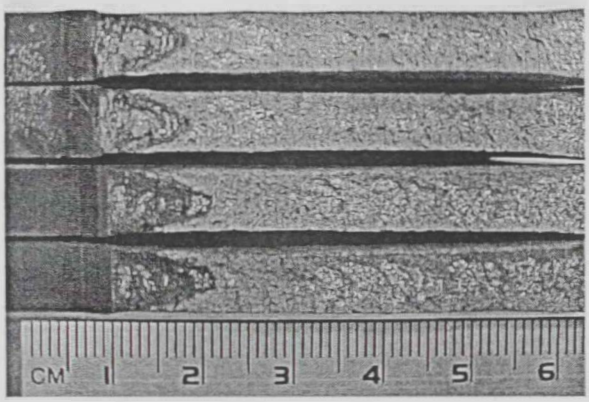

Fig. 2.10: Crack front tunelling.

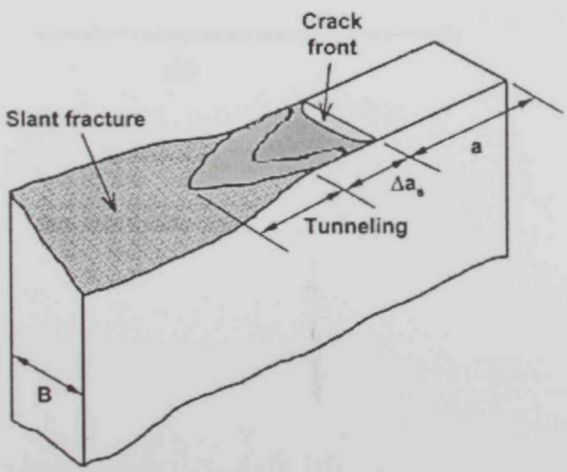

Fig. 2.11: Slant fracture surface (adapted from James and Newman [27]).

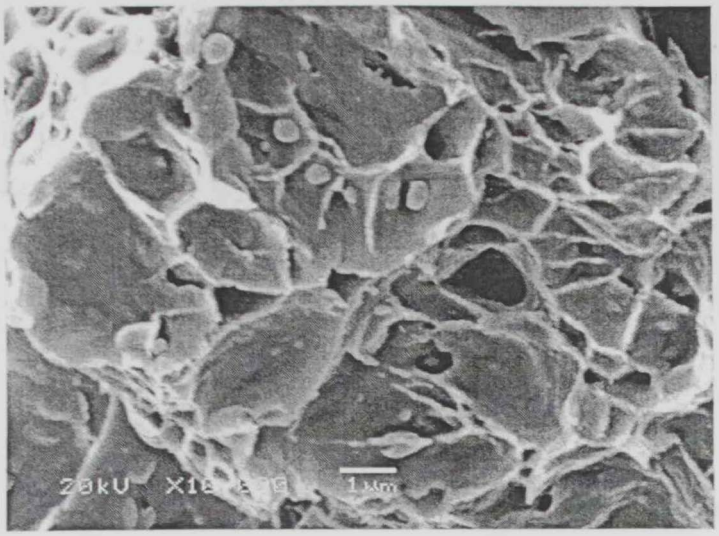

Fig. 2.12: Microvoid coalescence.

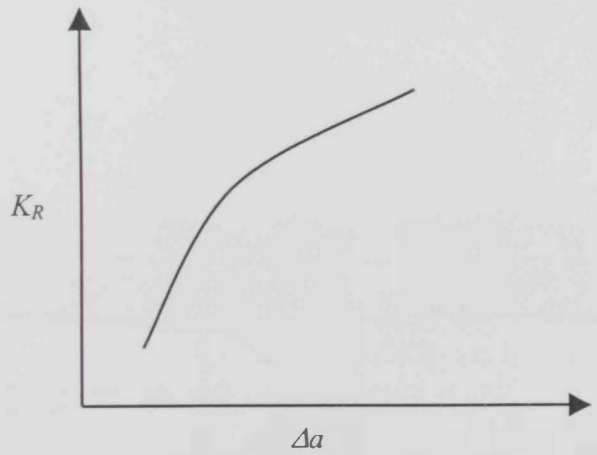

Fig. 2.13: Typical K_R curve.

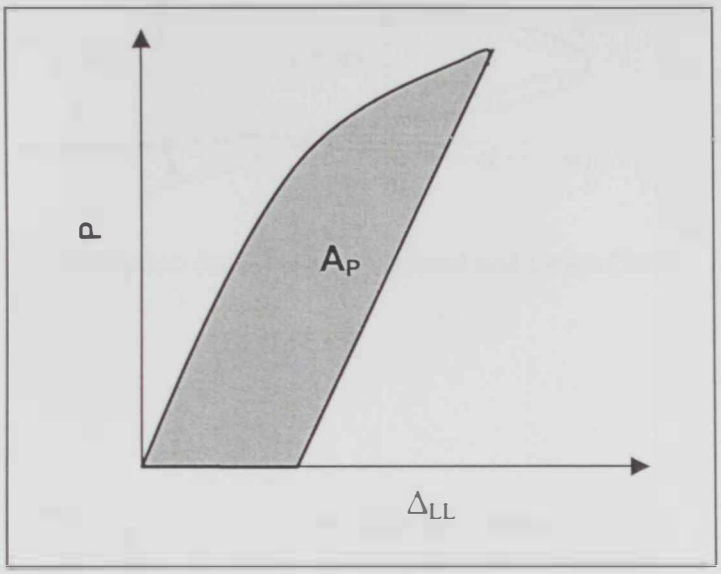

Fig. 2.14: A_{PL} for J calculation.

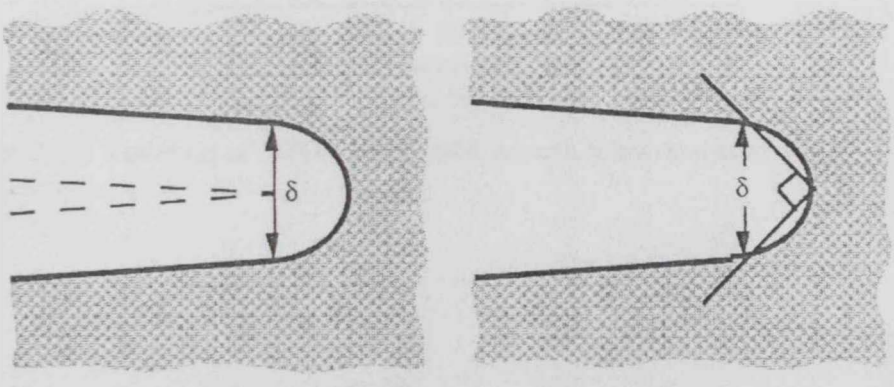

Fig. 2.15: Various definitions for CTOD (Anderson [1]).

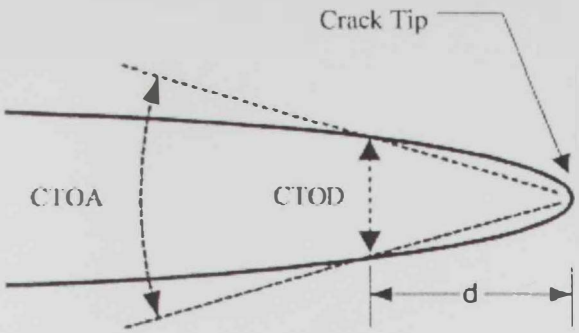

Fig. 2.16: Definition for CTOA (Mahmoud and Lease [26]).

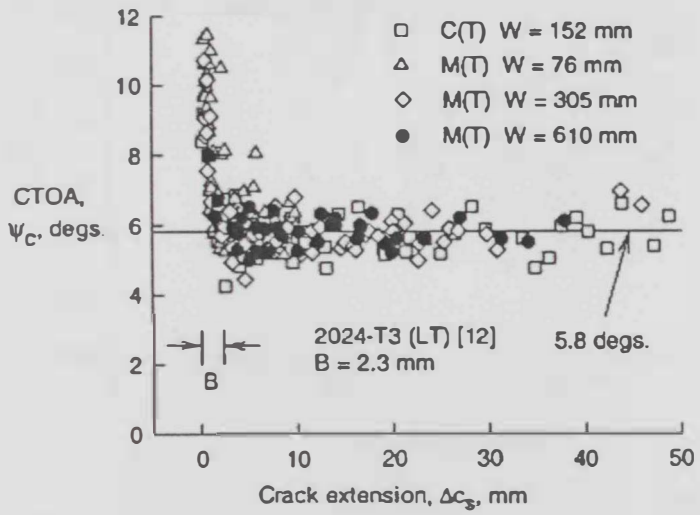

Fig. 2.17: Variation of CTOA with crack growth (Newman et al. [25]).

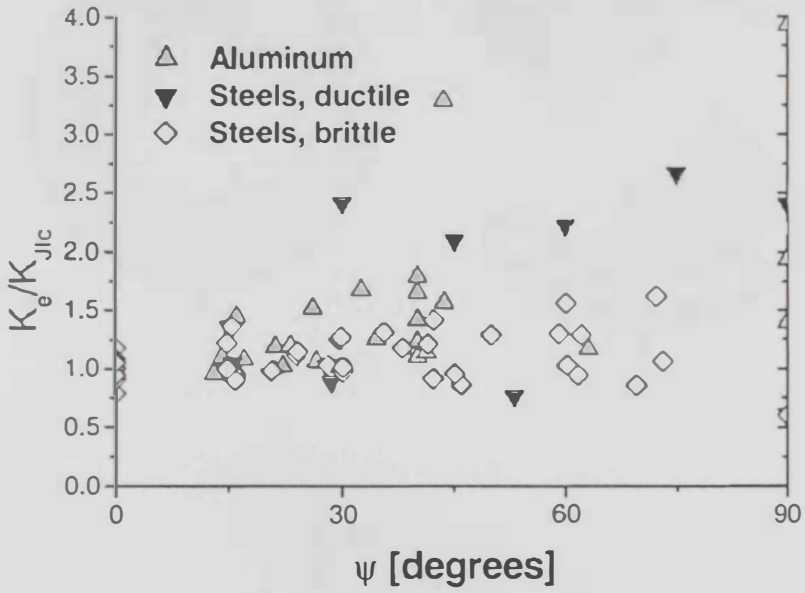

Fig. 2.18: Scatter regarding the effect of mode mixity (Laukkanen [50]).

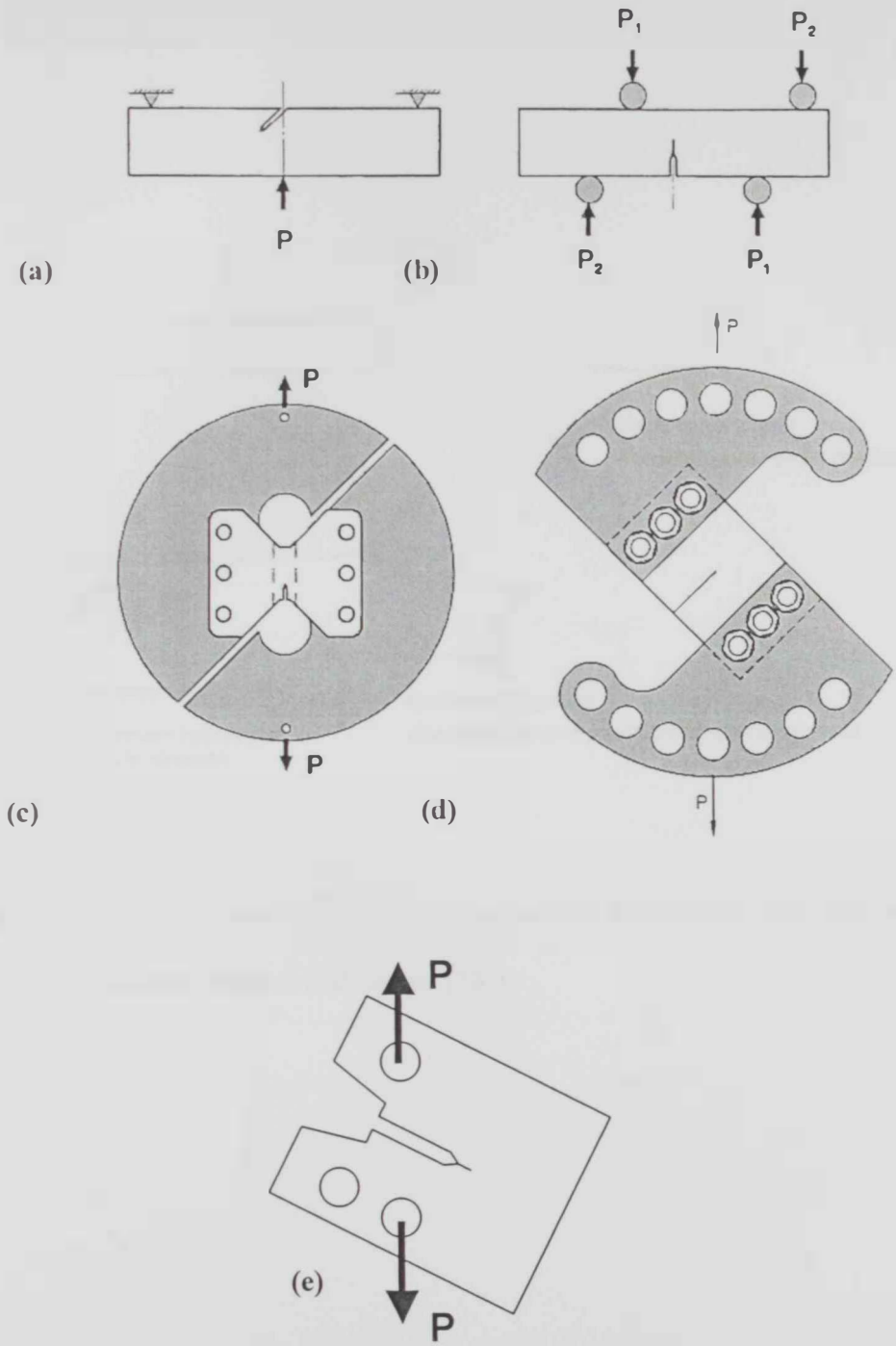

Fig. 2.19: Various specimen configurations for mixed-mode testing; (a) 3PB with inclined notch; (b) 4PB with offset loading; (c) Arcan configuration; (d) CTS configuration; (e) modified CT specimen.

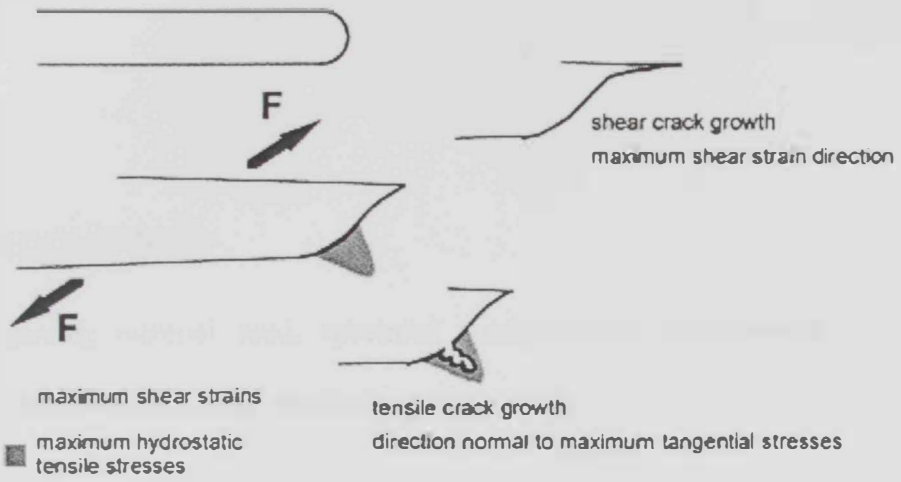

Fig. 2.20: Effect of mixed-mode loading on crack-tip deformation and crack propagation in ductile materials (Pirondi and Donne [58]).

CHAPTER 3

EXPERIMENTATION

3.1 INTRODUCTION

Details regarding material used, specimen configurations, experimental set-up and procedures are described in this chapter.

3.2 MATERIAL

Material chosen for current investigation is EN 34NiCrMo6 low alloy steel, which is equivalent to AISI 4330/4340 alloy class. The steel was supplied in rod form, 180 mm diameter x 2.8 m length. Composition for the alloy is given in **Table 3.1**.

3.3 TENSILE TEST

A section of the rod, approx. 200 mm was sawed and round surfaces flattened using a shaper machine into 120 mm x 120 mm square sections and then sawed to approx. 15 mm thick plates. One of the plates was used to manufacture tensile test specimens, in the R-C / C-R orientation (**Fig. 3.1**), similar to orientations of the modified CT specimens.

Geometry of the tensile test specimen is shown in **Fig. 3.2**. The tensile test specimen is of pin-holed type. The dimensions used for tensile specimen are non-standard. Dimensions for standard pin-holed specimens could not be machined with current plate dimensions - for the orientation of interest. Gripped-type specimens were discarded. This is due to in-house problems experienced in the gripping system when testing such specimens. Specimen thickness was slightly reduced at the centre by grinding – this was employed to enforce deformation and necking at the centre of the specimen.

Initial tests were conducted to measure Modulus of Elasticity, E and two more tests were conducted to obtain tensile and ultimate strengths, σ_Y and σ_{UTS}, and to obtain strain hardening constants α, and n. All tensile tests were conducted on an MTS universal testing machine with 100 kN rated load-cell. The strain was measured using an extensometer connected to an external strain-meter. This was so as technical problems were experienced regarding connection of extensometer to computerised data acquisition (DAQ) system of MTS machine. The strain measurements were manually logged during the test.

Tests were conducted under displacement control, at a cross-head displacement rate of 0.1 mm/min., which is equivalent to a strain-rate of approx. 2×10^{-3} /min. The stress-strain curve is shown in **Fig. 3.3**. The measured values are shown in **Table 3.2**. Average values for σ_{YS} and σ_{UTS} where 551 MPa and 779 MPa respectively.

According to Ramberg-Osgood Relationship:

$$\frac{\varepsilon}{\varepsilon_0} = \frac{\sigma}{\sigma_0} + \alpha\left(\frac{\sigma}{\sigma_0}\right)^n$$

Logarithmic plot of $\left(\frac{\varepsilon}{\varepsilon_0}-\frac{\sigma}{\sigma_0}\right)$ vs. $\left(\frac{\sigma}{\sigma_0}\right)$ beyond yield limit was plotted (stress range 600-750 MPa). The plot is shown in **Fig. 3.4**. A linear fit was obtained and the plastic constants were determined and shown in **Table 3.2**.

3.4 STABLE CRACK GROWTH TESTS

3.4.1 Specimen Preparation

Modified CT specimen configuration, as used by Mahanty and Maiti [59], Maiti and Mourad [60] and Mourad et al [61], was chosen for this investigation. The CT specimens were made from 120 mm x 120 mm plates of approx. 15 mm thick. These plates were obtained by flattening the round rod into 120 mm x 120 mm square section by milling the rounded edges. The section was sawed to approx. 15 mm – 20 mm sections using electrical-powered saw. These plates were then reduced to the required thickness (8 mm), and holes, knife-edges and pre-notches were machined. Some issues have arisen regarding effect of machining process on fracture behaviour, and this would be discussed in Chapter 5.

Various CT configurations were machined. Initially, two configurations; A1 and B1 were machined to produce a range of loading angle, ϕ, values. Note that loading angle, ϕ, would be defined as the angle between crack-plane and the load-line plane, as shown in schematic (**Fig. 3.5**). Configuration A1 is shown in **Fig. 3.6** and allows for loading angles

(ϕ) of 90° (hole #1), 65° (hole #2) and 50°(hole #3). Configuration B1 is shown in **Fig. 3.7** and allows for ϕ of 90° (hole #1), 70° (hole #2) and 60° (hole #3). It was found, through initial testing runs, that load required for ϕ value of 50° is nearing testing frame limits of 100 kN. Therefore, a modified configuration was then used, and they were A2, B2, and C2. Configuration A2 is shown in fig **Fig. 3.8** and allows for ϕ of 90° (hole #1) and 70° (hole #2). Configuration B2 is shown in **Fig. 3.9** and allows for ϕ of 80° (hole #1) and 65° (hole #2). Configuration C2 is shown in **Fig. 3.10** and allows for ϕ of 75° (hole #1) and 60° (hole #2).

3.4.2 EDM Pre-notch

A notch was machined into the specimens using Electron Discharge Machining (EDM) wire-cutting technique. Notch depths were 5mm, 10mm and 15mm to give a_0/W values of 0.45, 0.50 and 0.55 respectively. Two different wire diameters were used, 0.1 mm and 0.25 mm. These sizes gave notches of radii 0.08 mm (approx.) and 0.16 mm (approx.) respectively. Other notch sizes of radii 0.25 mm, 0.50 mm and 1.00 mm were also machined into some CT specimens.

3.4.3 Testing Procedures

CT specimens were loaded on the 100 kN MTS universal testing machine, with load cell rated at 100 kN. Load-line displacement, Δ_{LL}, was measured using a clip-gauge connected to an external strain-meter, which was previously calibrated. Readings were manually recorded during the test. All tests were conducted under displacement control.

Initial crosshead speed during testing was 0.1 mm/min. However, this was found to give undesirable long test durations (approx. +40 mins. per test). A pilot test, with crosshead speed of 0.25 mm/min, was conducted and results were compared with that conducted at 0.1 mm/min cross-head speed. Results, shown in **Fig. 3.11** were found to give comparable results within 5% difference. Later tests were conducted at the larger loading rate of 0.25 mm/min.

The specimens were loaded up to maximum load value, $P_{max,}$ and beyond. Test was then stopped for most specimens when load decreased by not more than 3 kN. Some tests were extended for longer periods for more load decrease. Dye penetrant was then applied and excess fluid soaked. Most specimens were unloaded slightly, by about 10 kN and reloaded until the specimen was broken into two halves. Fracture surfaces were then photographed and visually inspected.

Table 3.1: Composition of alloying elements (wt %) for EN 34NiCrMo6 Low Alloy Steel (Equivalent to AISI 4330/4340).

C	Si	Mn	P	S	Cr	Ni	Mo	Al	Cu
0.332	0.211	0.650	0.021	0.033	1.380	1.450	0.209	0.034	0.050

Table 3.2: Measured mechanical properties.

E (GPa)	σ_{YS} (MPa)	σ_{UTS} (MPa)	ε_{YS}	% *elongation*	α	n
217	551	779	4.295×10^{-3}	7.735	0.473	8.114

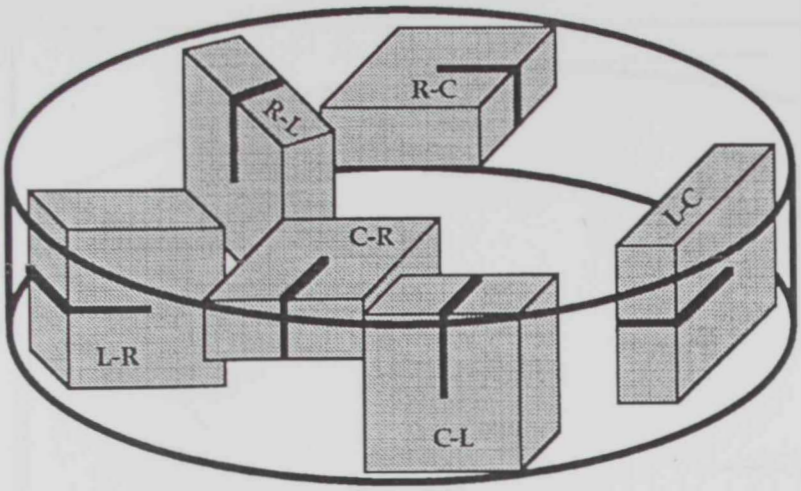

Fig. 3.1: ASTM notation for specimens extracted from disks [1].

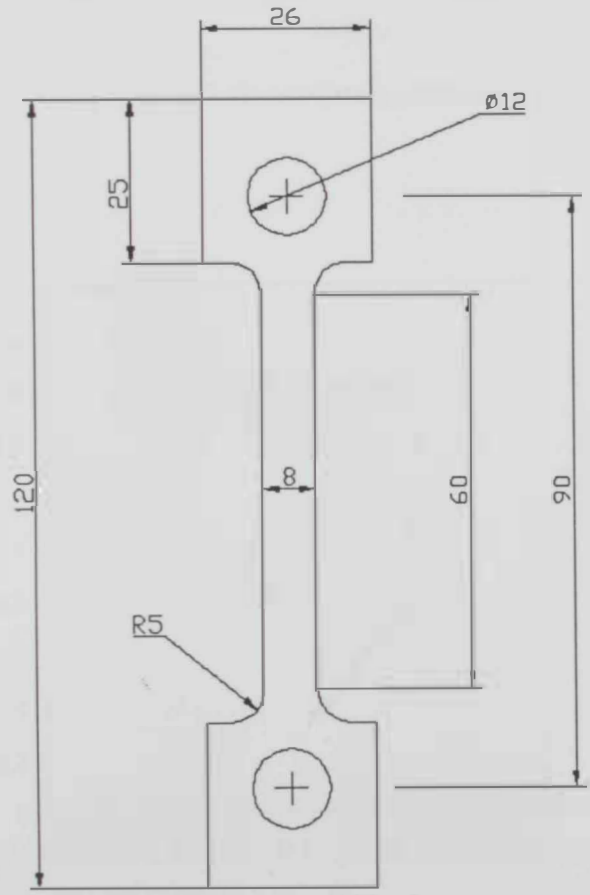

Fig. 3.2: Tensile specimen dimension (in mm).

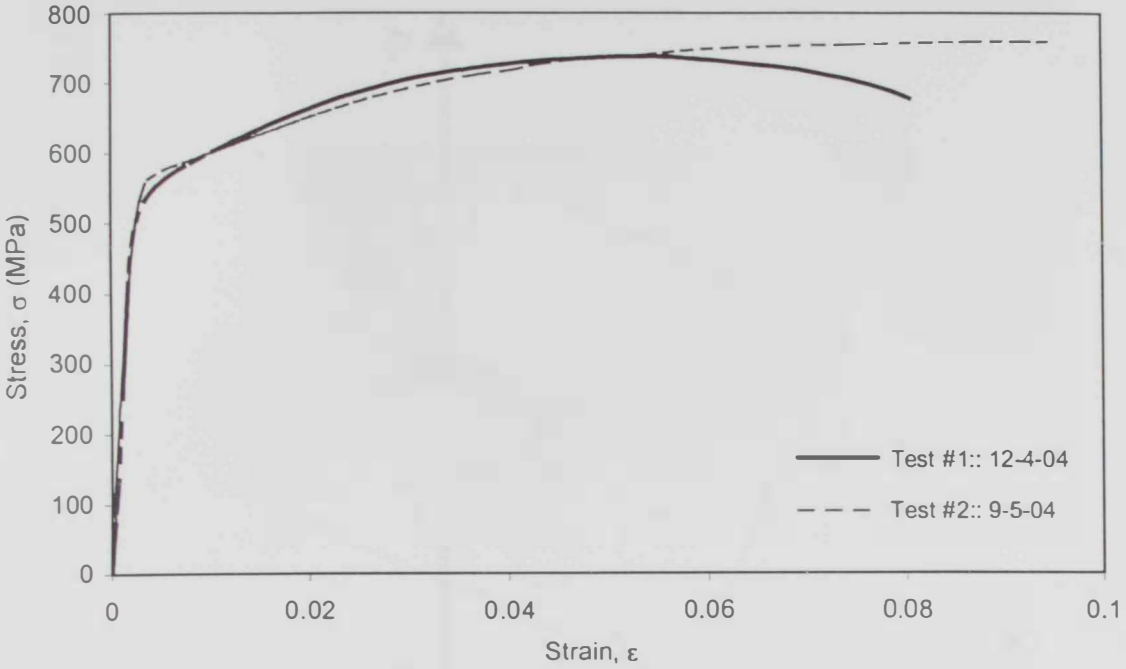

Fig. 3.3: Stress-Strain Curve.

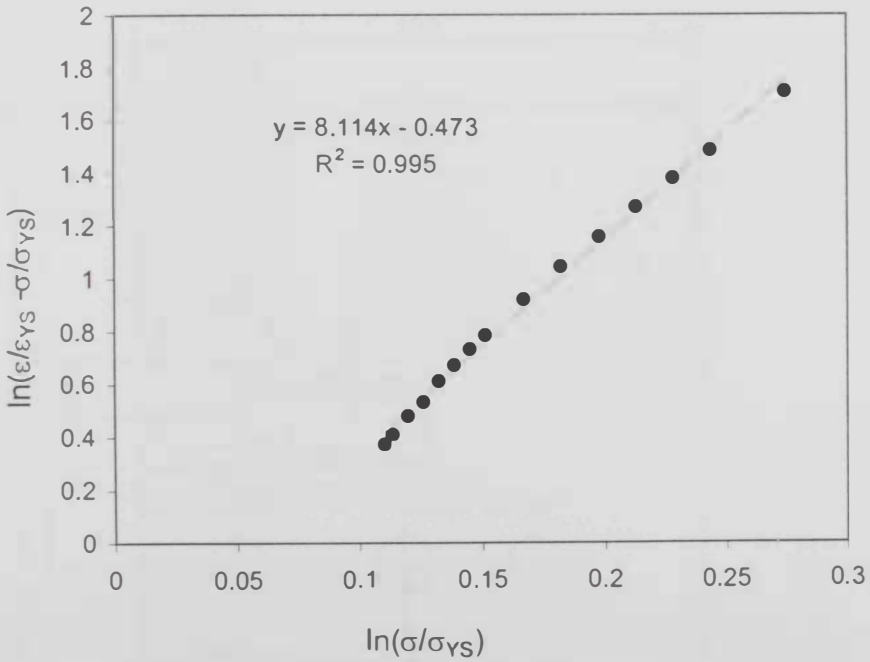

Fig. 3.4: Plot to obtain plastic Ramberg-Osgood Constants n and α.

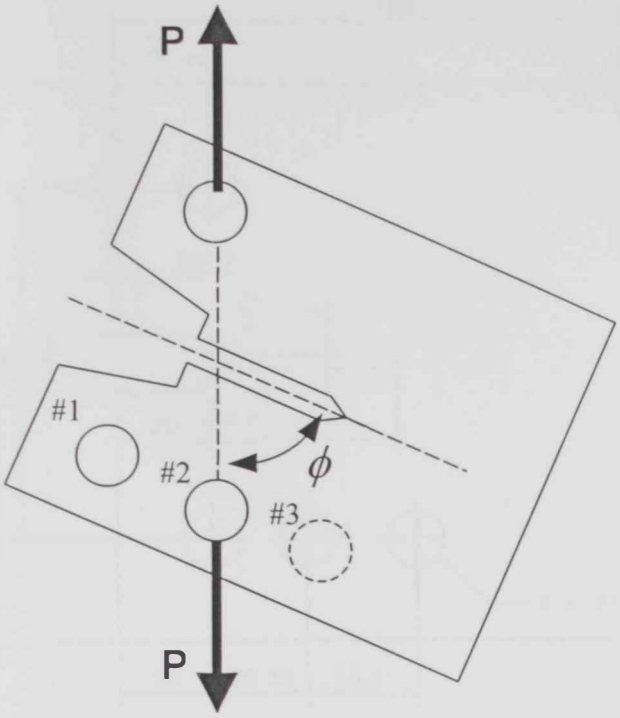

Fig. 3.5: Schematic for modified CT specimen configuration used.

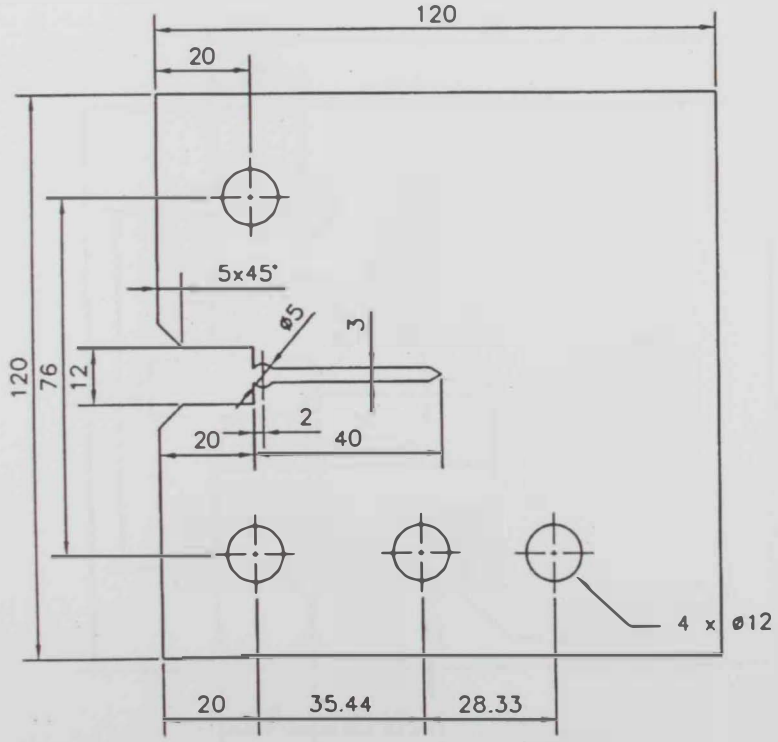

Fig. 3.6: Modified CT Specimen: Type A1.

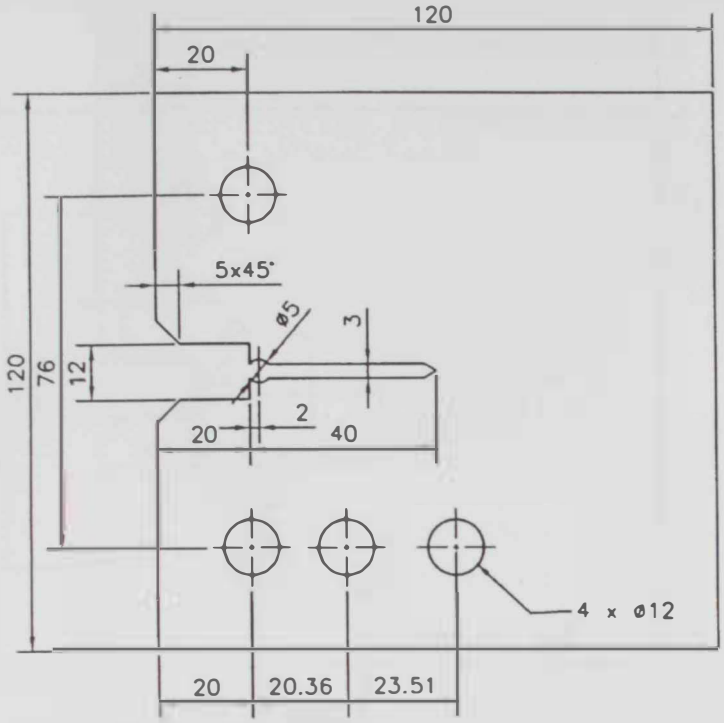

Fig. 3.7: Modified CT Specimen: Type B1.

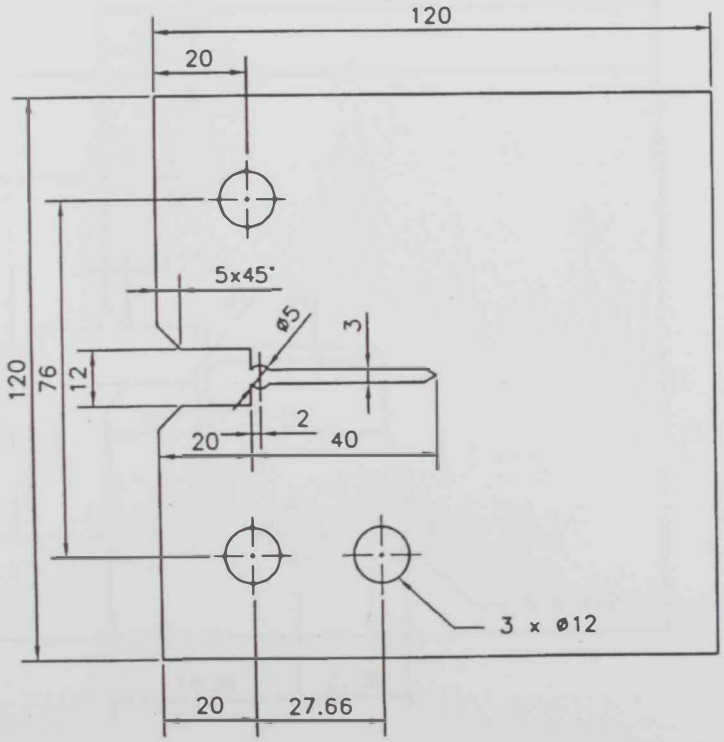

Fig. 3.8: Modified CT Specimen: Type A2.

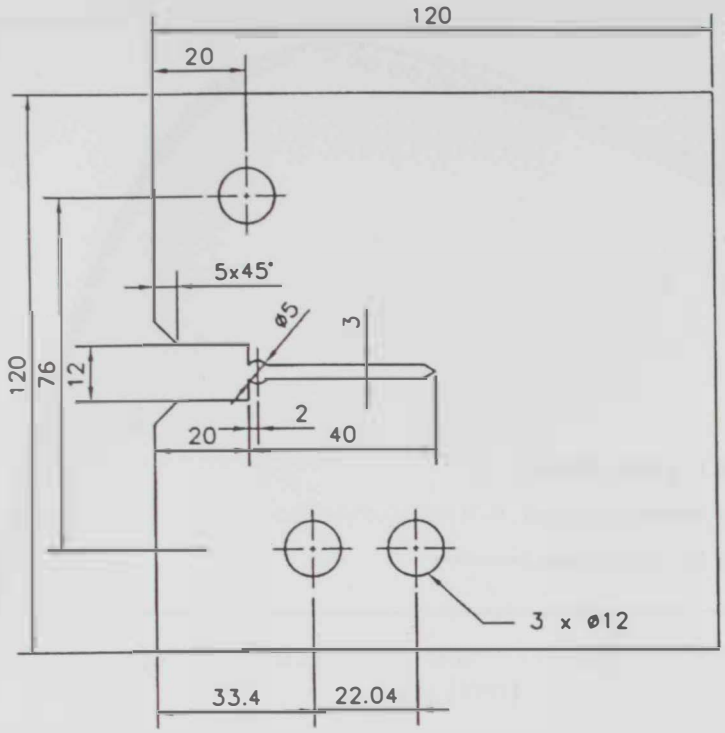

Fig. 3.9: Modified CT Specimen: Type B2.

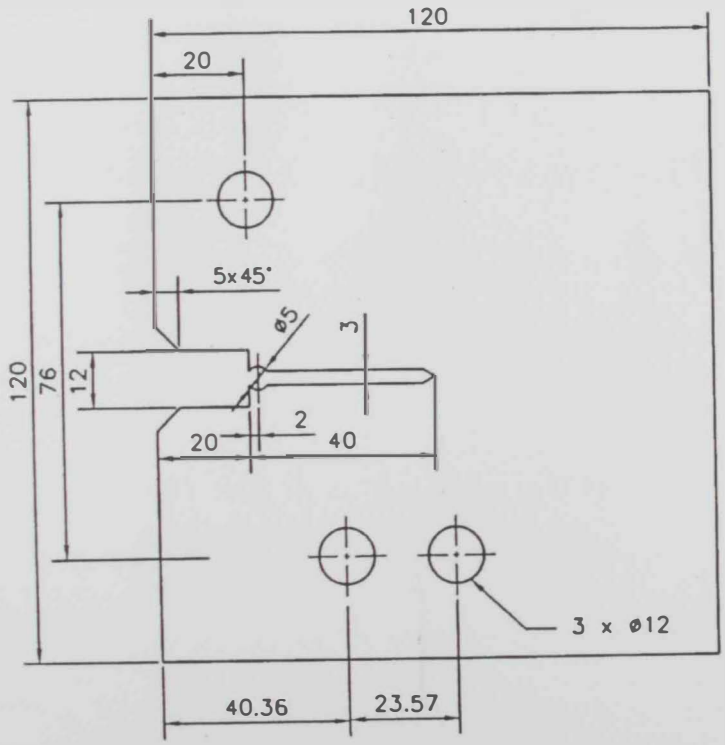

Fig. 3.10: Modified CT Specimen: Type C2.

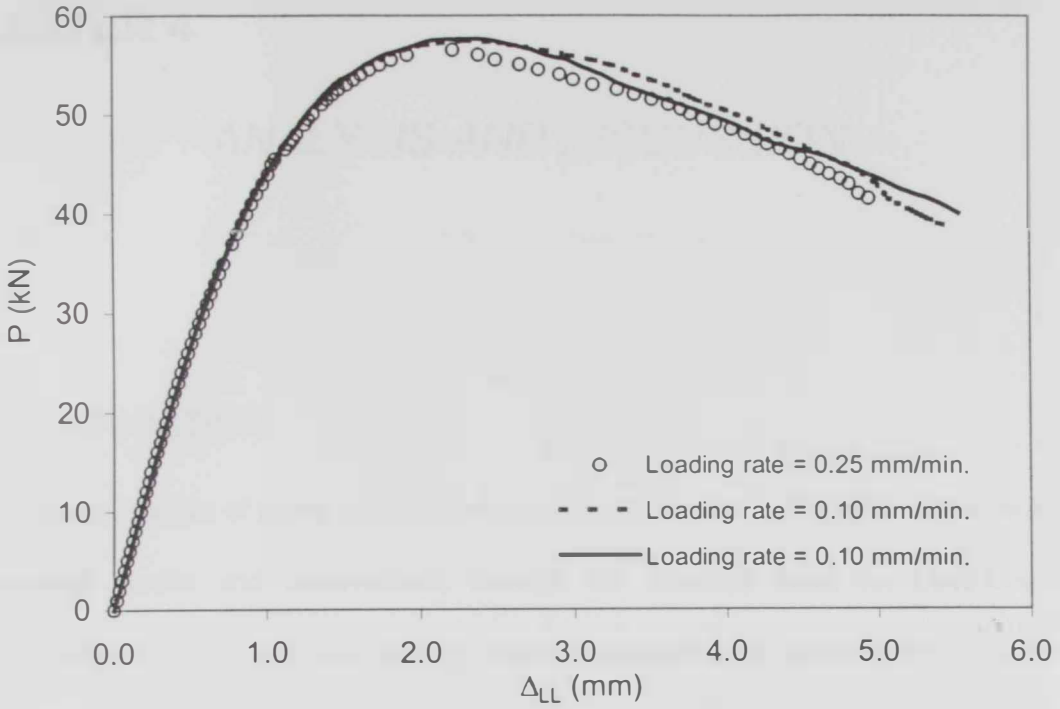

Fig. 3.11: Comparison between P-Δ_{LL} curves of two different loading rates.

CHAPTER 4

ANALYSIS AND DISCUSSION

4.1 INTRODUCTION

In this chapter, pattern of stable crack growth behaviour is examined in light of obtained experimental results and observations; through the obtained Load vs. Load-Line Displacement (P-Δ_{LL}) curves, and through visual examination of fracture surfaces and crack-front tunneling. Analysis is carried out and compared with experimental findings of other investigations. This is done to determine if there exists any consistent pattern of behaviour that can contribute towards a better understanding of stable crack growth.

4.2 LOAD LOAD-LINE DISPLACEMENT (P-Δ_{LL}) PLOTS

The P-Δ_{LL} plots are presented in **Figs 4.1-4.7**. Such plots are useful to obtain data pertaining to damage (crack) initation loads, P_i and P_Q, maximum loads, P_{max}, and load-line displacements at maximum load, Δ_{Pmax}. More detailed analysis on such data would be presented later. **Figs. 4.1-4.3** show P-Δ_{LL} plots in terms of the various loading modes for each a_0/W value. Plots show consistently a general trend of increasing maximum load, P_{max}, with loading angle, ϕ,. They also show an apparent increase in elastic stiffness of the specimens with ϕ. **Figs 4.4-4.7** show P-Δ_{LL} plots in terms of the a_0/W size for each loading angle, ϕ. They also show that with increasing a_0/W, stiffness and P_{max} diminishes.

4.2.1 Effect of Loading Angle, ϕ, on P_{max}:

Summary of various loads for notch radius of 0.08 mm is provided in Table 4.1. To investigate the effect of loading angle, ϕ, on P_{max}, the loads obtained have been normalised with P_{max} at $\phi = 90^{o}$, $P_{1\text{-}max}$. Plots were then obtained for $\frac{P_{max}}{P_{1-max}}$ vs. ϕ and are shown in Fig. 4.8. It has been found that there is a strong inverse-linear dependence of $\frac{P_{max}}{P_{1-max}}$ with ϕ. Plots were then reconstructed for $\left(\frac{P_{max}}{P_{1-max}}\right)^{-1}$ vs. ϕ, and are shown in Fig. 4.9. Moreover, such findings have been compared with experimental data from a recent study of a similar steel alloy (AISI 4340) by Mourad et al. [61]. Data from earlier experiments by Mahanty and Maiti [59] on D16AT aluminium alloy (equivalent to 2024-T3) are also included. All data are of experiments involving similar modified CT specimen configuration. Such comparisons have shown very similar relationships confirming the linear dependence of λ_{max}^{-1} on ϕ. Results are also shown in Fig. 4.9 for the various crack-sizes.

Although individual slopes, in Fig. 4.9, indicate a weak dependence on a_0/W, where the slope becomes slightly steeper with increasing a_0/W, one however can assume that an average slope fits all the data and therefore is reflective of the mechanical behaviour for the range $0.45 \leq a_0/W \leq 0.55$. The slope was found to be equal to 0.012 per deg.

4.2.2 Initiation Loads, P_i And P_Q

Two parameters were considered to indicate initiation of crack growth, P_i and P_Q. P_i was taken as the linear limit of the P-Δ_{LL} curve, where local damage is assumed to have started to take place, and hence the start of stable crack growth. In many cases, crack may

initiate at the core, with no indication of a presence of a crack at the surface. It is thus argued that any deviation from non-linearity is an indiaction of crack initation. There are two problems with such parameter; first, the exact position of the linear limit on P-Δ_{LL} curve is tentative and cannot be accurately and consistenly determined; second, blunting but not crack growth initiation may have taken place (and hence the term damage initiation is more accurate). On the other hand, P_Q is taken as the 95% secant slope to the linear portion of the P-Δ_{LL} curve. Even though no gaurantee that crack growth has initiated, it does prove a better estimate and consistent with definitions of initiation of unstable crack growth in plane-strain LEFM context.

P_i/P_{max} and P_Q/P_{max} ratios were plotted against loading angle, ϕ, as shown in **Figs. 4.10 and 4.11**. Plots show interesting results. P_i/P_{max} and P_Q/P_{max} ratios for a_0/W of 0.50 and 0.55 seem to be very consistent, the more so with P_Q. They do indicate a weak linear dependence of both P_i/P_{max} and P_Q/P_{max} ratios on a_0/W, but there is no clear pattern for the depencence of P_i/P_{max} and P_Q/P_{max} ratios on ϕ. P_i/P_{max} and P_Q/P_{max} ratios for a_0/W of 0.45, on the other hand, do not show any trend and most likely indicates a constant value. This suggests that P_i/P_{max} and P_Q/P_{max} ratios may not depend on loading angle after all, although more investigation on this issue may be needed. If that be the case, then one can determine an average ratio for all tests. Average P_i/P_{max} was found to be 0.430 (+/- 12% average deviation), while average P_Q/P_{max} was found to be 0.546 (+/-6% average deviation).

A recent study by Mourad et al. **[61]** showed that P_{max}/P_i remains fairly constant. This could not be confirmed due to scatter in current results, even though data from Mourad et al **[61]** were for an even narrower range of a_0/W, where $0.42 < a_0/W < 0.45$. The notion

of a constant P_i / P_{max} or P_Q / P_{max} ratios would not be refuted and indeed would be consolidated later, when normalisations of P-Δ_{LL} are presented.

4.2.3 Load-Line Displacement At P_{max} ($\Delta_{P\text{-}max}$)

$\Delta_{P\text{-}max}$ values were plotted against ϕ for the various a_0/W ratios to investigate if there was any parameter dependence. Graph plot, as shown in **Fig. 4.12**, shows scatter of data about an avergae value of 2.31 mm (+/-5.5% average deviation). This inidcates a constant Δ_{Pmax} too, which will prove to be interesting, especially when noted with P-Δ_{LL} normalisation, which is presented later.

4.2.4 Normalised P-Δ_{LL} Curves

The various P-Δ_{LL} curves are useful to understand the general stable crack growth behaviour for the various a_0/W ratios and loading angles tested. However, one needs to evaluate the intrinsic stable crack growth behaviour of the material. This is only possible if some form of normalisation is presented, where all the curves are normalised into a single material characteristic curve. This not only helps to characterise the intrinsic stable crack growth behaviour but also addresses transferability issue, where researchers have not yet found a straightforward method to related mechanical behaviour of specimens in experimentation to that of real-life structures and components. This is what was attempted, and results are presented.

4.2.5 Ananlysis for Mode–I Maximum Load, $P_{I\text{-}max}$ vs. Limit Load, P_L

Works by Giovanola et al. [67] and, Krompholz and Kalkhof [68] on blunt notches have presented normalised P-Δ_{LL} curves, where load, P, is normalised in terms of limit load, P_L, and load-line displacement, Δ_{LL}, in terms of specimen width, W. Solutions are provided in Anderson [1] for reference (notional) limit load, P_L , which corresponds to the load at which the net section, for geometry of interest, yields. P_L is obtained from [1]:

$$P_L = 1.072\,\eta\, B\, b\, \sigma_Y \tag{4.1}$$

where η, is a geomtery factor and is dependent on a_0/W:

$$\eta = \left\{ \left(\frac{2a}{b} \right)^2 + 4\frac{a}{b} + 2 \right\}^{\frac{1}{2}} - \left(\frac{2a}{b} + 1 \right) \tag{4.2}$$

where B is specimen thickness, a is crack length, b is ligamnet length ($=W$-a), and σ_Y, is termed flow stress and is defined as average of ultimate and yield strengths:

$$\sigma_Y = \frac{\sigma_{UTS} + \sigma_{YS}}{2} \tag{4.3}$$

The solution presented is for a plane-stress condition.

Calculated values for P_L are shown in **Table 4.2** and are compared with experimental results for $P_{I\text{-}max}$. Results obtained for $P_{I\text{-}max}$ are consistent with P_L to within 5% .

This was not expected, since this could indicate that plastic yielding crierion may be valid for estimating fracture limit loads, for sharply notched structures despite stable crack growth behaviour. In order to confirm or refute such indication, a series of comparisons with of other experimental data were made. Results, for P_L-P_{max} values, of recent investigation on sharply notched CT specimens by Mourad et al. [61] are listed in **Table**

4.3. Results show an average difference of 25% of P_L. It does seem that difference is dependant on a_0/W. Other comparisons were also made with results of tests conducted on pre-cracked CT specimens by Mahmoud and Lease [26] and, Mahanty and Maiti [59], listed in **Table 4.4**. Results show a much larger difference of more than 45% of P_L, and also show dependence on a_0/W. Reslts of Mahanty and Savant [51] on 3PB tests are also listed.

Therefore, one cannot say that P_L does direclty predict P_{max} for sharply notched specimens, but some form of empirical relationship may be possible. However, for purpose of normalisation, an alternative parameter was sought.

4.2.6 Normalisation with P_{max}

If all specimens share the same criterion that governs stable crack growth, then an obvious and straightforward normalisation parameter is P_{max}. If all curves where "forced" to coincide at the same maximum, one can then evaluate any difference in characteristic behaviour for a material. P-Δ_{LL} curves in **Figs. 4.1–4.3**, showing various loading angles for a single a_0/W ratio, were normalised and presented as **Figs. 4.13–4.15**. The normalised curves do coincide, although one can see that higher loading angles in a_0/W = 0.45 and 0.50 seem rather shifted, but only minutely. P-Δ_{LL} curves in **Figs. 4.4-4.7**, showing various a_0/W for each loading angle, where also normalised and presented as **Figs. 4.16-4.19**. They all also conincide, apart from minor discrepencies that can be seen for $\phi = 65^\circ$ **(Fig. 4.19)**, where a_0/W values seem minutely shifted. All the normalised curves where then assembled in one single chart and presented in **Fig. 4.20**. The plot exhibits a single trend, and indeed it does suggest that all P-Δ_{LL} curves can be represented as a single characteristic curve. Hence, validity of normalisation parameter, P_{max}.

4.2.7 Comparisons with a Similar Material

To confirm that such normalisation is valid, more fittings are needed. Experimental results from Mourad et al. [61] where therefore normalised and presented in **Fig. 4.21**. Indeed once can see that all the results obtained can be presented as a single charactaristic curve.

4.2.8 Comparison of Different Configurations

It would be interesting to see if such normalisation approach does work for specimens of different configurations (and constraints) and specifically with fatigue precracks. Experimental inverigation on stable crack growth on D16AT (akin to 2024-T3) aluminium alloy was carried out using CT specimens by Mahanty and Maiti [59] and using 3PB by Maiti and Mourad [52]. Earlier Experiments have also been conducted by Dawicke et al. [28] using CT and MT specimens on 2024-T3 Aluminium Alloy. Comparison between mechanical properties of both materials are shown in **Table 4.5**. Experimental data were normalised and are presented in **Fig. 4.22**. It may worth to mention that all load-line displacements were normalised, with specimen width, W, except for MT specimens, where it was found that $W/2$ gave the required normalisation. As can bee seen from **Fig. 4.22**, all of the normalised P-Δ_{LL} curves show a general trend, which can be interpretd as a single characteristic curve. It may worth mentioning that the curves obtained by Mahanty and Maiti [59] and Maiti and Mourad [52] are more consitent with each other than with that of Dawicke et al. [28] –although the overall general trend is very similar, indiating a common stable crack growth behaviour. This distinction between them can be explained in terms of various sources of discrepencies; mainly that materials are similar but not identical; and that errors may have risen from digitisation of experimental data. One should also bear in mind the varied range of

constraints and loading angles, expressesd in terms of *b/B*, but, one can assert that indeed all curves share the same trend during stable crack growth. Also, normalised Δ_{Pmax} values are very similar. One should also note that after maximum loads, the curves no longer share a common trend, but this is not of interest in this investigation since after maximum load, crack growth is no longer stable.

4.2.9 Comparison for Different Thicknesses

Mahmoud and Lease [26] conducted an investigation on stable crack behaviour for an aluminium alloy (2024-T351) at four different thicknesses, B, of 2.3 mm, 6.35 mm, 12.7 mm and 25.4 mm thick. The various P-Δ_{LL} charts were normalised and are presented in **Fig. 4.23**. With the exception of curve of B = 25.4 mm, all other curves were very similar upto normalised maximum, where they depart. This confirms the applicability of normalisation of various thickness (2.3 mm $\leq B \leq$ 12.7 mm). The disparity of curve corresponding to thickest of specimens (B = 25.4 mm) can be attributed to either or both of the following causes.

First, the specimen was machined differently than other 3 specimens, since no thickness reduction was done. Investigation findings in this thesis, to be presented in chapter 5, indicate a significant machining effect on stable crack growth behaviour in alloy steel under investigation. The aluminium alloy used by Mahmoud and Lease [26] may have also been affected by machining, even though this would require further invertigation for confirmation.

Second, investigation of the fracture surface shows that the specimen did not develop a slant fracture, unlike the other three. Later numerical and FE analyses by Mahmoud and

Lease [29] indicated that the constraint, quantified in terms of plastic constraint factor (p.c.f) was different (higher) in the case of B = 25.4 mm. This therefore may suggest that the proposed normalisation scheme may only work for low constraint behaviour specimens – even though it was demonstrated in **Fig 4.22** that even proposed normalisation was valid for a range of b/B ratios and as low as 2.75. Also further investigation is need for this issue.

4.3 CRACK GROWTH AND TUNNELING ANALYSIS

Fracture specimens were inspected visually. All specimens showed tunneling growth and, and when broken, have shown slanted fracture surface.

4.3.1 $\Delta a_{P\text{-}max}$ Measurements

Crack front tunneling profiles have been obtained for some specimens (notch radius of 0.08 mm and 0.16 mm) using dye-pentrant technique. Electronic photographs have been taken for the profiles and are shown in **Figs. 4.24**. Only values at the mid-thickness were reported as there was minimal crack growth at the surface (range approximately 1-2 mm) and reasonable measurements were not possible (**Fig. 4.25**). Measurements of crack extensions at the mid-thickness (core) gave mean values of around 5.71 mm, 5.34 mm and 4.74 mm for a_0/W =0.45, a_0/W = 0.50 and a_0/W = 0.55 respectively (**Fig. 4.26**). However, the overall pattern is scattered. During testing, the loading drop beyond P_{max}, though limited, was varied. This may have contributed to the scatter. The average values suggest that for crack ratios tested, there is fairly a narrow range of stable crack extension values, regardless of loading angle; and this would be further supported when normalised

data for other experimental investigations, of fatigue precracked specimnes, are presented.

4.3.2 Normalised *P-Δa* Curves

P-Δa plots are also used to charecterise stable crack behaviour. If normalised P/P_{max} is indeed a valid characterising parameter for precracked specimens, then one should also obtain a similar characteristic curve, when normalising *P-Δa* curves, similar to the normalised P-Δ_{LL} plots. Amstutz et al. [54] and Sutton et al. [55] have conducted investigations on mixed-mode behaviour of 2024-T3 (aluminium alloy) using Arcan specimen configuration. The specimen size in [54] is different than in [55] (**Table 4.6**). Published *P-Δa* plots were digitised, normalised and presented in **Fig. 4.27-4.28**. The chart interstingly shows that indeed a general trend for all specimens, despite loading angle and differing sizes, prior and after maximum normalised load (**Fig. 4.29**). Note however, that data points near intiation were rather scattered. $\Delta a_{Pmax}/W$ values also lie within a narrow range. Normalisations of *P-Δa* from Mahmoud and Lease [26] were carried also out and do show similar observations and are presented in **Fig. 4.30**. Note that discrepancy that has been shown previously for B=25.4 mm (**Fig. 4.23**) is not prominent. If constraint has been the cause for the observed discrepancy, then **Fig 4.30** suggests that $\Delta a_{P\text{-}max}/W$ is relatively less sensitive to constraint.

4.4 EFFECT OF NOTCH RADIUS ON STABLE CRACK GROWTH

Initial tests with different notches have shown that there seems to be little difference in fracture behaviour, as shown in **Fig. 4.31** and **4.32**. This prompted investigation into larger notch radii. P-Δ_{LL} curves of specimens with varying notch radii are shown in **Fig.**

4.33. Results show that, despite of the notch radius increase of twelve folds, maximum load, P_{max}, only increased by about 13%. A plot of P_{max} vs. notch radii has been obtained and is shown in **Fig. 4.34**. The plot shows that there is a linear fit, but one should note that the slope is shallow. What is also noteworthy about **Fig 4.34** is that it is possible to extend the trend to zero intercept, i.e. case were radius is zero (sharp crack). This would predict P_{max} for a fatigue-precracked specimen, which would be approximately 37.0 kN, and this will be verified experimentally. One can deduce from the plot that difference of P_{max} between a sharp notch and a fatigue-precrack is expected to be minimal indeed.

P-Δ_{LL} normalisations have also been obtained and are shown in **Fig. 4.35**. Results show that, apart from the largest of tested radii (r = 1.00 mm), all curves do coincide, indicating similar stable crack growth behaviour.

Crack Growth measurements at the core have also been obtained through fracture surface examination and are listed in **Table 4.7**. A noteworthy observation is that for largest of radii (r = 1.00 mm) crack growth was observed to have grown, minutely and only at the core, as shown in **Fig 4.34.**

4.5 CONCLUSIONS

Experimental Investigation was conducetd to investigate stable crack growth behaviour from notches in 34CrNiMo6 alloy steel. Findings were as follows:

1- Maximum Mode-I load, $P_{I\text{-}max}$ could be predicted using empirical relationships based on elastic-plastic limit load solutions, P_L. Results were very consistent and comparable with P_L values.

2- Maximum Load, P_{max}, was inversly related to loading angles, ϕ. A linear dependence has been found to occur between the inverse of normalised P_{max} with loading angle.

3- There is general indication that Δ_{Pmax} and Δa_{Pmax} were scatter within a narrow range of values for the tests conducted. This indicated that such parameters can regarded as constants. Such assertion was reinforced in the light of normalisations used for P-Δ_{LL} plots and comparisons with fatigue-precracked specimens.

4- Normalisation of P-Δ_{LL} results was possible using P/P_{max} and Δ_{LL}/W. Such normalisation was able to represent all of current experimental into a single general trend. Further validations from various experimental data, for fatigue precracked specimens, were obtained, where various specimen configurations and sizes shared the same normalised trend.

5- Tests on notches show that there a weak effect of notch radius on P_{max}, and thus hints to the fact that stable crack growth behaviour for fatigue-precracked specimens and sharp notches are very similar.

6- Overall, there are indications that normalised P/P_{max}, Δ_{Pmax} and Δa_{Pmax} are candidate charecterising parameteres for stable crack growth behaviour for both, notched and cracked specimens.

Table 4.1: Various Loads vs. loading angles for notch radius = 0.08 mm.

ϕ (deg.)	P_i	P_Q	P_{max}
a_0/W =0.45			
90	25.0	31.0	57.5
80	23.0	25.5	67.5
75	24.0	30.5	69.0
70	28.0	35.5	74.0
65	30.0	48.5	81.5
a_0/W =0.50			
90	23.0	27.5	48.0
80	28.0	31.5	53.5
70	26.0	32.0	61.0
65	31.0	36.0	68.5
60	27.0	37.0	74.2
a_0/W = 0.55			
90	20.0	23.0	37.6
80	22.0	25.5	43.0
75	21.0	25.0	46.0
70	23.0	27.5	49.1
65	22.0	28.0	55.1
60	24.0	30.0	60.5

Table 4.2: Comparison for P_L estimates with $P_{I\text{-}max}$

a_0/W	P_L (kN)	$P_{I\text{-}max}$ (kN)	Difference
0.45	57.50	57.50	-0.0%
0.50	46.27	48.00	-4.0%
0.55	36.50	37.60	-3.0%

Table 4.3: Comparison for P_L estimates with $P_{I\text{-}max}$ for sharp-notched specimens.

Material	a_0/W	P_L (kN)	$P_{I\text{-}max}$ (kN)	Difference
4340 Low Alloys Steel (Mourad et al. [61])	0.41	58.37	45.47	22%
	0.42	56.11	44.00	22%
	0.43	53.91	40.40	25%
	0.44	51.76	39.00	25%
	0.45	49.67	36.00	28%

Table 4.4: Comparison for P_L estimates with $P_{I\text{-}max}$ for fatigue pre-cracked specimens by other researchers.

Material	a_0/W	$P_{L\text{-}P.s}$ (kN)	$P_{I\text{-}max}$ (kN)	Difference (%)
2024 –T351 Aluminium Alloy (Mahmoud and Lease [26])	0.4	25.89	14.20	45%
	0.4	71.48	37.50	48%
	0.4	142.95	76.00	47%
	0.4	285.91	127.80	55%
D16AT – 2024-T3 Aluminium Alloy (Mahanty and Maiti [59])	0.45	41.53	19.00	54%
	0.55	26.37	10.35	61%
D16AT – 2024-T3 Aluminium Alloy (Mahanty and Savant [51])	0.50	8.00	6.17	23%

Table 4.5: Comparison for mechanical properties for 2024-T3.

Source	E (GPa)	σ_{YS} (MPa)	σ_{UTS} (MPa)
Maiti and Mourad [52]	72.6	353	457
Dawicke et al. [28]	71.4	345	490

Table 4.6: Arcan Specimen Sizes comparison for Amstutz et al. [54] and Sutton et al. [55].

Source	W (mm)	B (mm)	h/B
Amstutz et al. [54]	38.1	2.3	13.75
Sutton et al. [55]	152.4	6.4	19.84

Table 4.7: Notch radii and resulting K_T and measured Δa_{core}.

Notch radius (mm)	0.08	0.16	0.25	0.50	1.00
K_T	27.22	19.54	15.83	11.49	8.42
Δa_{core}	5.33	n/a	4.51	3.74	2.95

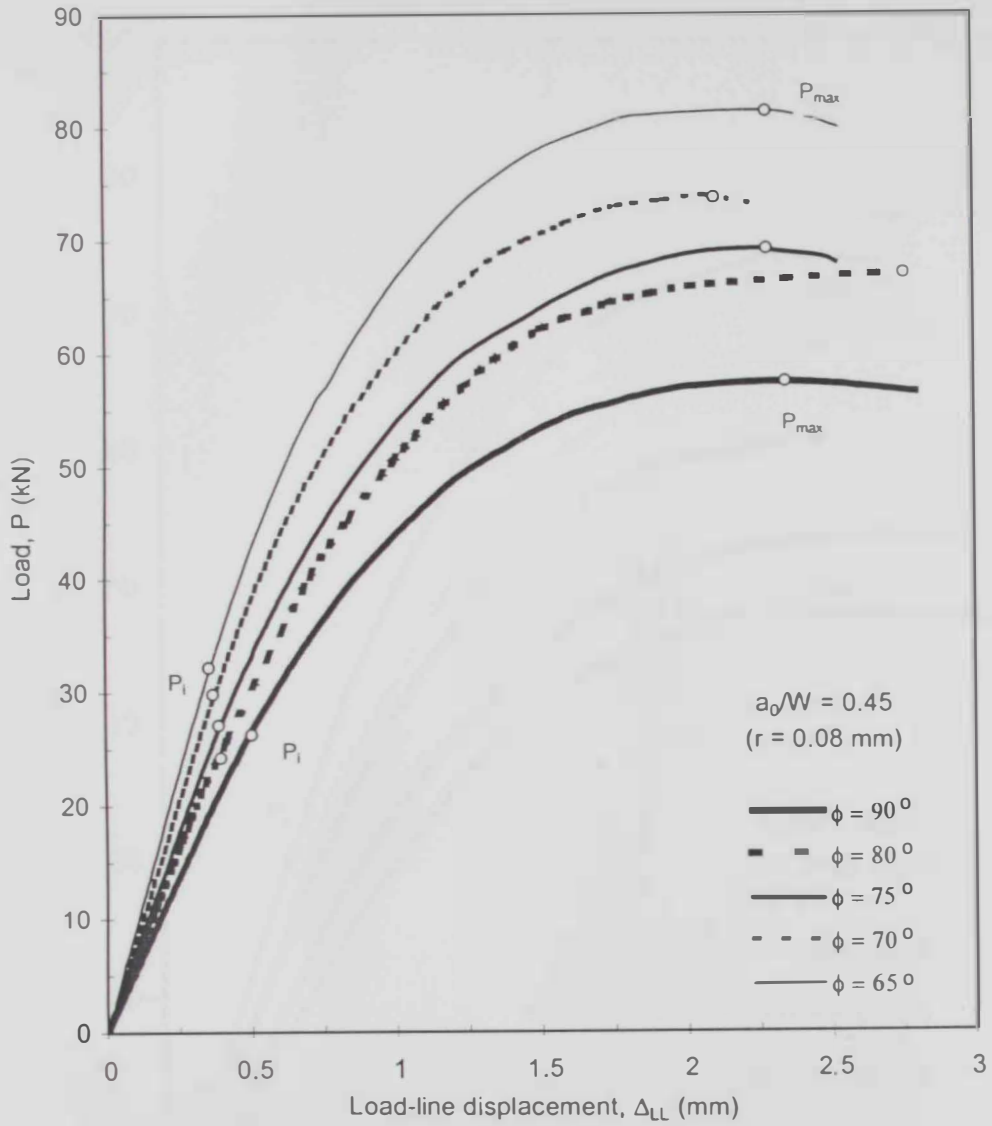

Fig. 4.1:P-Δ_{LL} curves for a_0/W = 0.45 (notch radius = 0.08 mm).

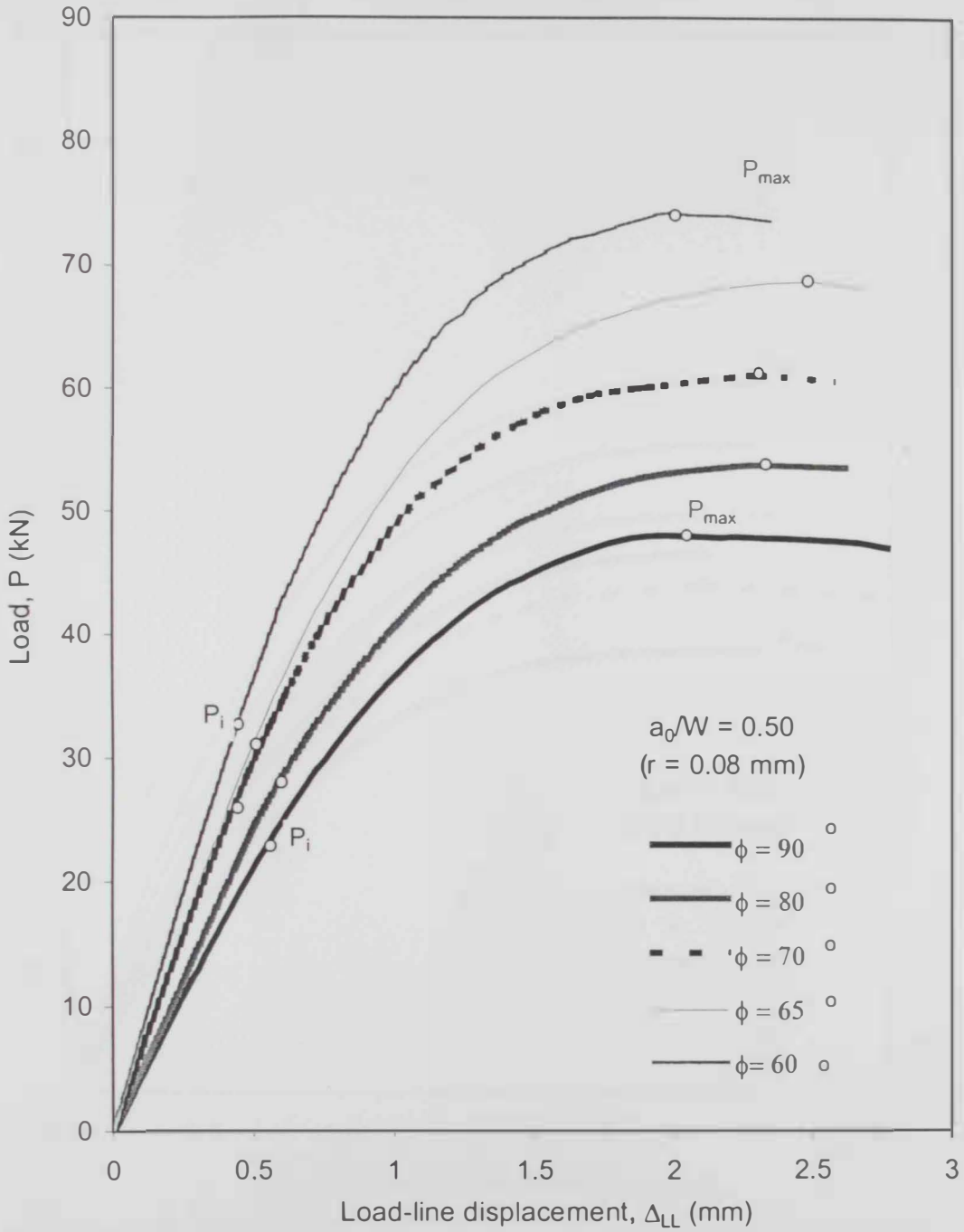

Fig. 4.2: P-Δ_{LL} curves for a_0/W = 0.50 (notch radius = 0.08 mm).

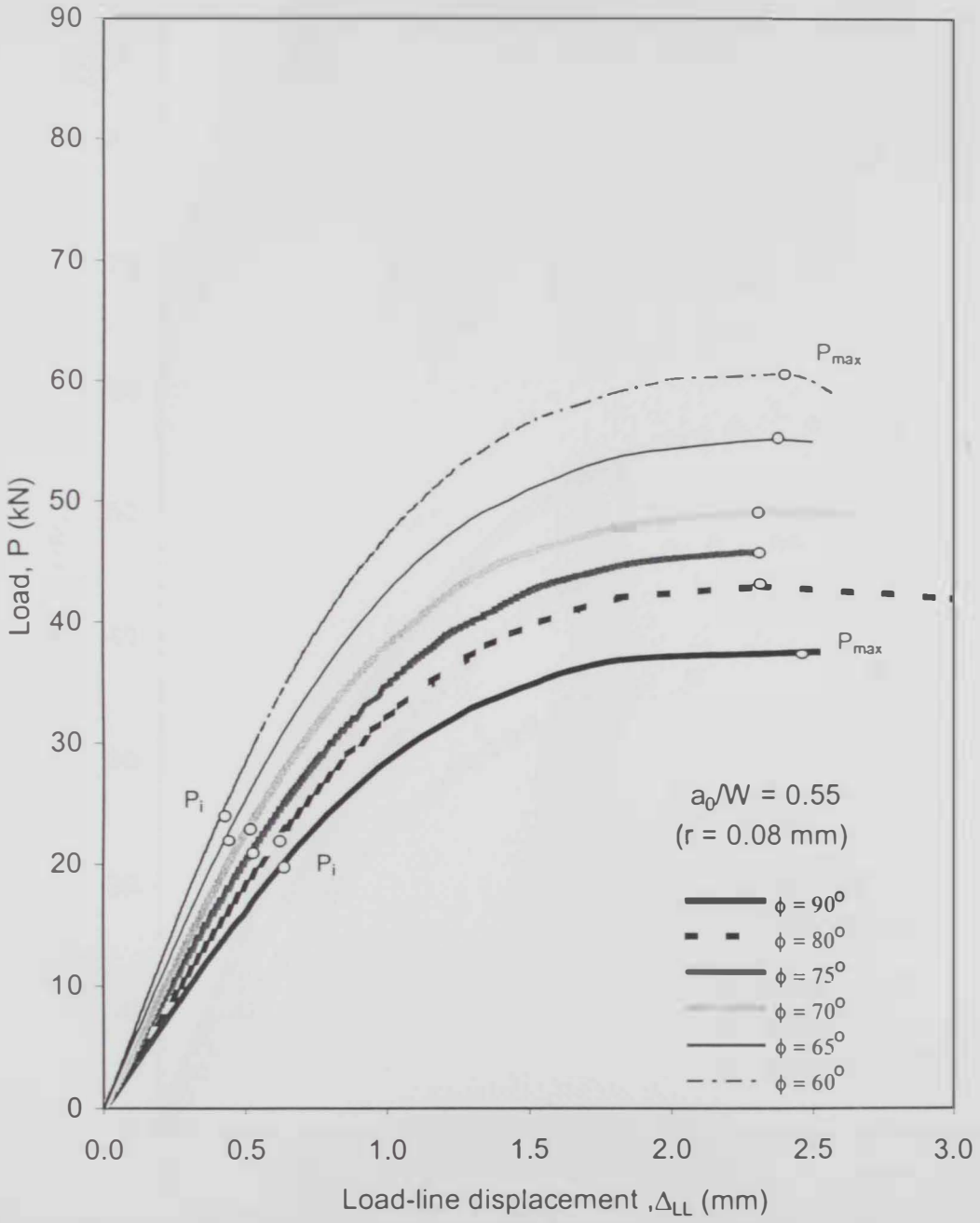

Fig. 4.3:P-Δ_{LL} curves for $a_0/W = 0.55$ (notch radius = 0.08 mm).

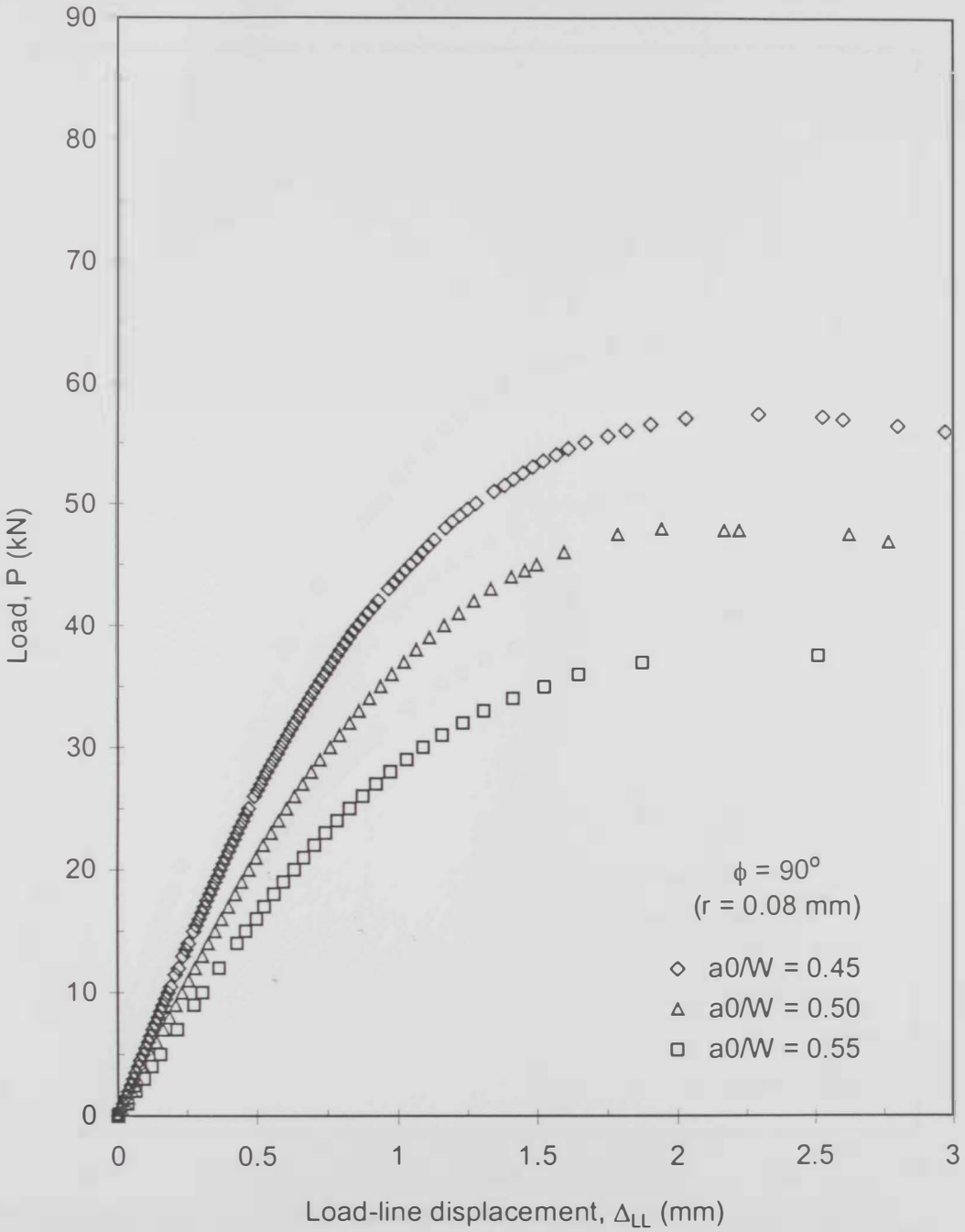

Fig. 4.4:P-Δ_{LL} curves for $\phi = 90^o$ (notch radius = 0.08 mm).

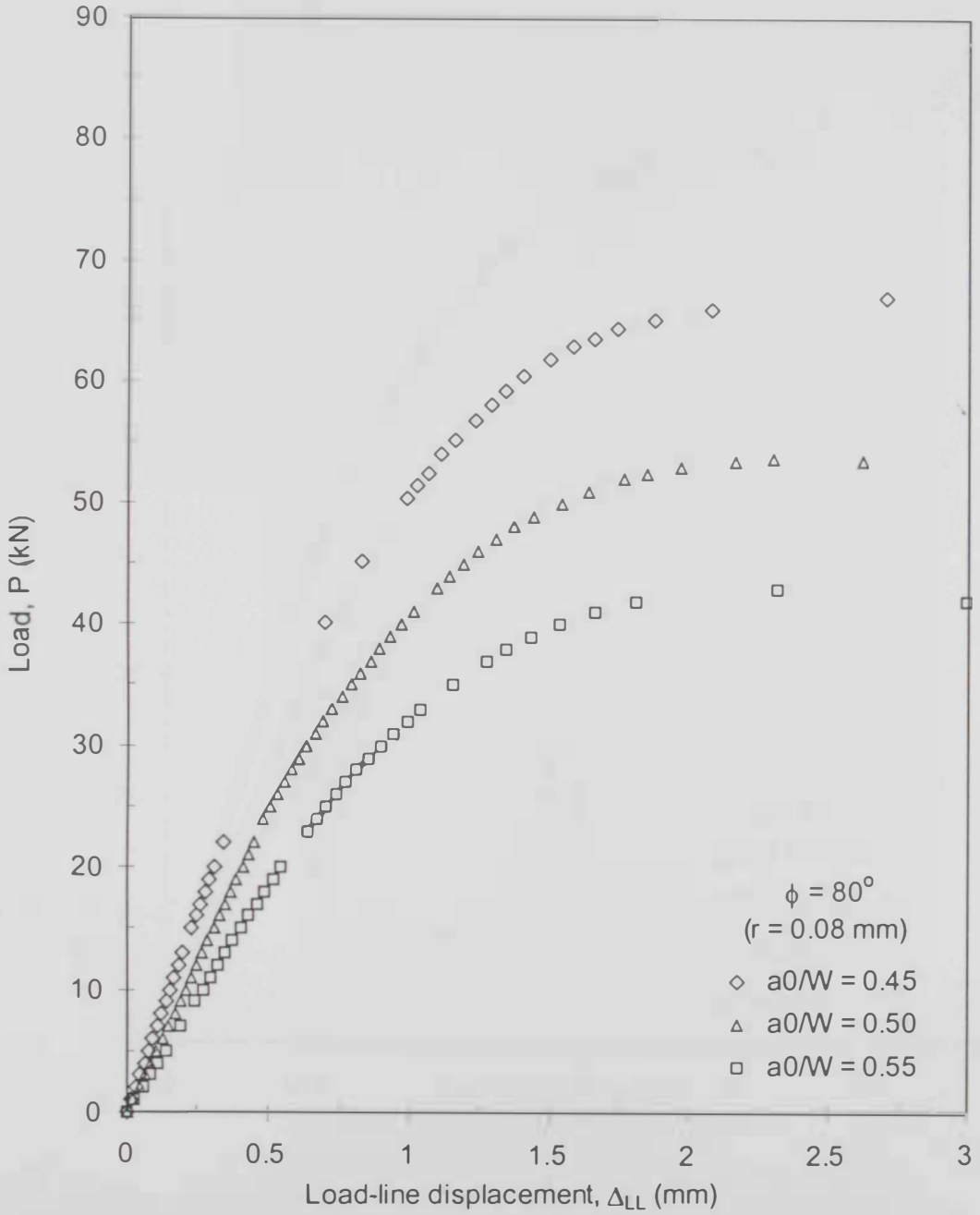

Fig. 4.5:P-Δ_{LL} curves for $\phi = 80^{o}$ (notch radius = 0.08 mm).

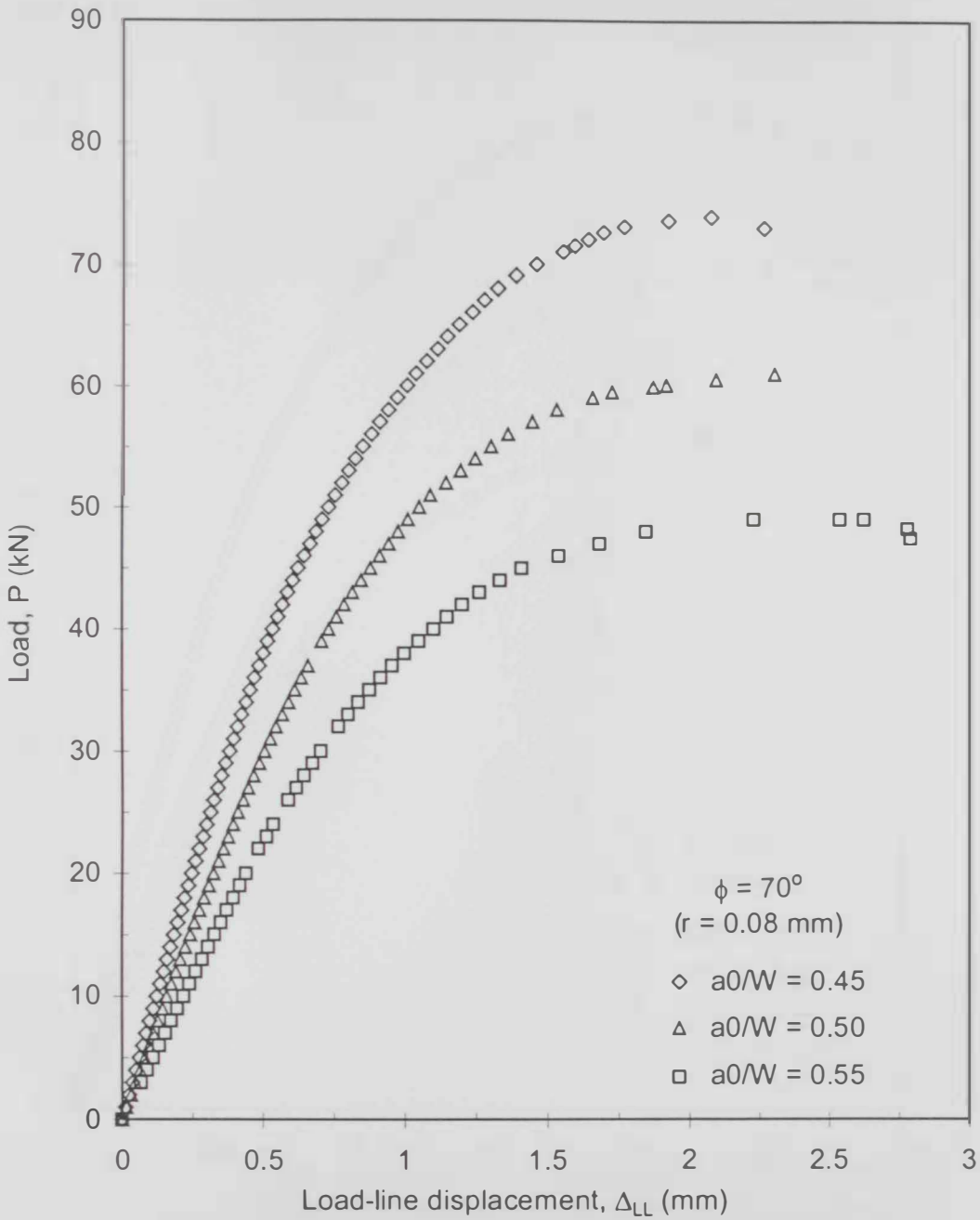

Fig. 4.6:P-Δ_{LL} curves for $\phi = 70^{o}$ (notch radius = 0.08 mm).

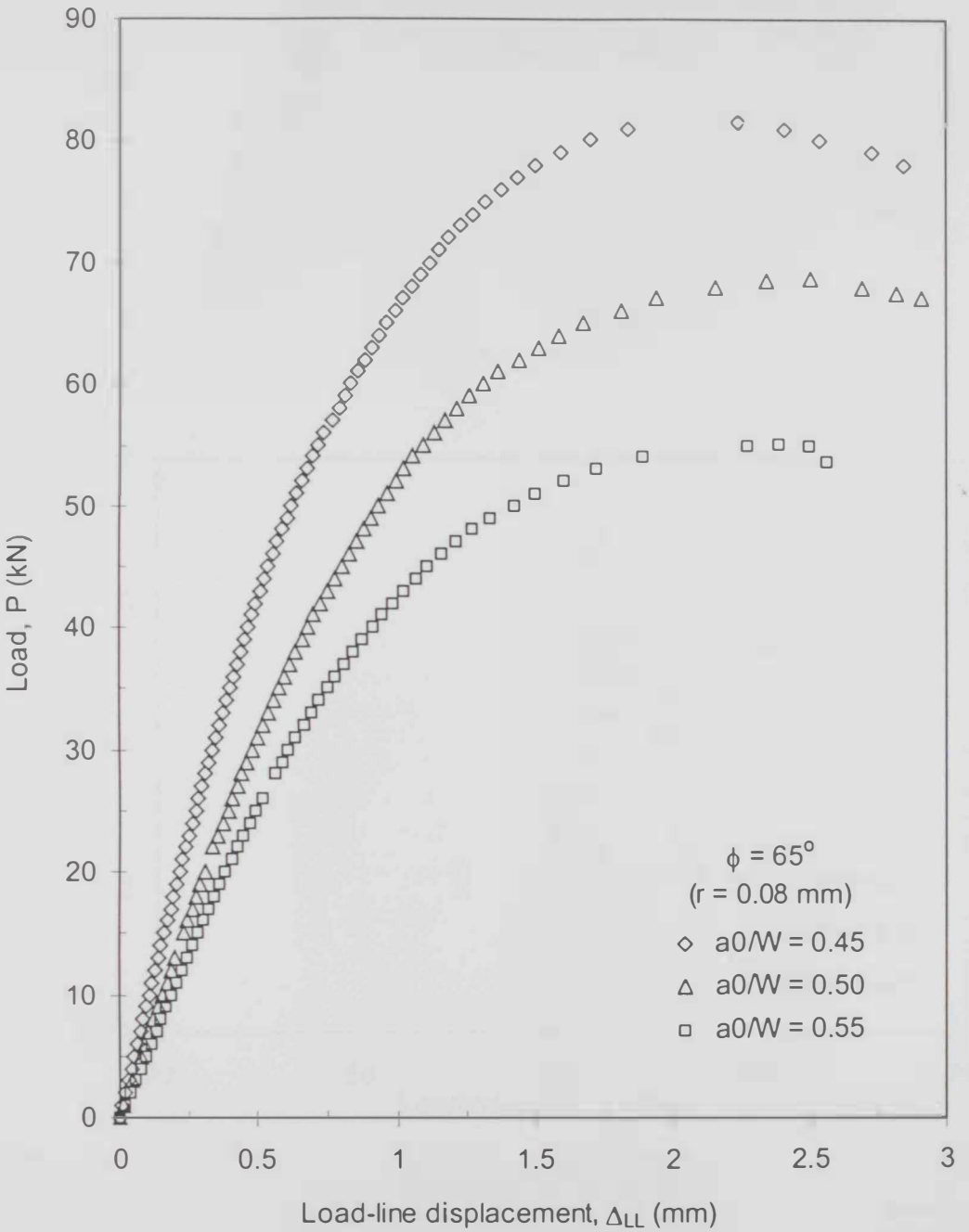

Fig. 4.7:P-Δ_{LL} curves for $\phi = 65^{o}$ (notch radius = 0.08 mm).

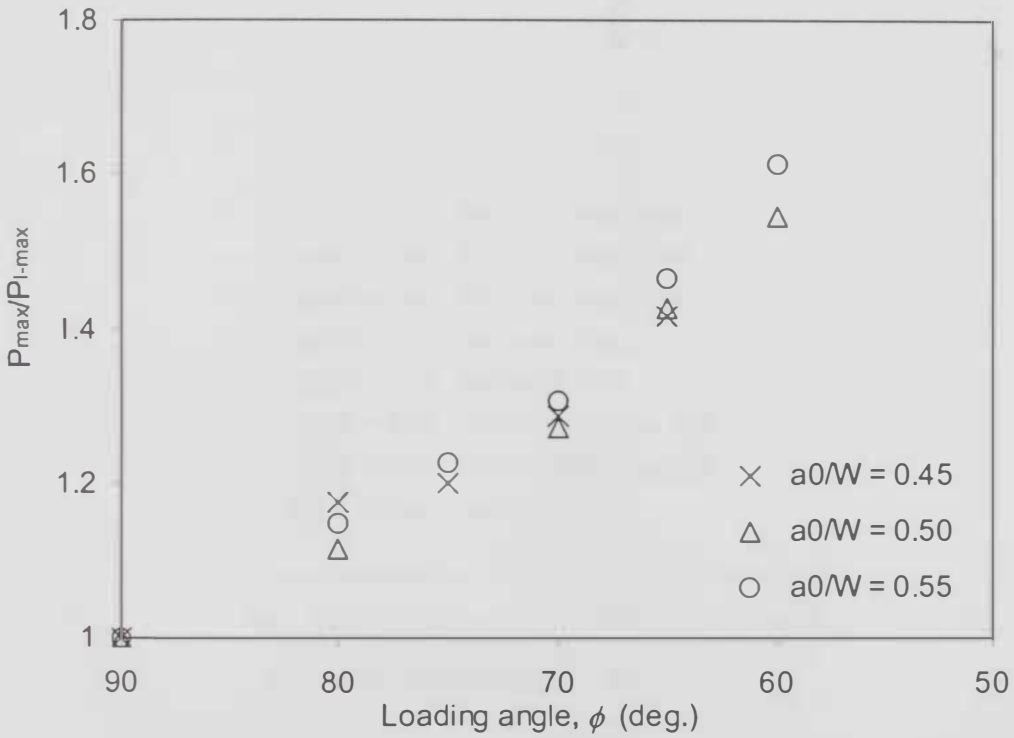

Fig. 4.8: Normalised maximum load variation with loading angle ($P_{max}/P_{I\text{-}max}$ *vs.* ϕ).

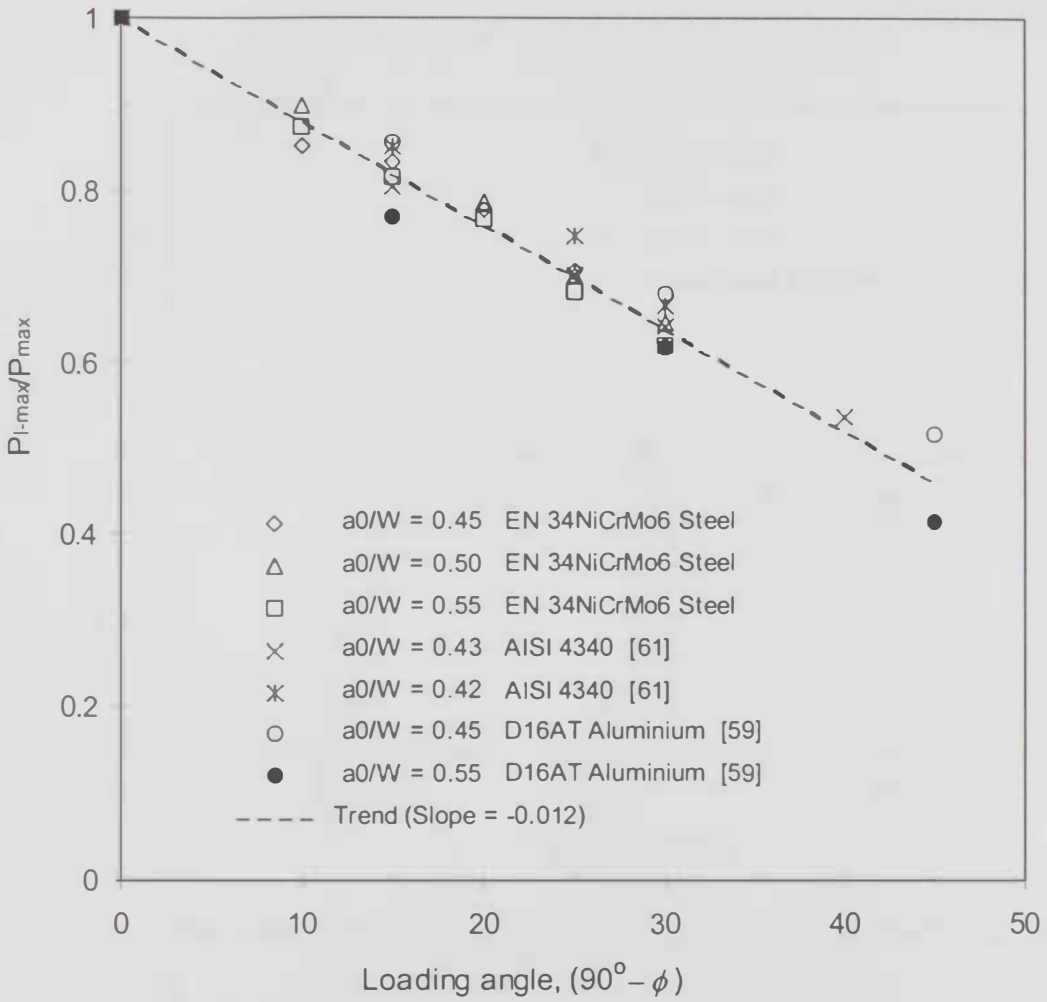

Fig. 4.9: Linear fit for normalised maximum load variation with loading angle ($P_{max}/P_{I\text{-}max}$ *vs.* ϕ) and comparison with results of other investigations.

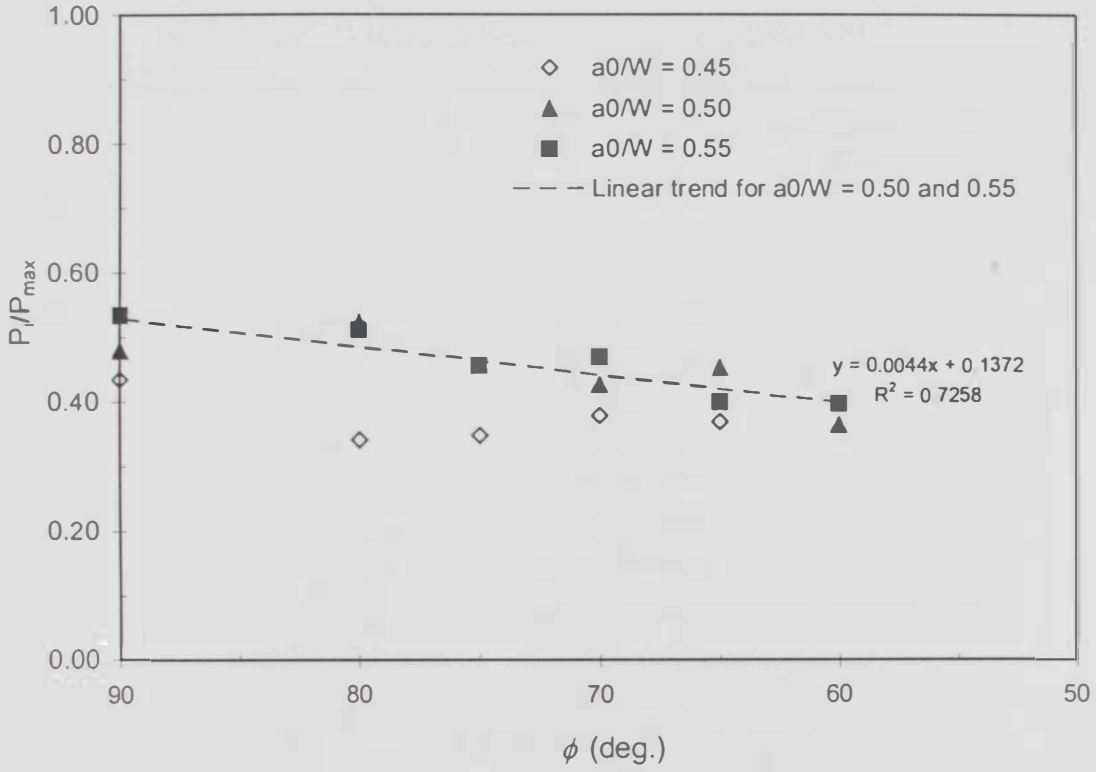

Fig. 4.10: Normalised initiation load (P_i) vs. loading angle.(P_i/P_{max} vs. ϕ).

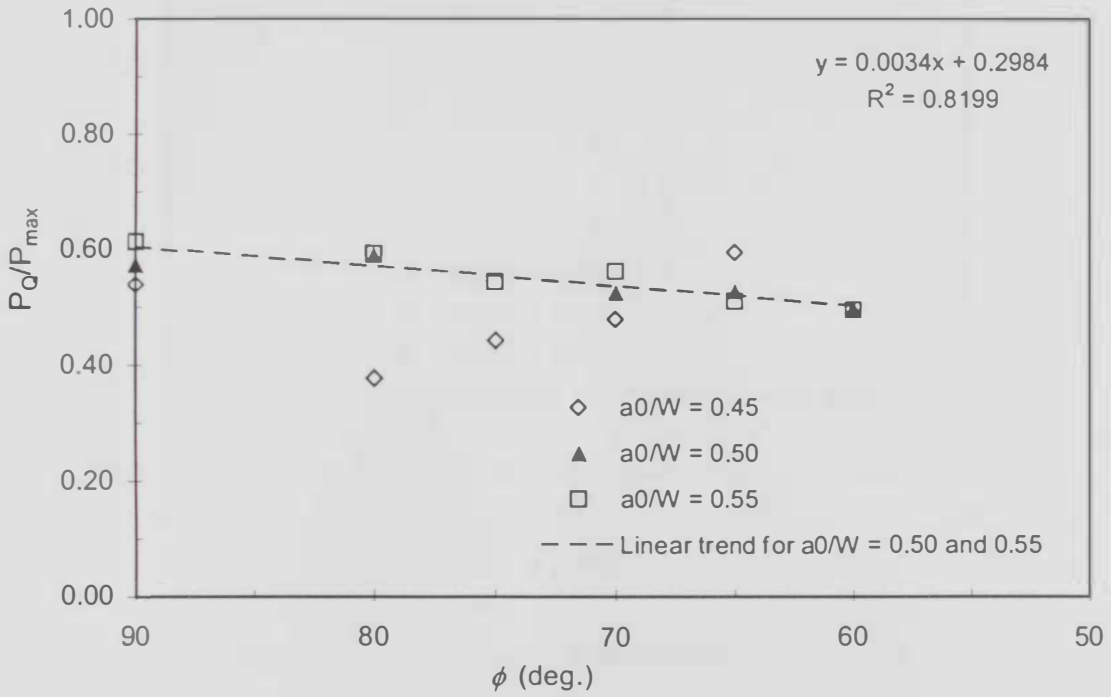

Fig. 4.11: Normalised initiation load (P_Q) vs. loading angle.(P_Q/P_{max} vs. ϕ).

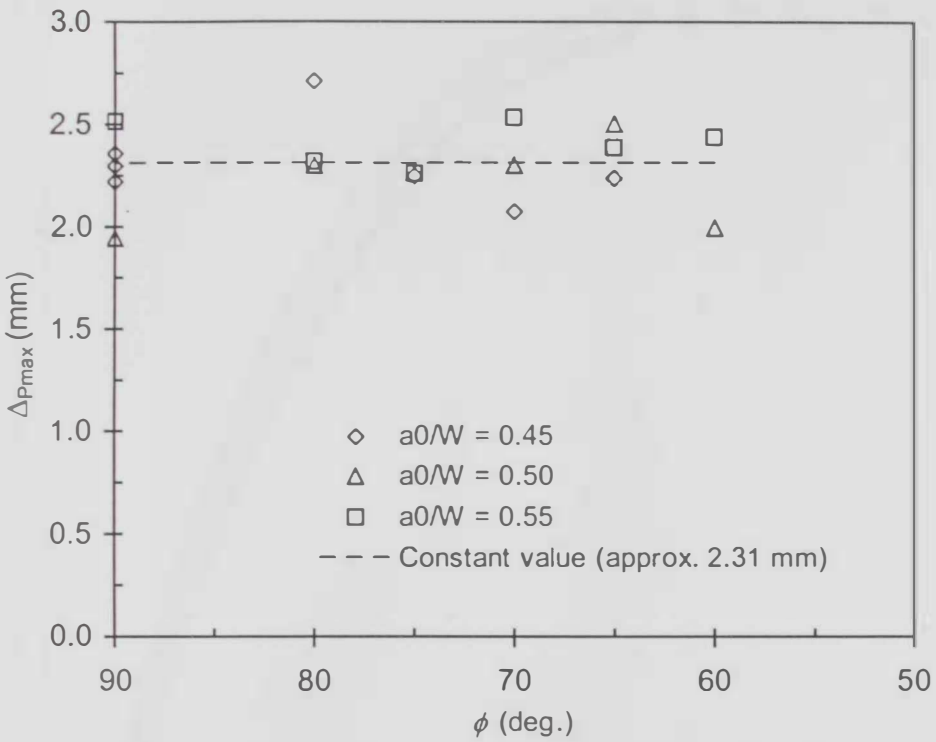

Fig. 4.12: Δ_{LL} at P_{max} vs. loading angle ($\Delta_{P\text{-}max}$ vs. ϕ).

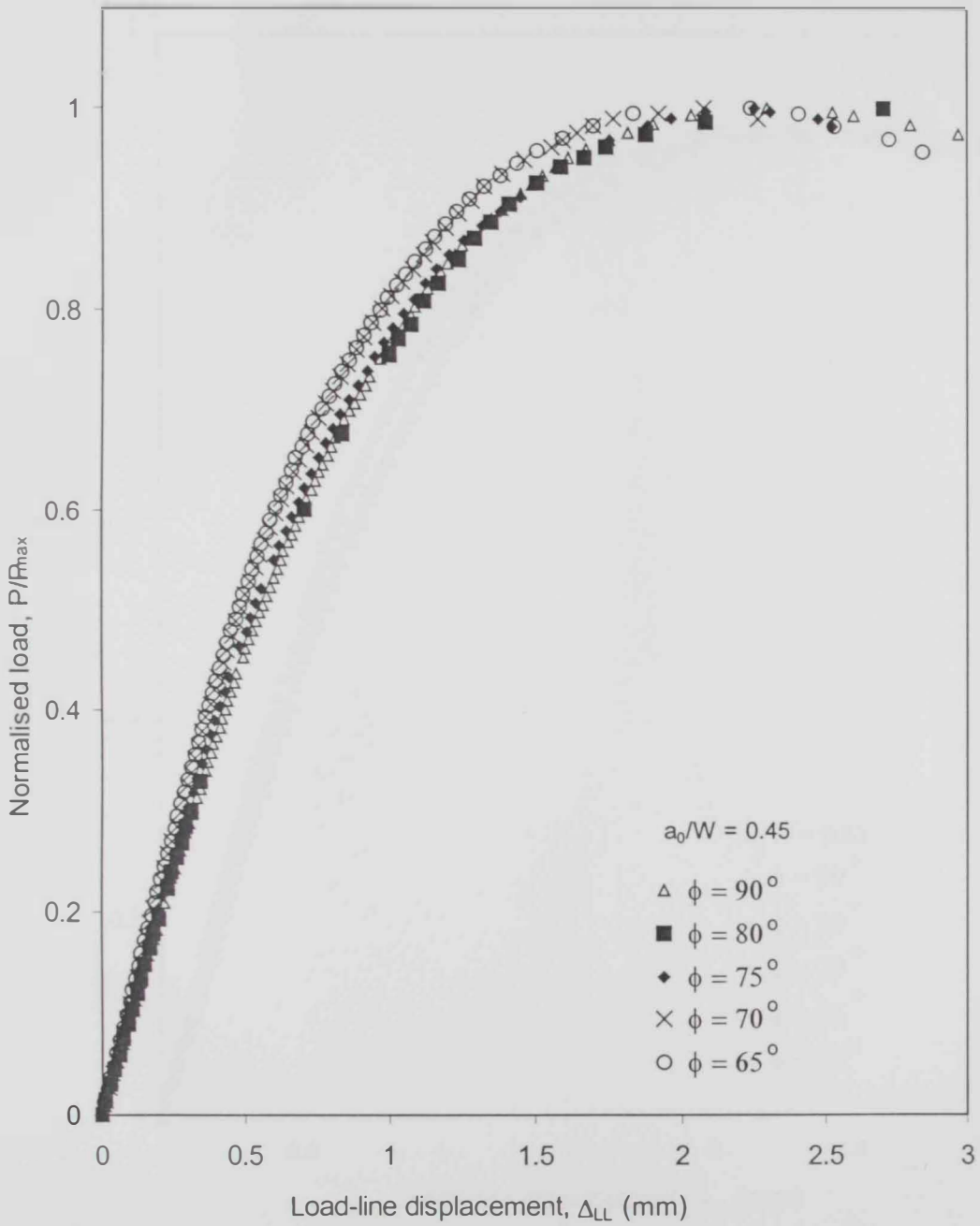

Fig. 4.13: Normalised P-Δ_{LL} curves for $a_0/W = 0.45$ (notch radius = 0.08).

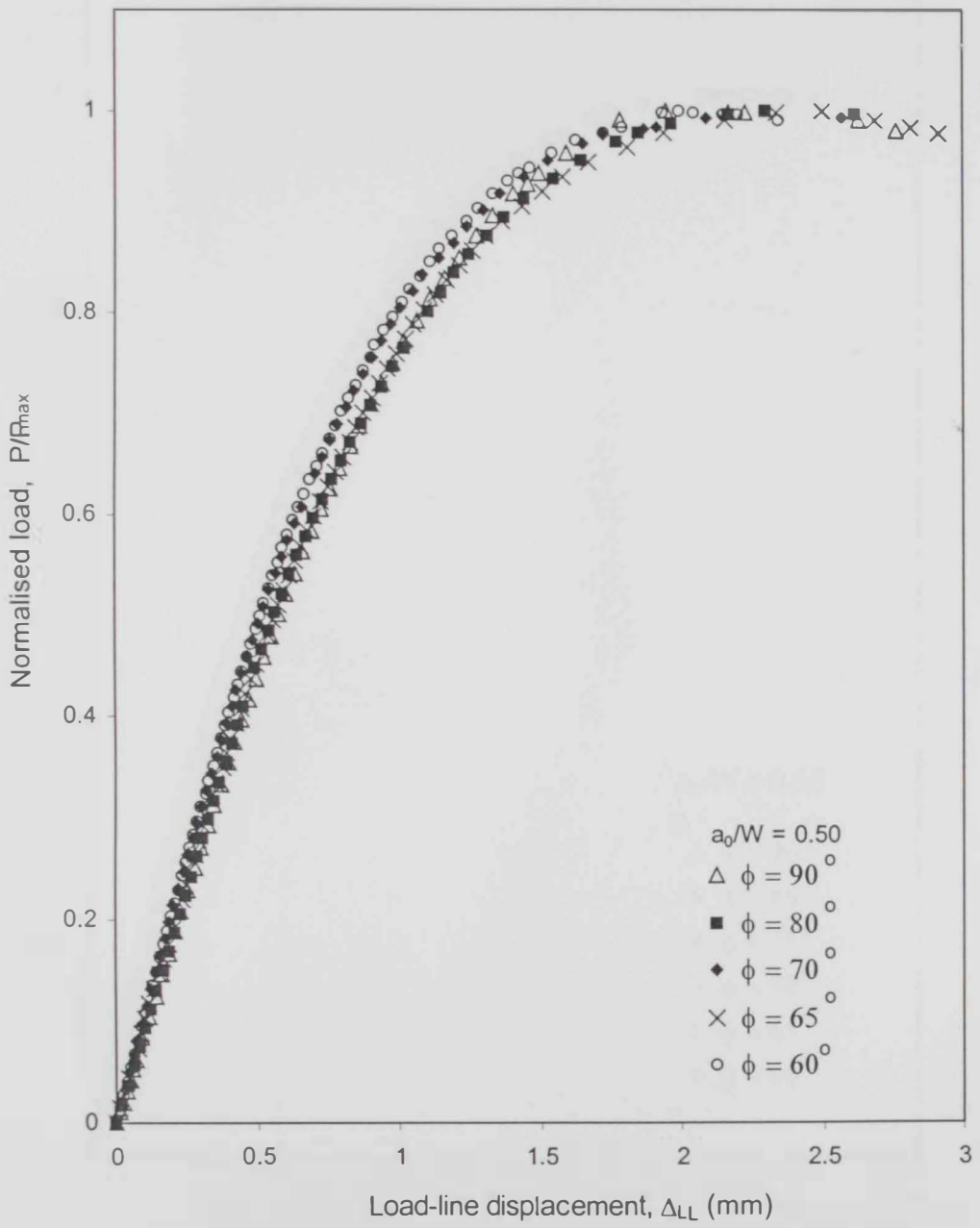

Fig. 4.14: Normalised P-Δ_{LL} curves for $a_0/W = 0.50$ (notch radius = 0.08).

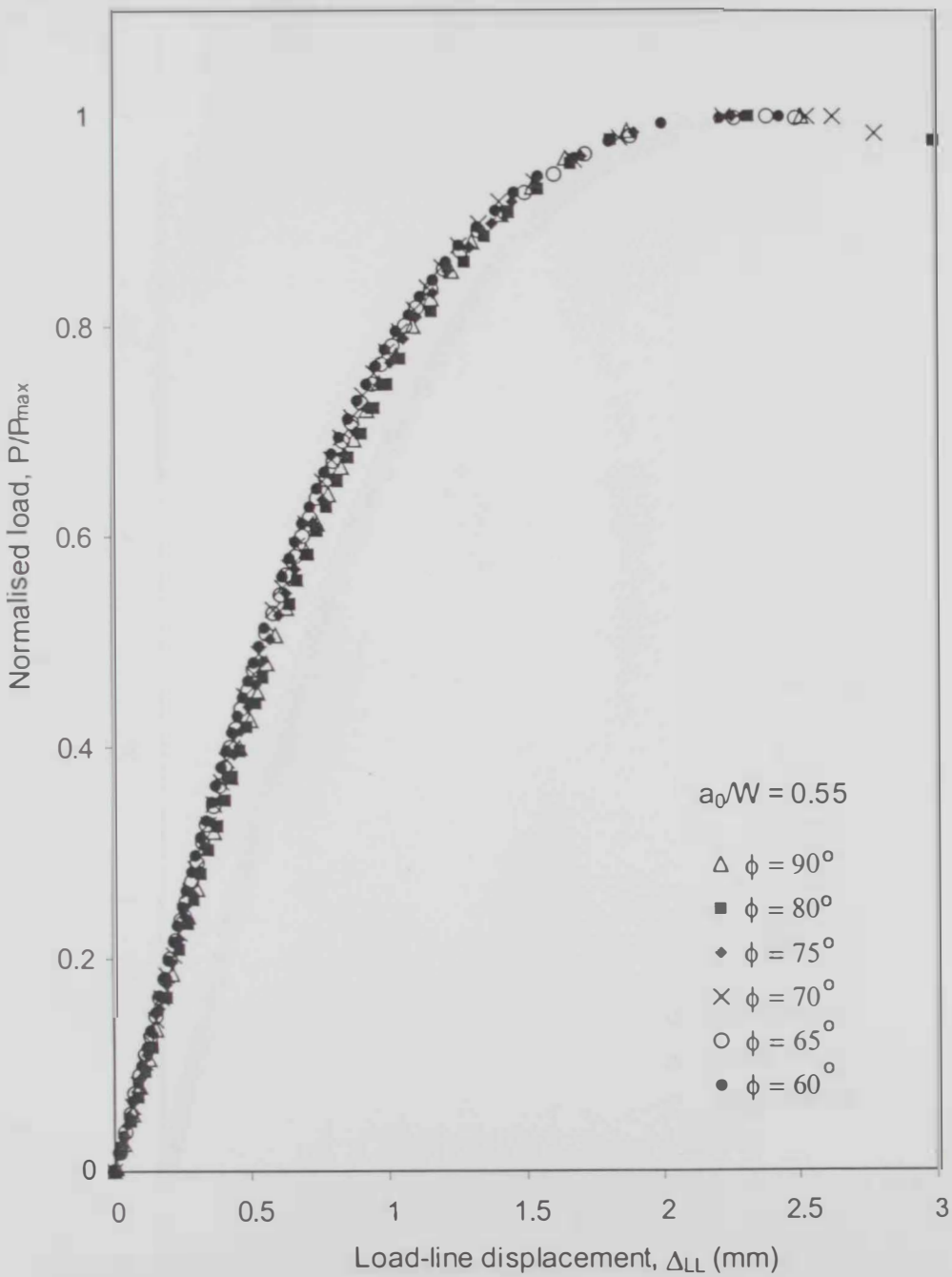

Fig. 4.15: Normalised P-Δ_{LL} curves for $a_0/W = 0.55$ (notch radius = 0.08).

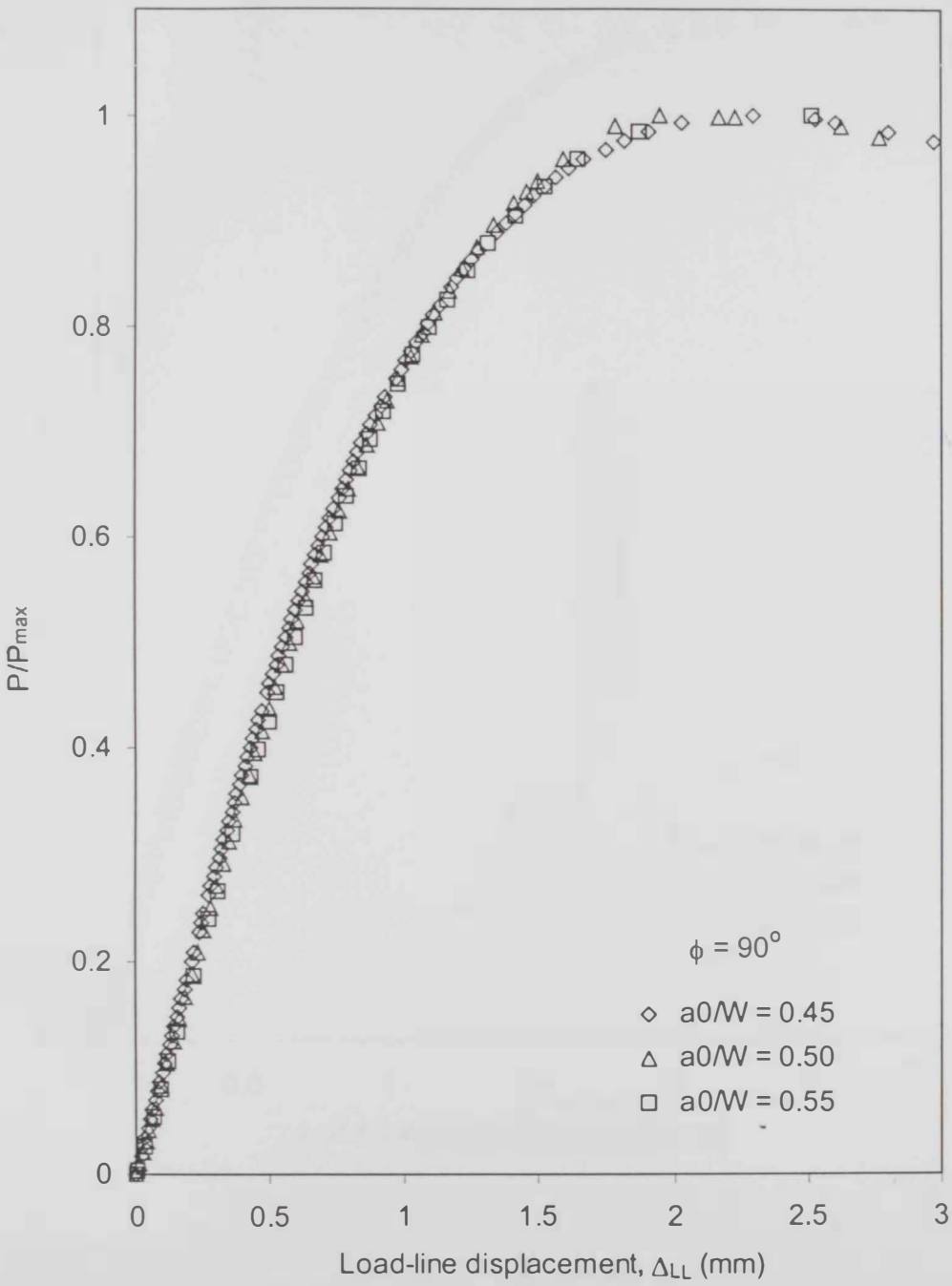

Fig. 4.16: Normalised P-Δ_{LL} curves for $\phi = 90^{o}$ (notch radius = 0.08).

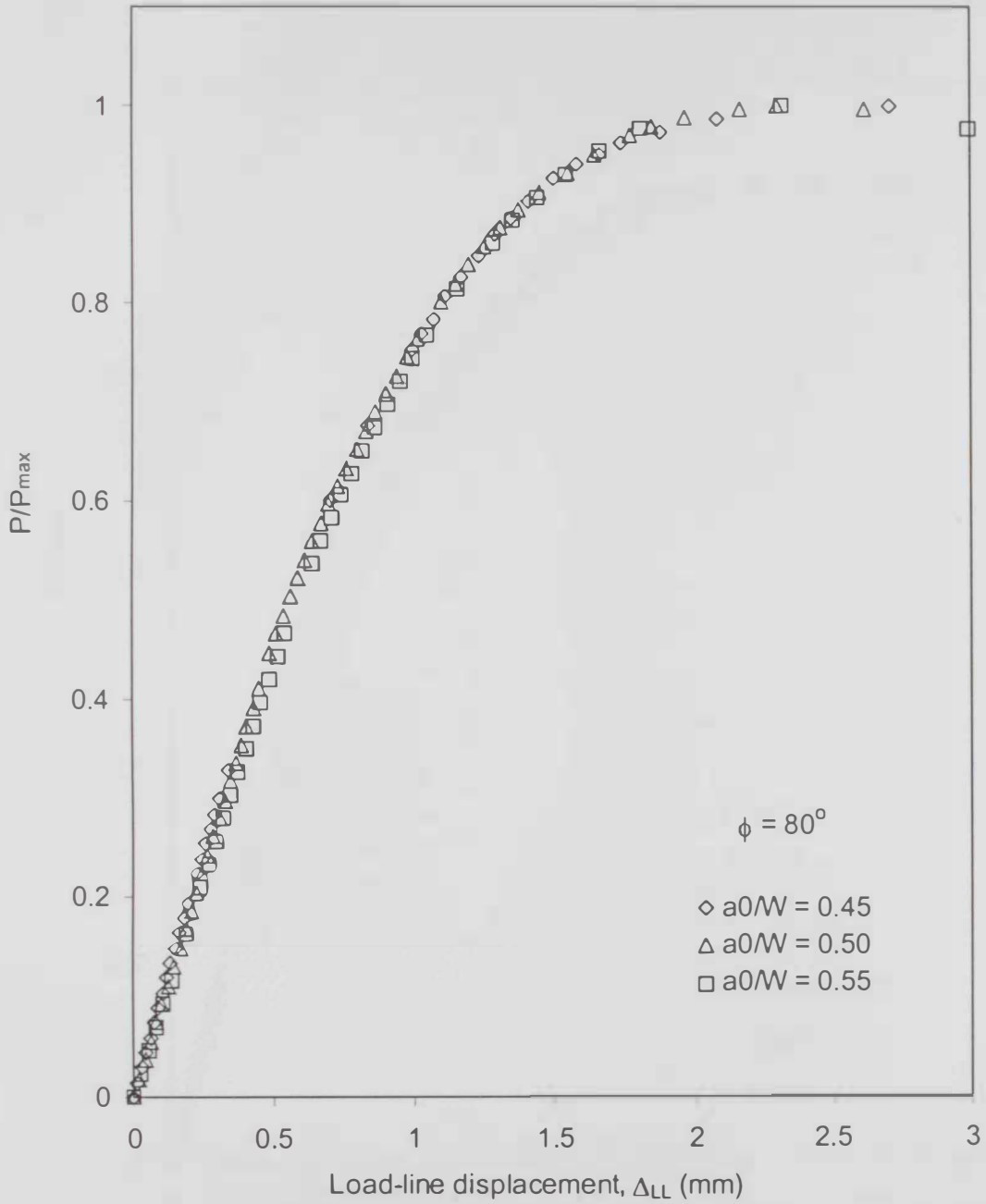

Fig. 4.17: Normalised P-Δ_{LL} curves for $\phi = 80^{o}$ (notch radius = 0.08).

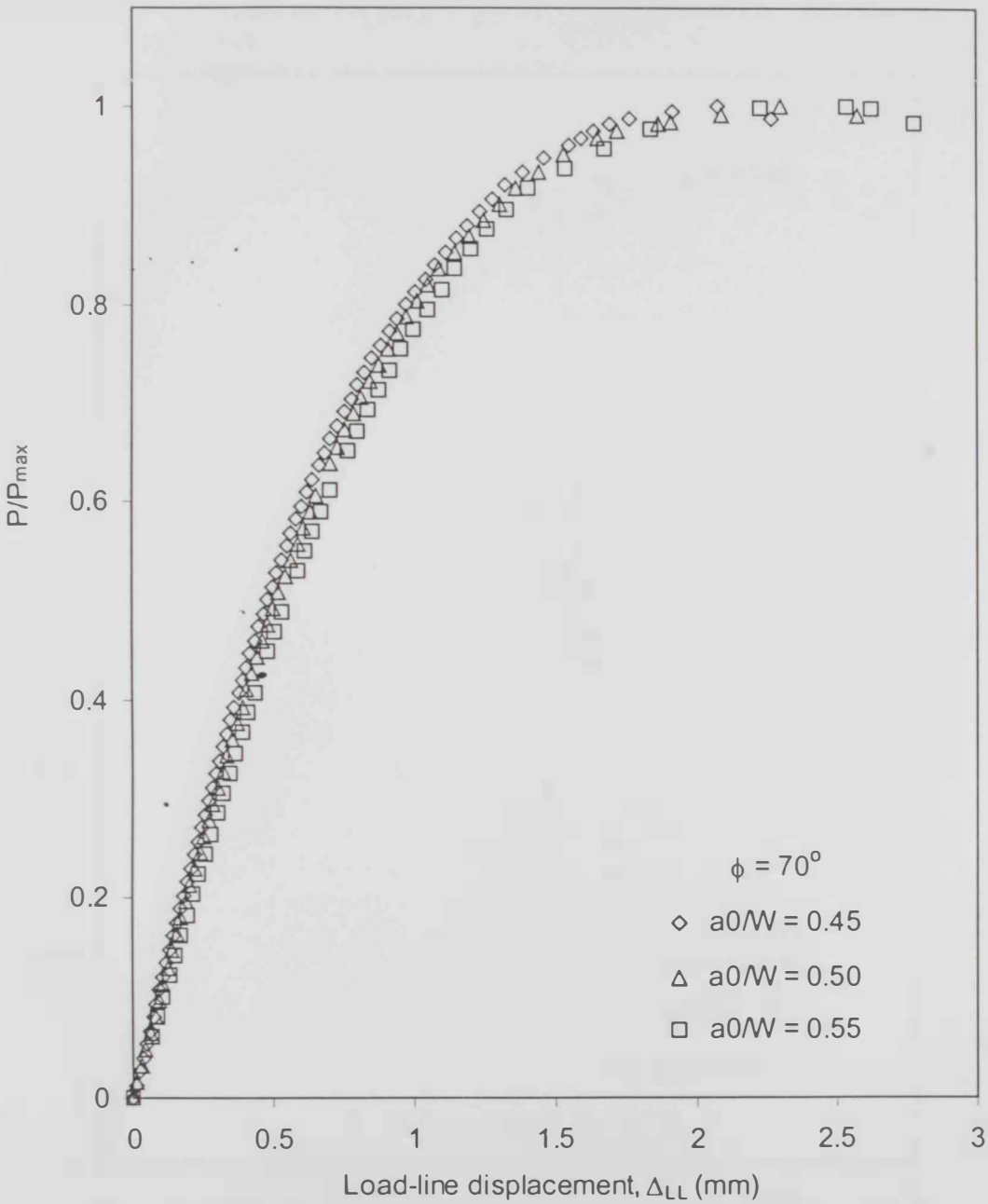

Fig. 4.18: Normalised P-Δ_{LL} curves for $\phi = 70^{o}$ (notch radius = 0.08).

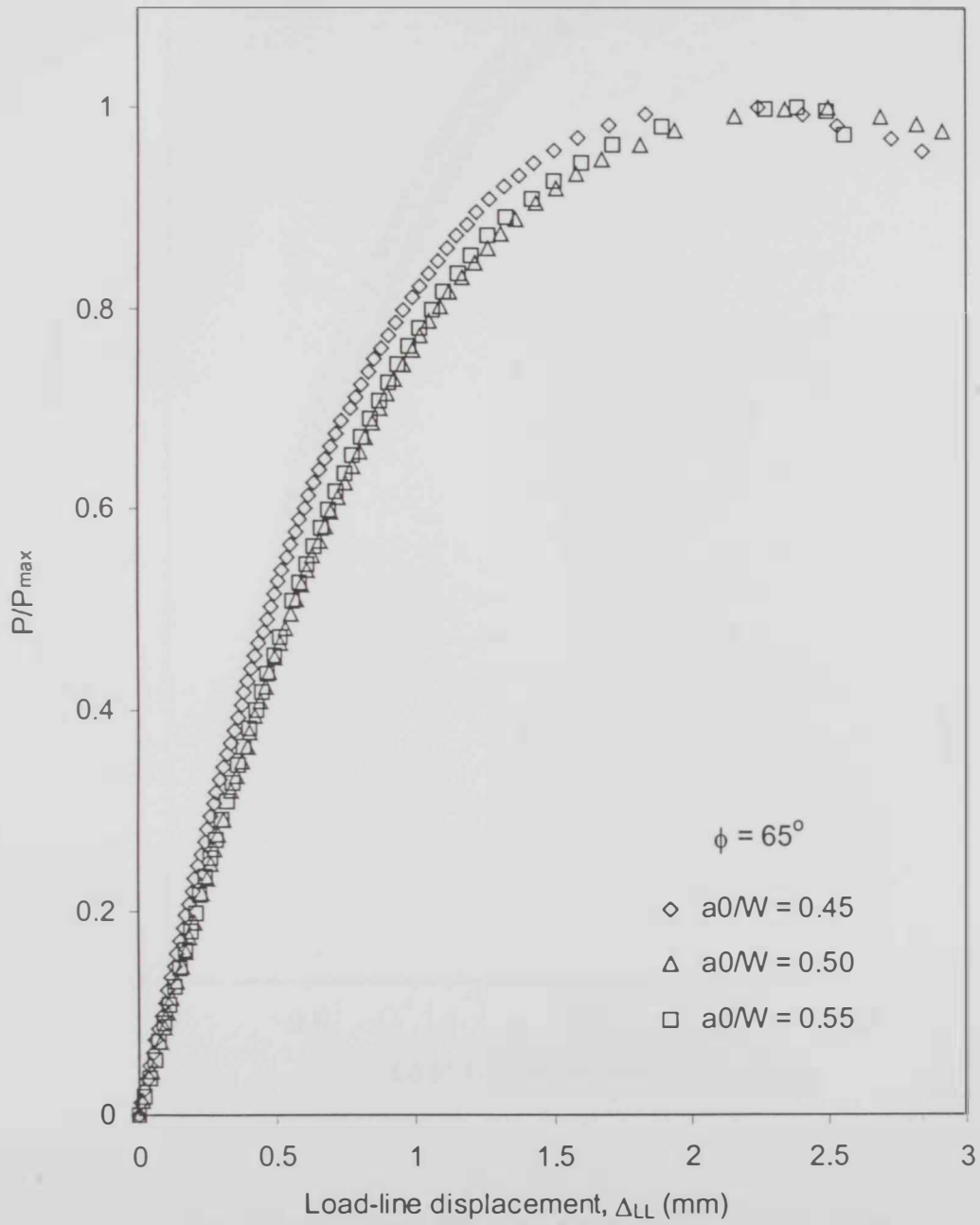

Fig. 4.19: Normalised P-Δ_{LL} curves for $\phi = 65^{\circ}$ (notch radius = 0.08).

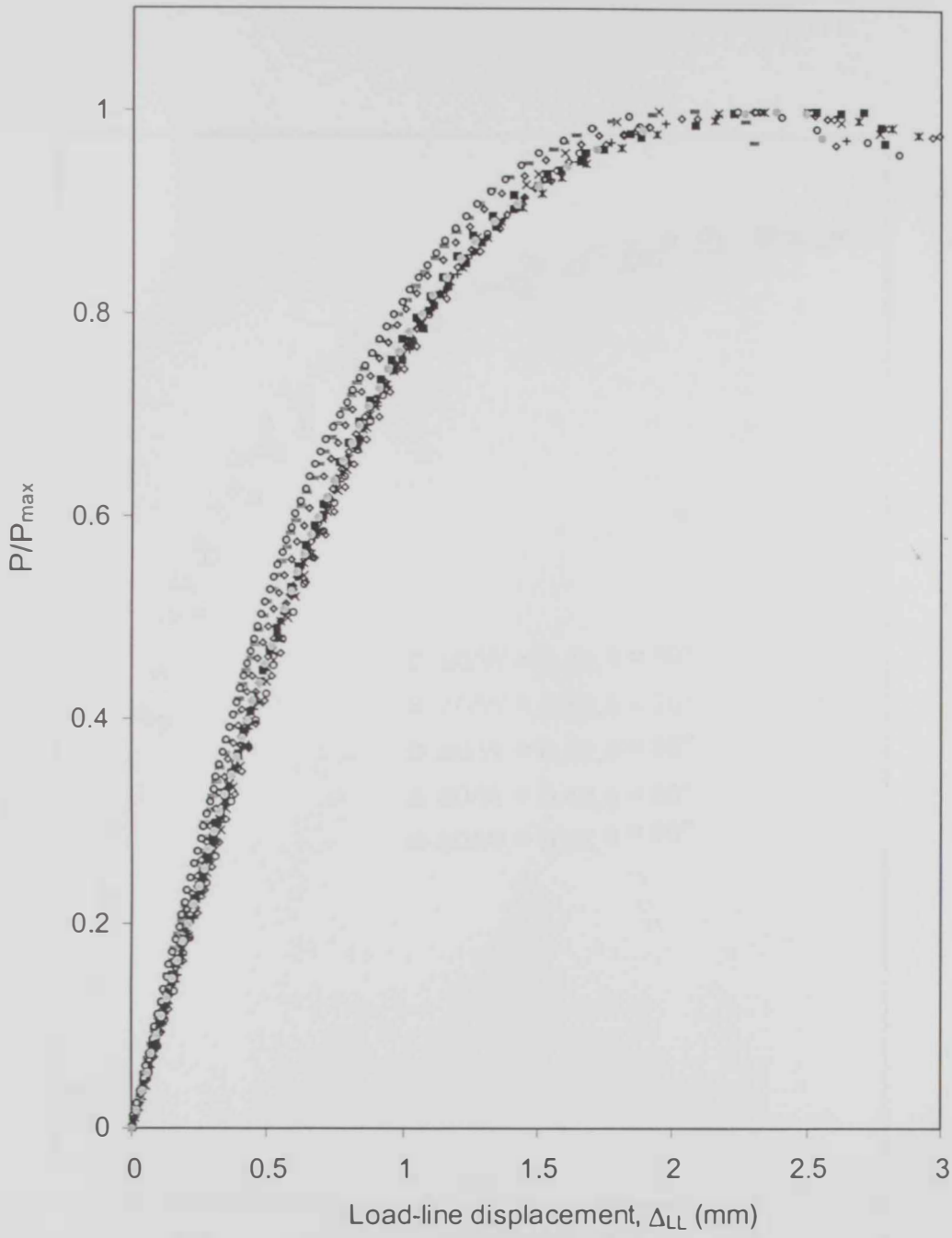

Fig. 4.20: All normalised P-Δ_{LL} curves (notch radius = 0.08).

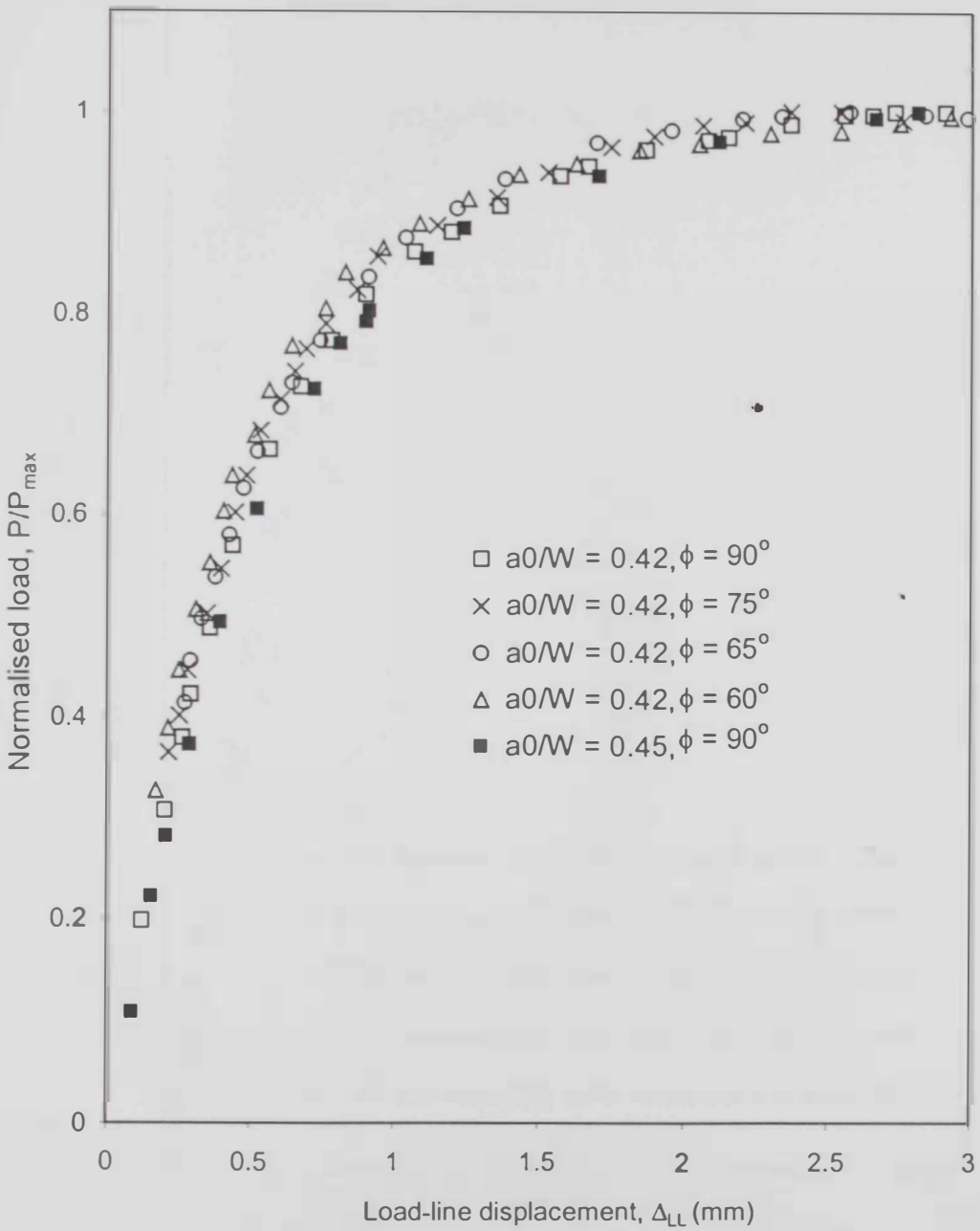

Fig. 4.21: Normalised P-Δ_{LL} curves for selected results by Mourad et al. [61].

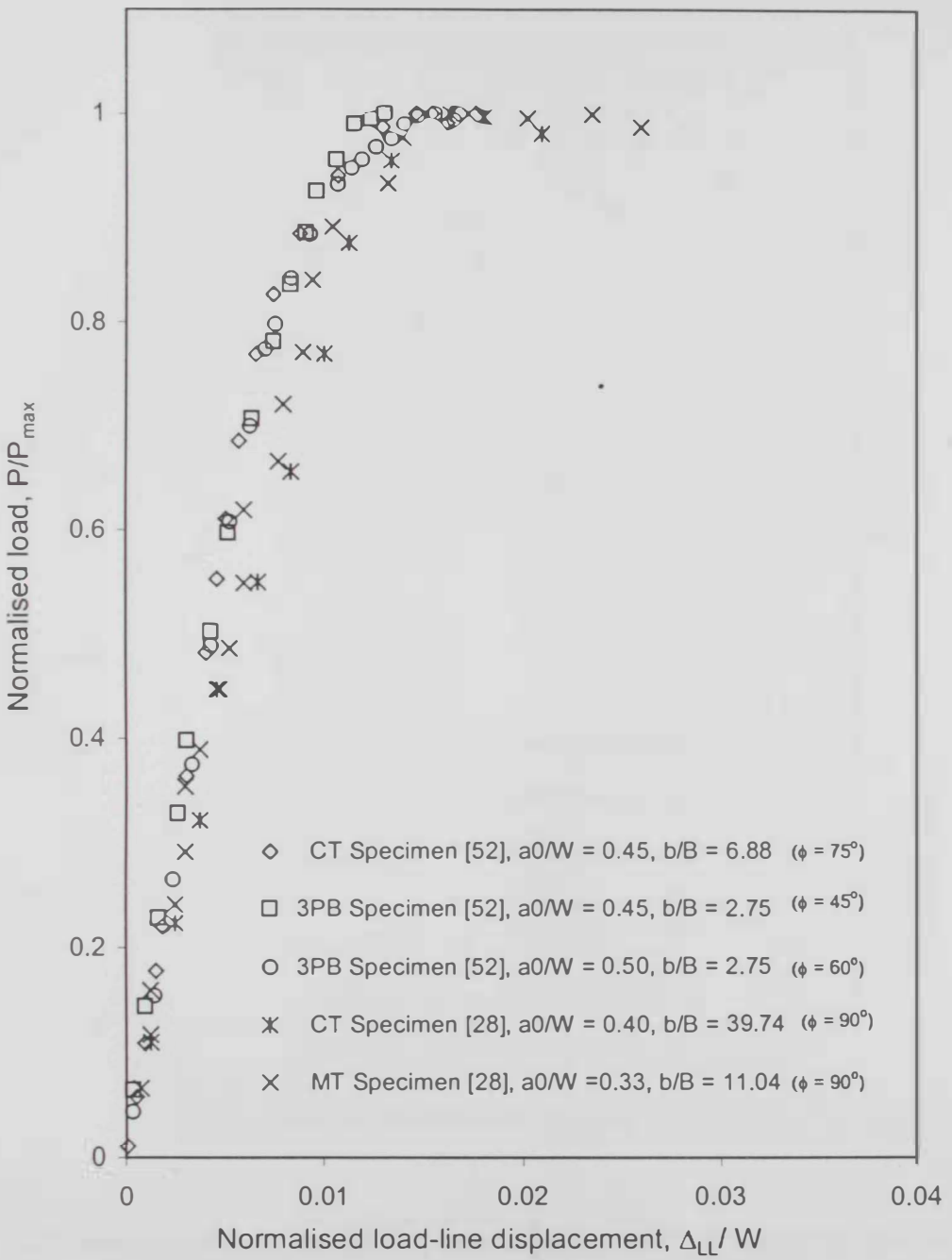

Fig. 4.22: Normalised P-Δ_{LL} curves for selected results for 2024-T3 aluminium alloy.

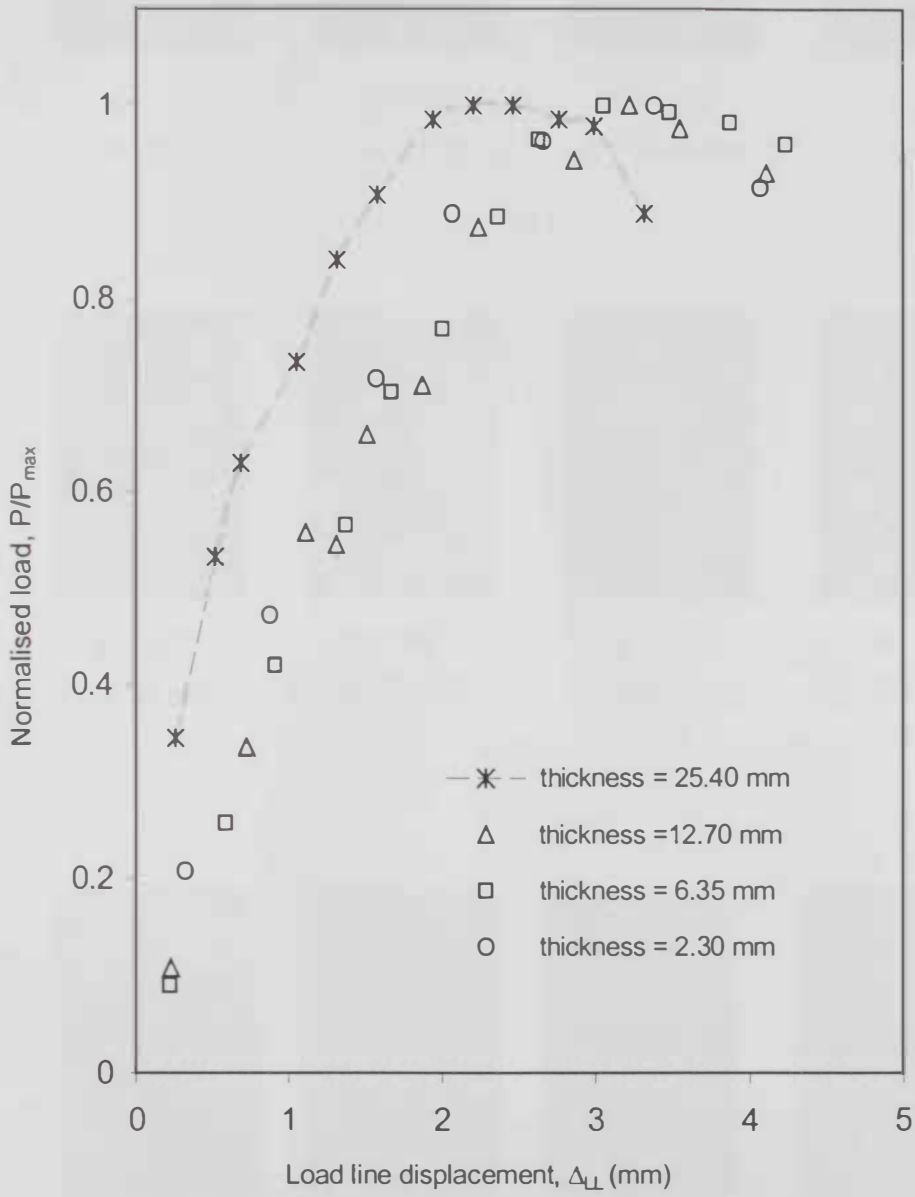

Fig. 4.23: Normalised P-Δ_{LL} curves for various thicknesses for 2024-T351 aluminium alloy by Mahmoud and Lease [26].

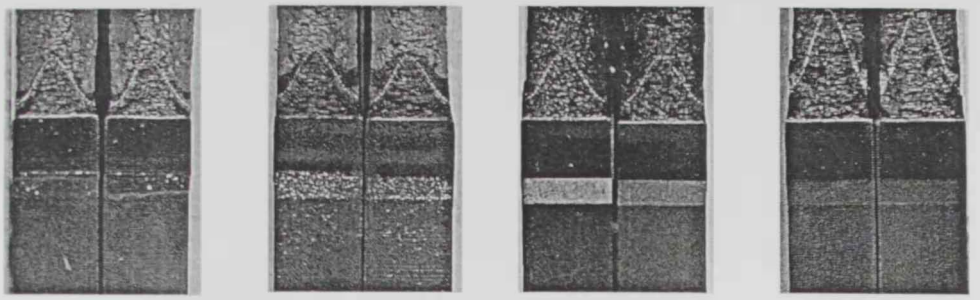

$\phi = 90^{o}$ (r =0.16 mm) $\phi = 80^{o}$ (r =0.16 mm) $\phi = 70^{o}$ (r =0.08 mm) $\phi = 65^{o}$ (r =0.08 mm)

(a)

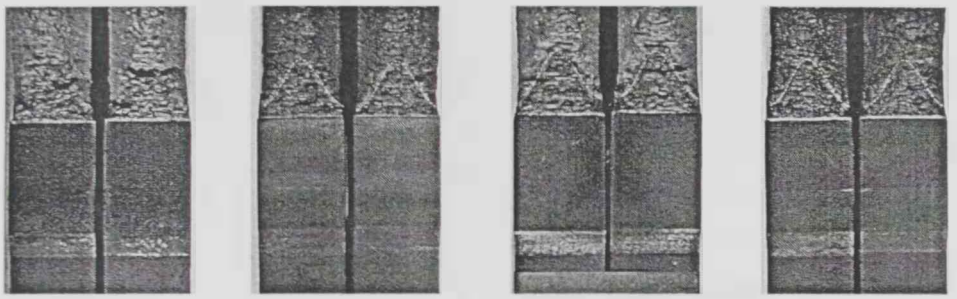

$\phi = 90^{o}$ (r =0.16 mm) $\phi = 80^{o}$ (r =0.16 mm) $\phi = 80^{o}$ (r =0.08 mm) $\phi = 70^{o}$ (r =0.08 mm)

(b)

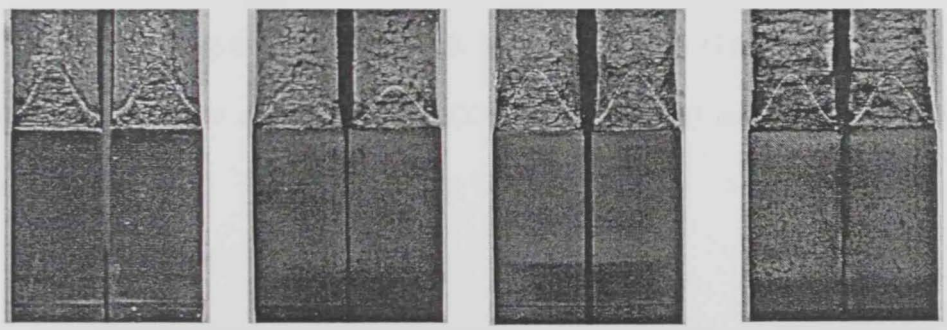

$\phi = 90^{o}$ (r =0.08 mm) $\phi = 80^{o}$ (r =0.08 mm) $\phi = 65^{o}$ (r =0.08 mm) $\phi = 60^{o}$ (r =0.08 mm)

(c)

Fig. 4.24: Crack front photographs showing crack growth at mid-thickness for (a) a_0/W = 0.45, (b) a_0/W = 0.50, and (c) a_0/W = 0.55.

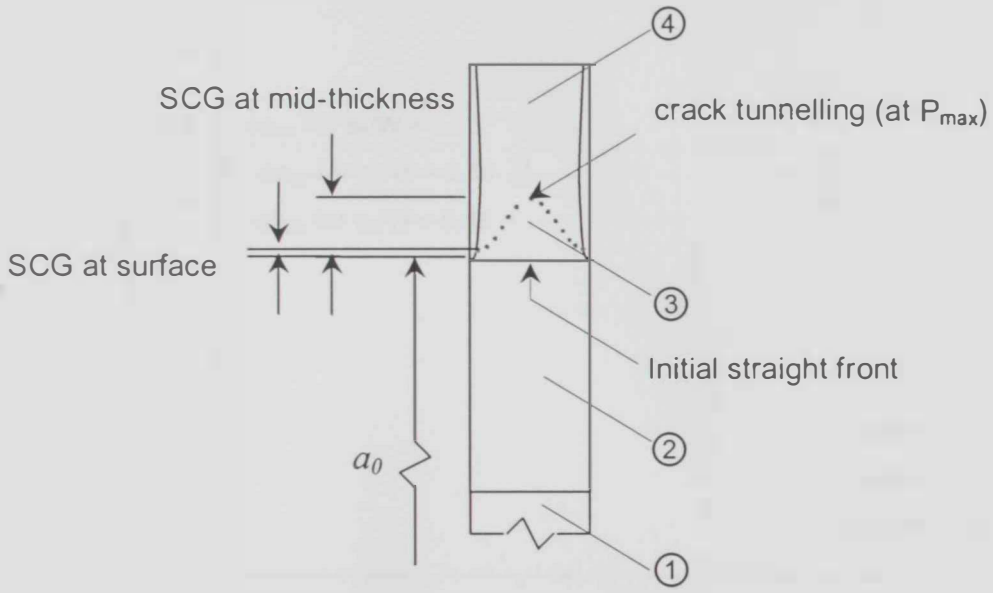

Fig. 4.25: Schematic diagram showing crack surface features; (1) "starter" notch, (2) EDM pre-notch, (3) stable crack growth (SCG) region, and (4) unstable crack growth (and slanting).

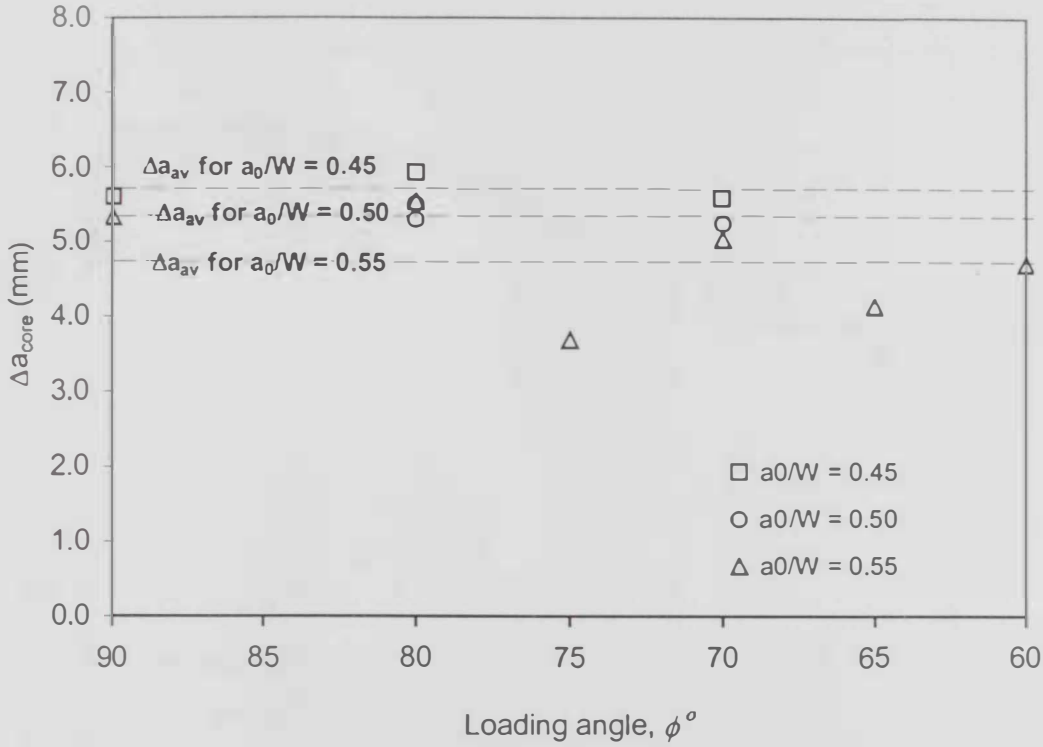

Fig. 4.26: Chart showing $\Delta a_{P\text{-}max}$ measurements at mid-thickness (Δa_{core}) vs. loading angle (Δa_{core} vs. ϕ),

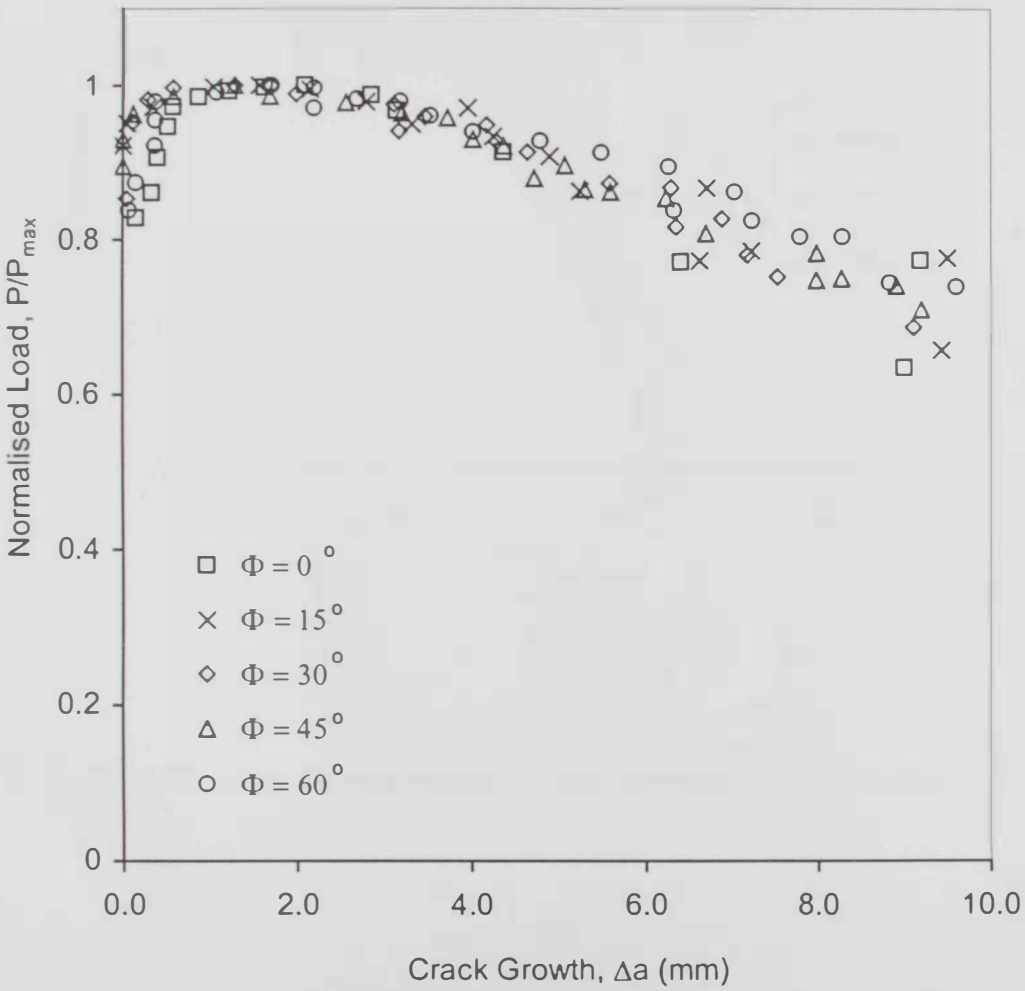

Fig. 4.27: Chart showing normalise P-Δa curves by Amstutz et al. [54] on 2024-T3.

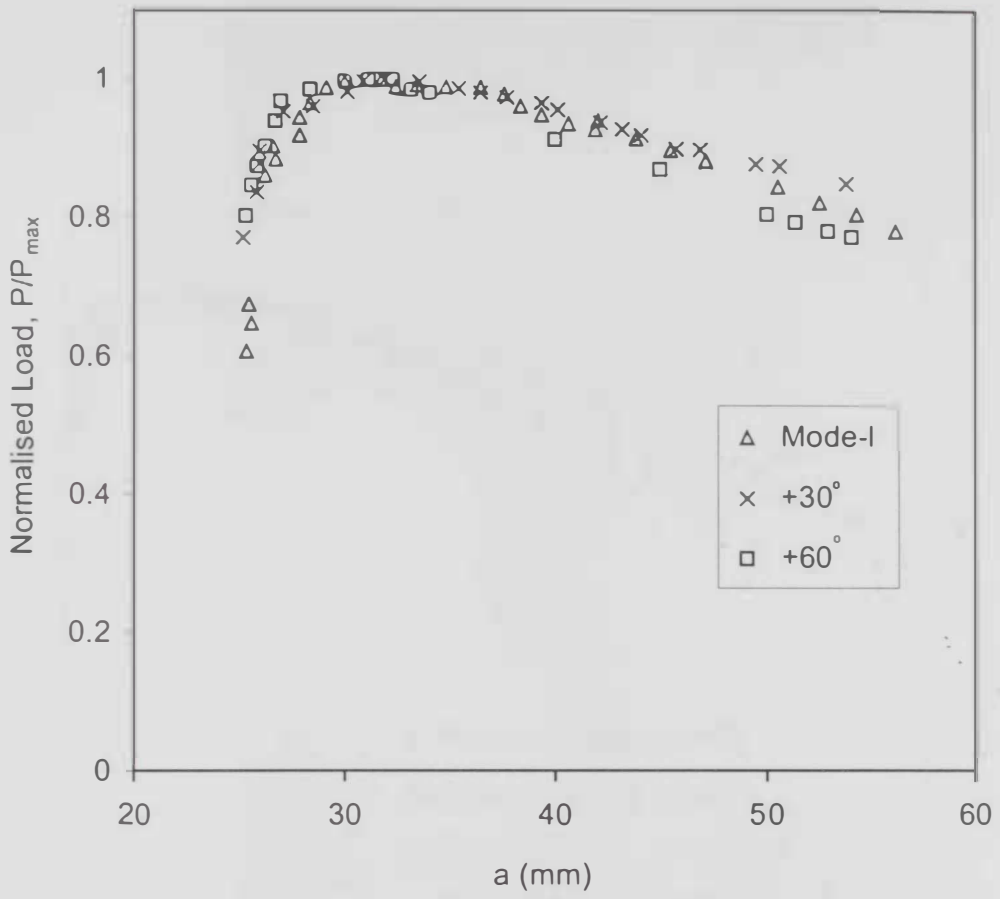

Fig. 4.28: Chart showing normalise P-Δa curves by Sutton et al. [55] on 2024-T3.

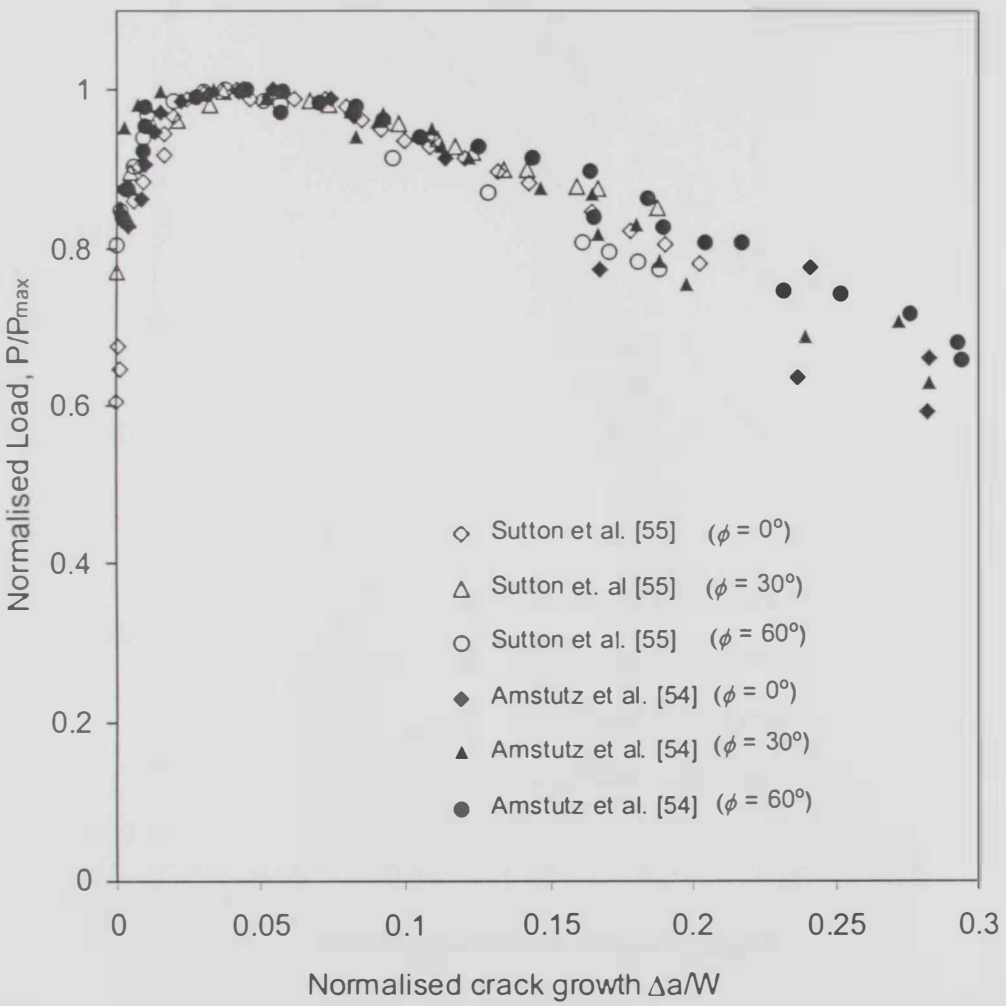

Fig. 4.29: Chart showing combined normalise P-Δa curves for works by Amstutz et al. [54] and Sutton et al. [55] on 2024-T3.

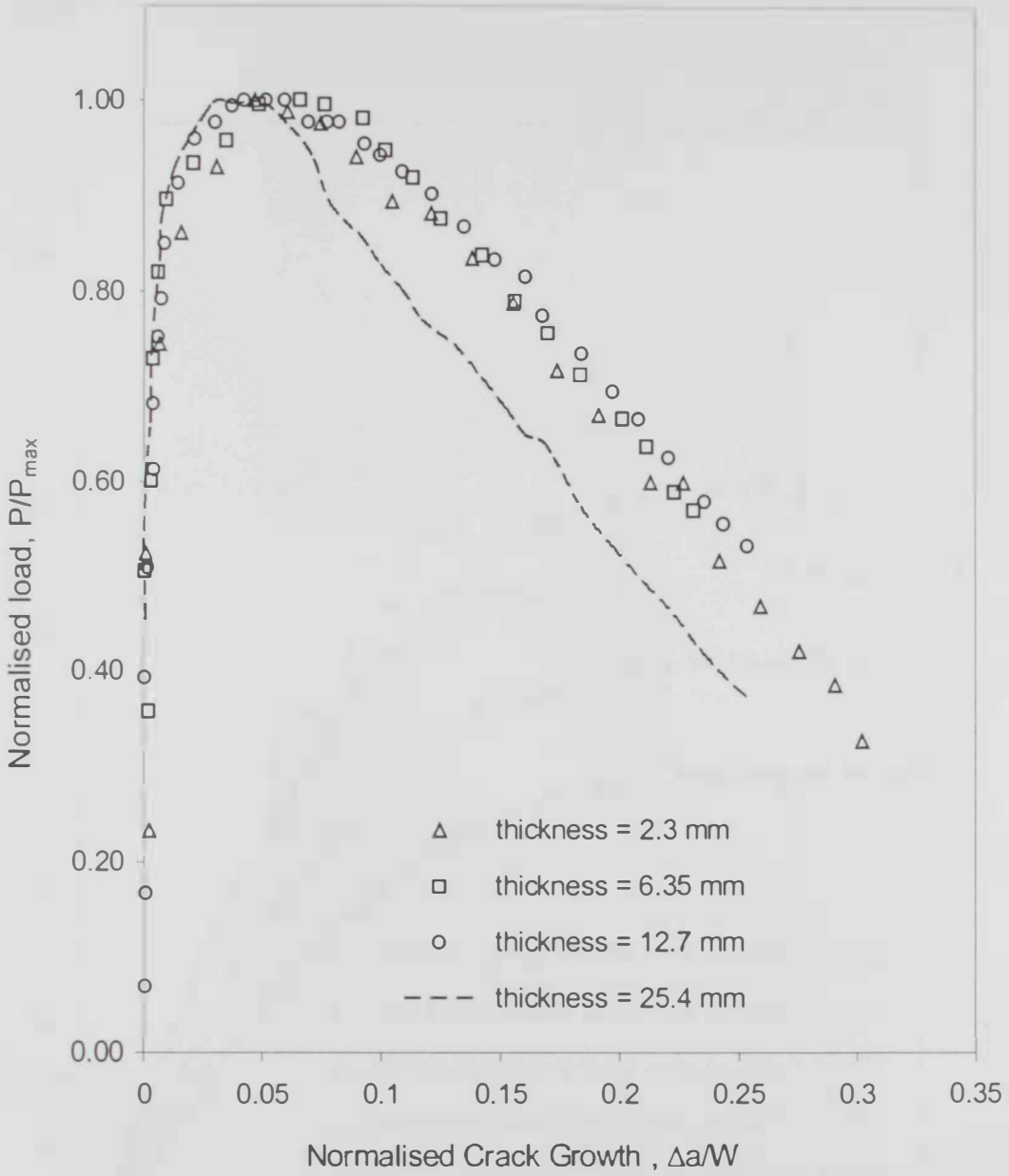

Fig. 4.30: Chart showing combined normalise P-Δa curves for works by Amstutz et al. [54] and Sutton et al. [55] on 2024-T3.

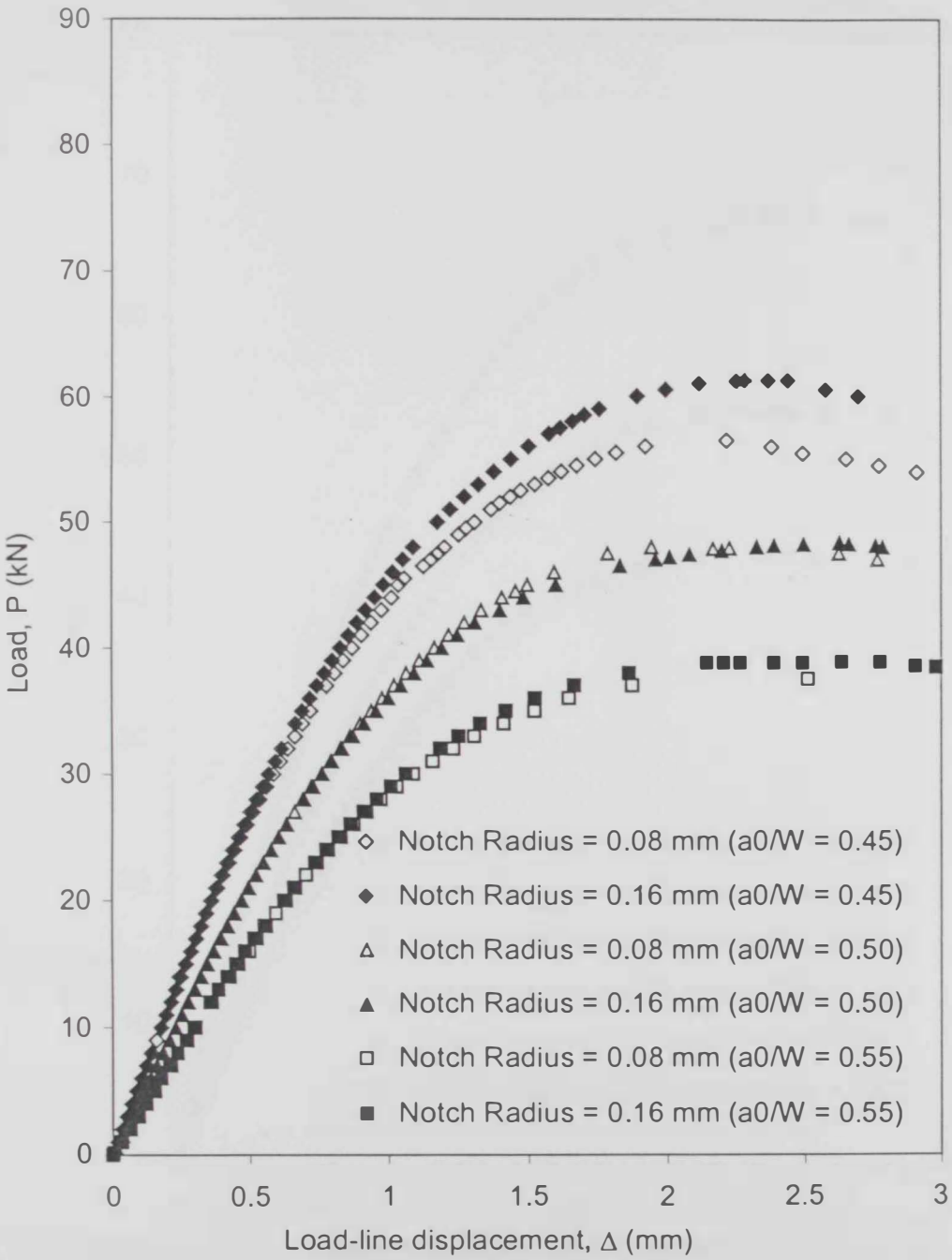

Fig. 4.31: Chart showing normalised P-Δ_{LL} curves for notch radii of 0.08 mm and 0.16 mm for $\phi = 90^{\circ}$.

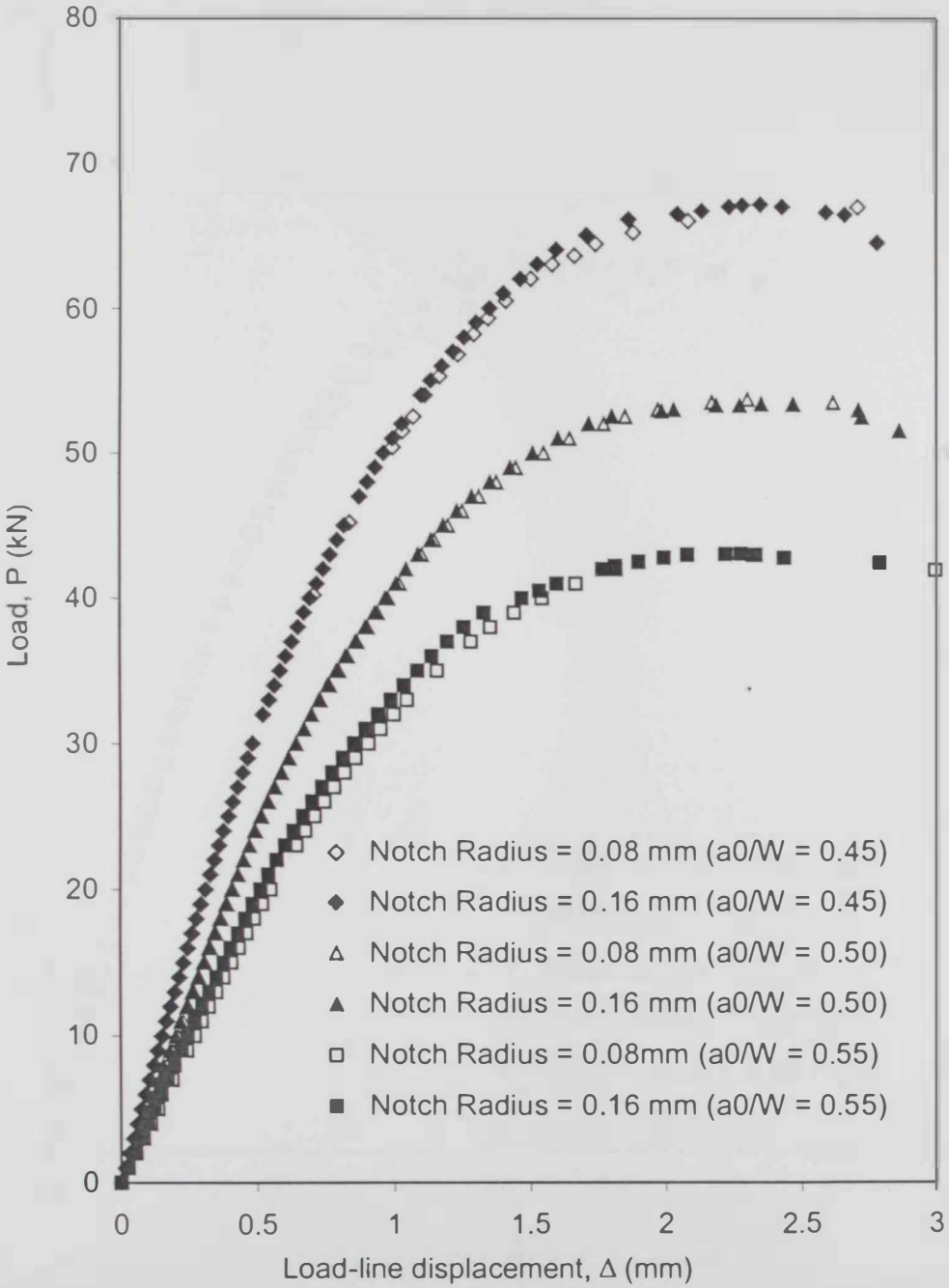

Fig. 4.32: Chart showing normalised P-Δ_{LL} curves for notch radii of 0.08 mm and 0.16 mm for $\phi = 80^{\circ}$.

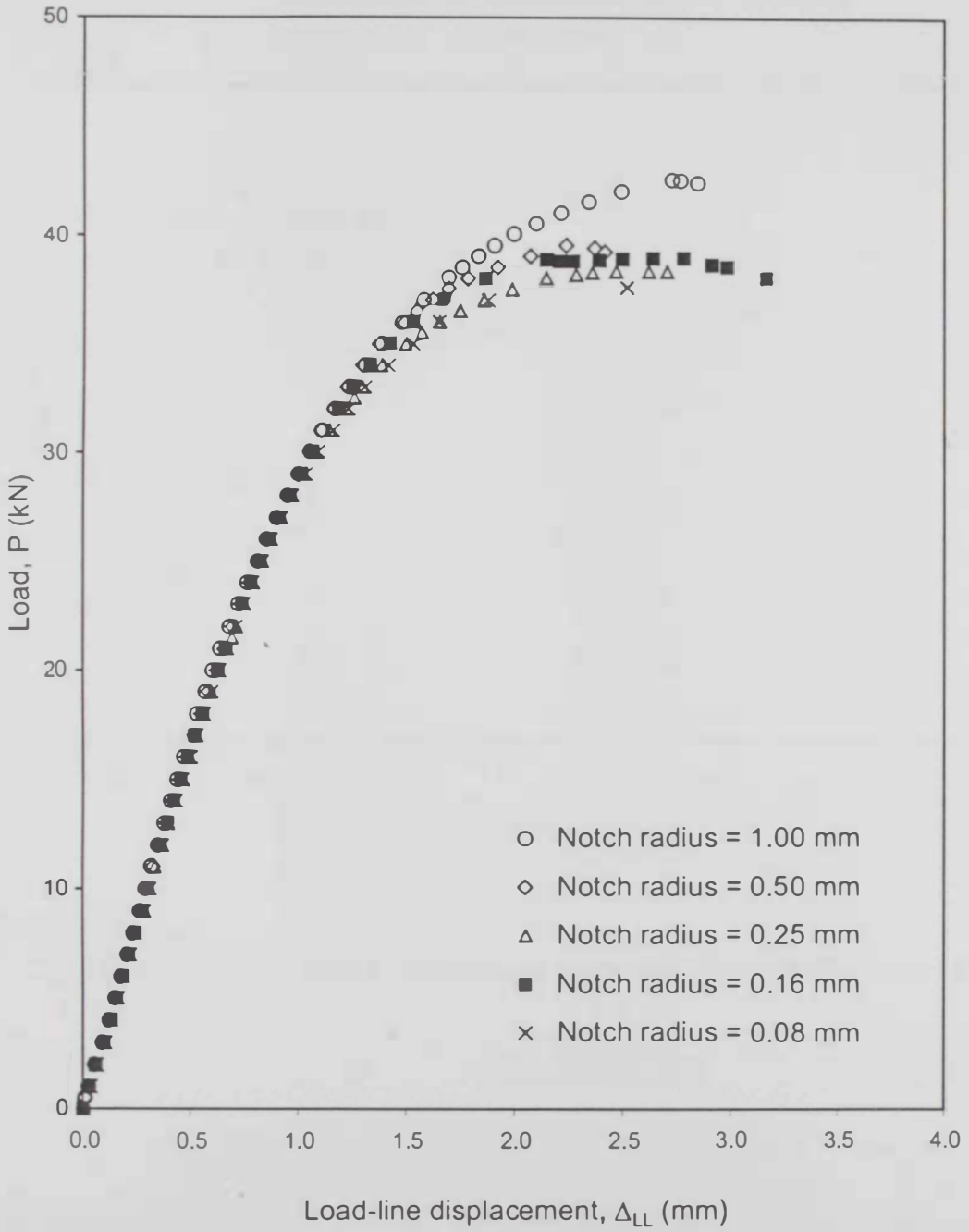

Fig. 4.33: P-Δ_{LL} curves for various notch radii for $a_0/W = 0.55$ and $\phi = 90^{\circ}$.

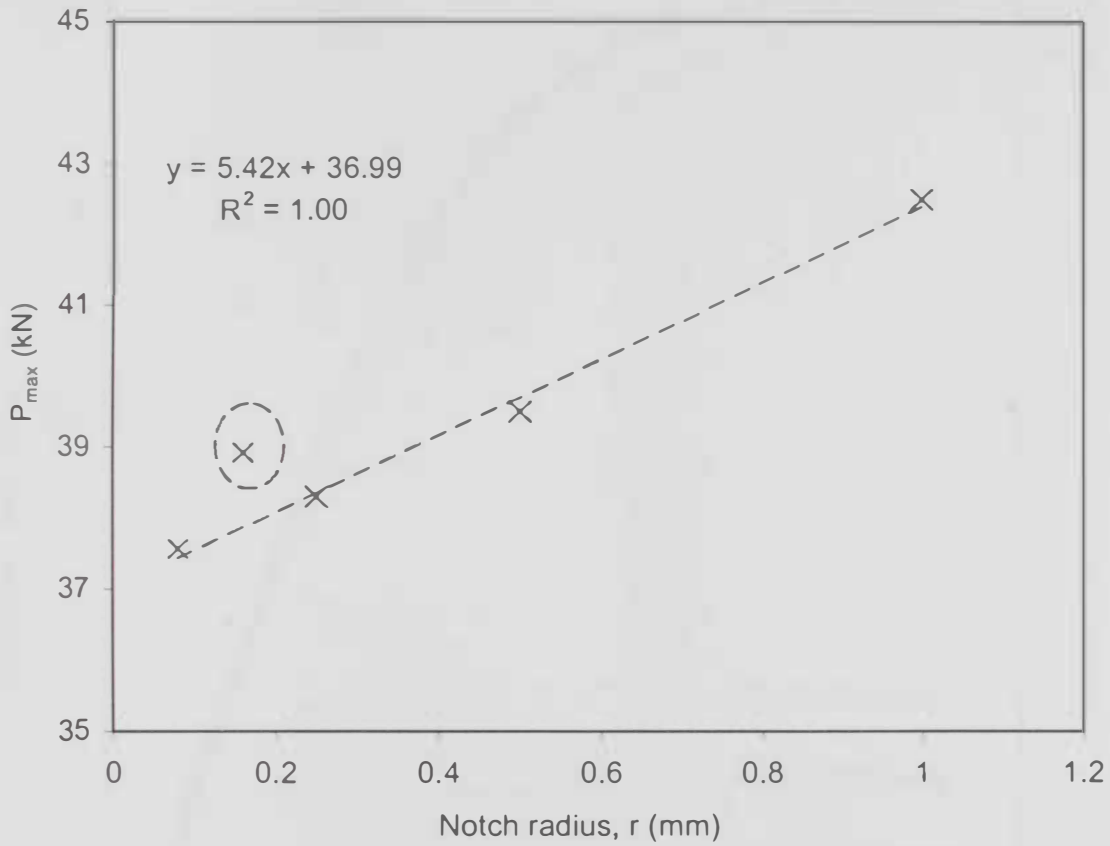

Fig. 4.34: Linear fit for P_{max} for various notch radii , $a_0/W = 0.55$ and $\phi = 90^{o}$.

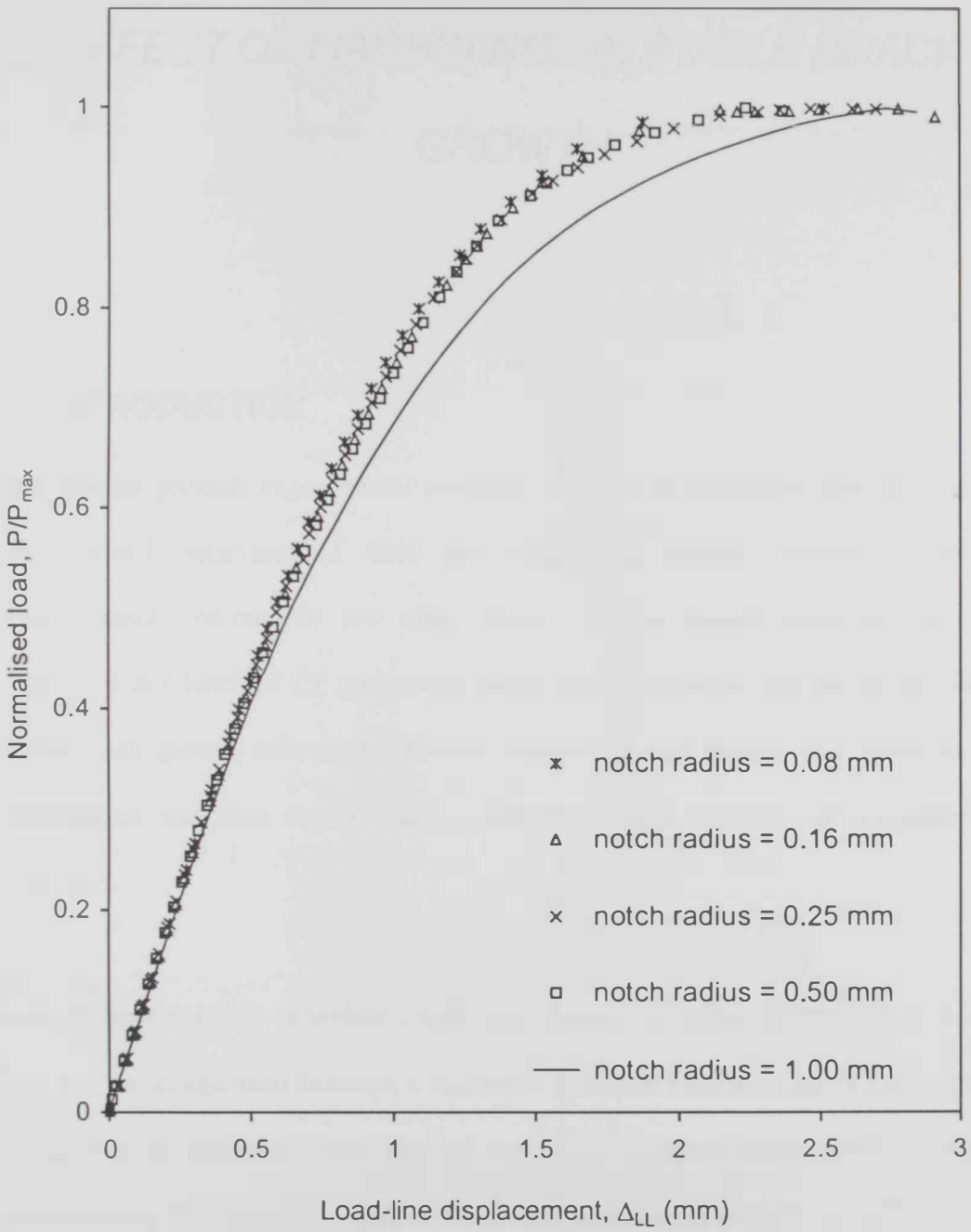

Fig. 4.35: Normalised P-Δ_{LL} curves for specimens of various notch radii, $a_0/W = 0.55$ and $\phi = 90^{\circ}$.

CHAPTER 5

EFFECT OF MACHINING ON STABLE CRACK GROWTH

5.1 INTRODUCTION

This chapter presents experimental evidence of effect of machining process on stable crack growth behaviour of 4340 low alloy steel; causing tempered martensite embrittlement, common to low alloy steels. Brittle fracture behaviour had been discovered in a batch of CT specimens, unlike previous batches that had shown ductile (stable crack growth) behaviour. This was unexpected, and indeed, was anomalous. An investigation was thus carried out to understand what processes have affected the behaviour.

Such anomalous brittle behaviour can be seen from P-Δ_{LL} plots shown in **Figs. 5.1-5.3**. One can see comparison between a "normal" specimen exhibiting stable crack growth and anomalous specimen. Note that the non-linear region, in the anomalous curve, is rather limited. This indicates very limited, if any, stable crack growth.

5.2 POSSIBLE CAUSES TO ANOMALOUS (BRITTLE) BEHAVIOUR

Material used for mentioned batch was rather different than one used and mentioned in chapter 3, which is similar but not identical. **Table 5.1** shows composition of low alloy steel used-that exhibited embrittled behaviour. CT specimens that exhibited this anomalous behaviour were only exposed to machining processes. As mentioned before, raw material was received as round rod, 180 mm diameter. The cross-section was then flattened by milling, i.e. the round section was milled into a square-section of 120 mm x 120 mm. Thick plates, of approx. 15-20 mm thickness, were then cut from squared rod, using automated electrical saw. The plates were then milled into required 8 mm thickness and, holes and notches were machined into plate. The CT specimen was then notched using EDM-wire cutting.

Communications with workshop staff revealed that "normal" specimens were not machined similarly; the round section was flattened using a shaper machine, rather than milled. Moreover, the material had the longest exposure during flattening – in either method. Therefore, milling process during flattening became the focus of more attention.

5.2.1 Milling Process: Primary Cause

Advances in materials technology with regard to end-bits used in machine tools has meant that machine operators can tolerate more aggressive machining than before. Such aggressive machining can save substantial production lead times. However, temperature rise resulting from such aggressive machining, or excessive strain rates, can affect some aspects of mechanical behaviour of materials being machined.

Therefore, two causes were initially suspected to have caused such change of behaviour; either excessive residual stresses (either from high machining strain rates, or cooling-rate differentials), or tempered martensite embrittlement (TME) common to low alloy steels.

5.2.2 Residual Stresses

Formation of residual stresses is not uncommon during machining. They can arise from the surface plastic deformation that has occurred leading to compressive residual stresses. Other residual stresses may arise from the different cooling rates/cooling gradients that cause hardness variations throughout the section, and such would lead to residual stresses. Residual stresses are often relieved using tempering.

5.2.3 Martensitic Embrittlement

Indeed several heat treatments (heat cycles) can cause degradation in the mechanical properties of low alloy steels one of which is Tempered Martensite Embrittlement (TME), where tempering in the range of 250 – 400 ^{o}C [69].

TME can lead to transgranular fracture or intergranular fracture depending on embrittlement mechanism. Transgranular fracture of TME results from either decomposition (thermal or mechanical) of interlath retained austenite into cementite or the coarsening of existing interlath cementite. There has been some controversy in the past on whether interlath cementite deposition and coarsening can be the cause of transgranular feature, or whether instability and decomposition of retained austenite was the real cause [70, 71, 73]. Intergranular fracture, on the other hand, arises from

formation of carbides at prior austenite grain boundaries that are already weakened by segregation of impurity elements [70, 72].

One of the serious problems with regard to TME, and specifically transgranular TME, is that its characterisation is very difficult. Only through transmission electron microscopy (TEM) could interlath cementite be seen, which would give a confirmation of TME. Mechanical Testing, such as tensile testing, cannot characterise TME. Charpy Impact however, can give indication of TME [69].

5.3 EXPERIMENTAL PROCEDURE

Fracture tests were carried out to characterise on CT specimens with different heat treatments to find the cause of this unexpected embrittlement. Micro-hardness measurements, tensile tests and microscopic (SEM) examination were also carried out and are reported.

5.3.1. Heat Treatments

Various heat-treatment schemes were employed: tempering and austenitisation. In tempering, the specimen was put in an oven at about 200 °C for about 1 hr and the air-cooled (normalised). In austenitisation, the specimen was placed at about 800 °C and then left to cool slowly in the oven (annealed). Note that oven environments were not inert, and therefore after treatment, the surface was black indicating some decarburisation.

The idea behind such schemes is that if the CT specimens were affected by residual stresses, then tempering would be sufficient in alleviating brittle behaviour. However, if

it were TME that caused brittle behaviour, then austenitisation followed by annealing would eliminate brittle behaviour.

5.3.2. Stable Crack Growth Tests

CT specimens were loaded in Mode-I configuration. The specimens were loaded at a crosshead speed of 0.25 mm/min. P-Δ_{LL} Plots of the various tests are shown in **Fig. 5.4.**

5.3.3 Microhardness Tests

Samples were taken from the various CT specimen edges and were prepared for microhardness testing. The Vickers microhardness profile was measured at 0.5 mm steps across the thickness of samples, using 300g-indentation mass for an indentation period of 20s. Microhardness profiles are shown in **Fig 5.5**.

5.3.4 Tensile Tests

Tensile test specimens were manufactured from 8 mm thick (untested) CT plates. Dimensions of specimens are shown in **Chapter 3**. Tensile test results are shown in **Table. 5.2**. The tensile tests were conducted at a crosshead speed of 0.1 mm/min using a universal MTS testing machine.

5.3.5 SEM Fractography

Fracture surfaces were prepared from a normal (ductile) specimen and an anomalous (brittle) one. They were then examined under scanning electron microscope (SEM). Fractography was taking at magnification of x1000.

5.4 RESULTS AND DISCUSSION

Fig 5.3 and Fig. 5.4 clearly indicates the difference in crack growth behaviour for specimens of a_0/W ratio of 0.44. Note that initial slope is essentially identical but the embrittled specimen did not show extending non-linearity, i.e. it did not show any stable crack growth. This does correspond to the observed instant crack (and brittle) fracture behaviour and the absence of any prior blunting. Therefore maximum loads are different. For austinitised specimens, maximum load was recorded at 37.2 kN, i.e. restored to 95% of normal specimen (Fig. 5.4).

Note also the difference between the tempered and austinitised specimens. The tempered specimen, even though showing relatively more non-linearity than the anomalous (brittle) specimen, it still does show limited stable crack growth. This does correspond to the observed behaviour of limited blunting prior unstable crack growth. The austinitised specimen, on the other hand, does show more stable crack growth, and indeed it is similar to the normal (ductile) specimen, indicating that ductile (stable crack growth) behaviour had been restored in the austenitising process.

Microhardness profiling through specimen thickness shows lower microhardness levels for embrittled specimen sample. Moreover, the profile suffered scatter with a general trend to soften slightly at the core. This may indicate the machine heating and the surface-core temperature variations during thickness reduction (milling) process. Note the austenitisation did not restore original hardness of ductile specimen.

SEM fractographs are shown in Figs. 5.6 and 5.7. Fractographs of embrittled specimen

fractographs shown intergranular behaviour, then type of embrittlement mechanism would have been difficult to identify without further examination using spectroscopy.

Such transgranular feature is interesting and can be explained in terms of decomposition of retained interlath austenite promoted by combined effects of temperature and high strain rates during machining.

5.5 CONCLUSION

Unexpected brittle behaviour of 4340 CT specimens was explained as TME. Various mechanical and fractographic examinations have confirmed such thesis. The only exposure the specimens had to heat was during machining and therefore it was presumed that heating to TME embrittlement temperatures during machining to be the likely source of embrittlement.

Such detrimental effect of machining process may explain the various scatter in lab results obtained during various round robins on fracture behaviour of steel alloys where substantial scatter may prevent reasonable interpretation of test data.

Therefore great attention is needed during machining to avoid accidental embrittlement to avoid heat treatment after machining may reverse some, but may not restore all of material's properties. Moreover, great attention to machining process is warranted when round-robin results, on steel alloys, are obtained and compared, in order to avoid misleading experimental results.

Table 5. 1: Alloying elements composition for 4340 low alloy steel used.

Element	C	Mn	Si	P	S	Cr	Ni	Mo	V	Cu	Al
Wt. %	0.408	0.633	0.254	0.015	0.004	1.050	1.310	0.220	0.014	0.214	0.012

Table 5. 2: Results for mechanical testing.

Specimen	σ_{YS} (MPa)	σ_{UTS} (MPa)
Ductile	487	662
Embrittled	320	660
Austinitised	386	680

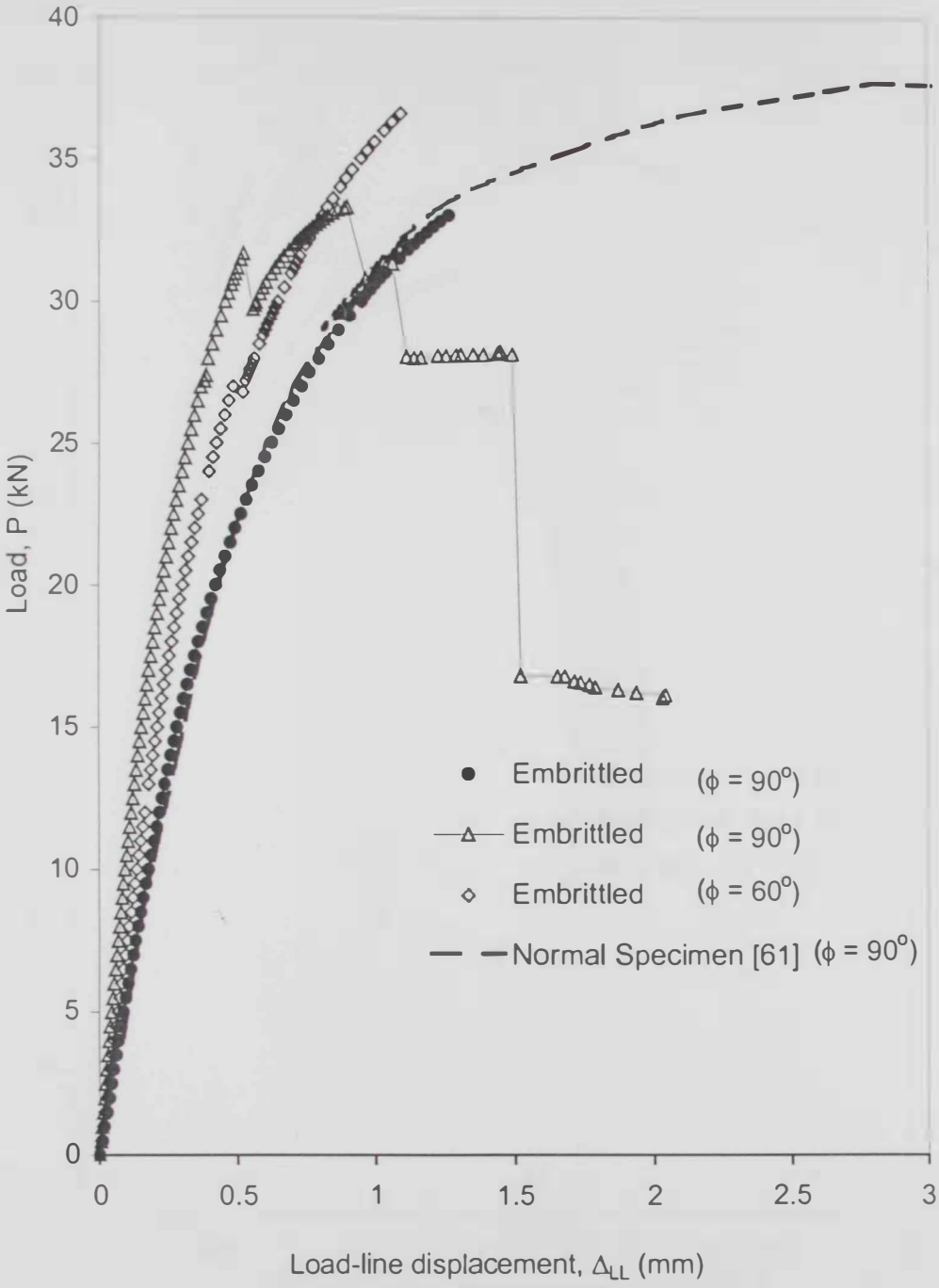

Fig. 5.1: P-Δ_{LL} curves for $a_0/W = 0.45$ (notch radius = 0.16 mm) showing embrittled behaviour.

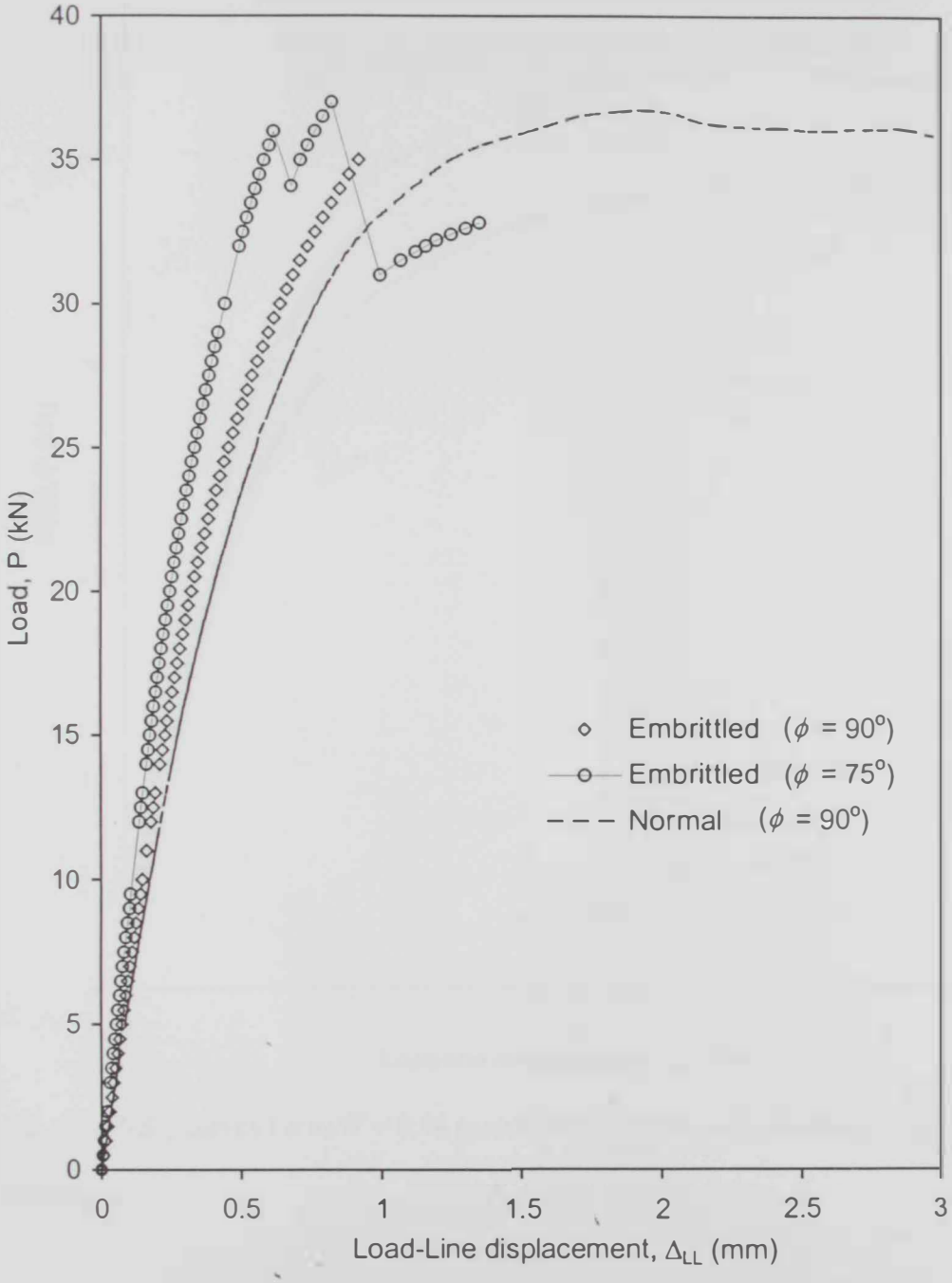

Fig. 5.2: P-Δ_{LL} curves for $a_0/W = 0.41$ (notch radius = 0.16 mm) showing embrittled behaviour.

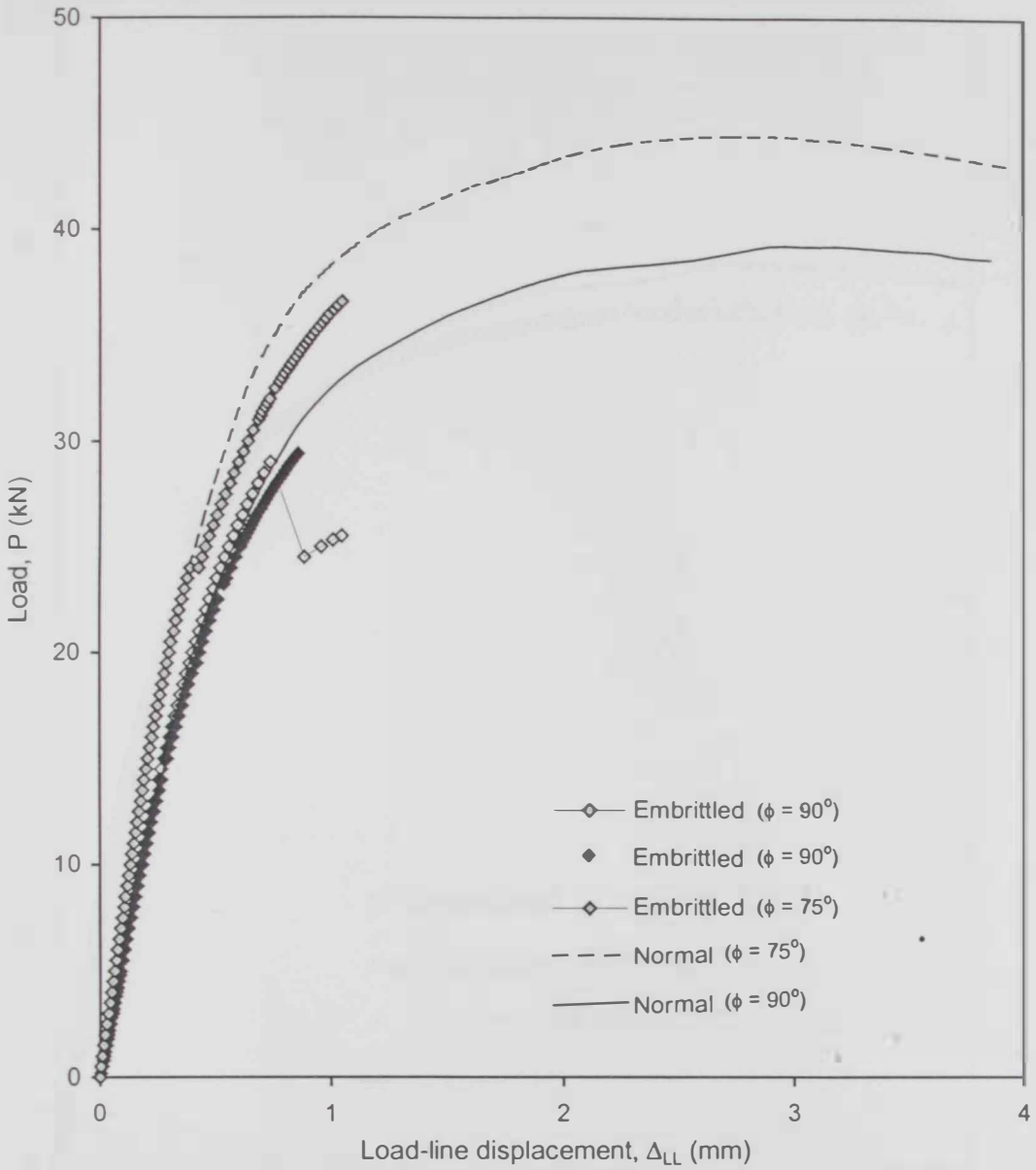

Fig. 5.3: P-Δ_{LL} curves for a_0/W = 0.44 (notch radius = 0.08 mm) showing embrittled behaviour.

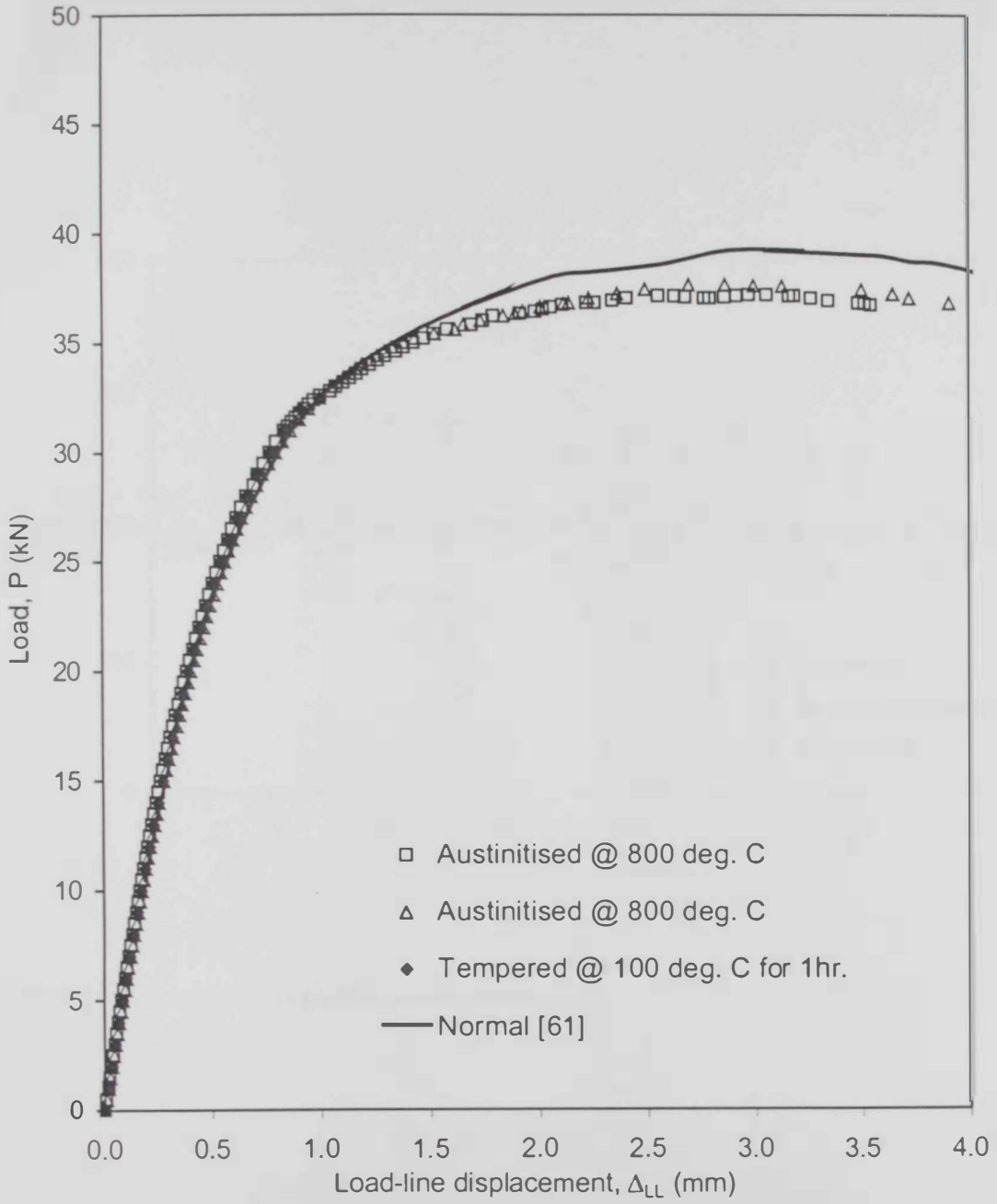

Fig. 5.4: Results of various heat treatment schemes and comparison with normal specimen.

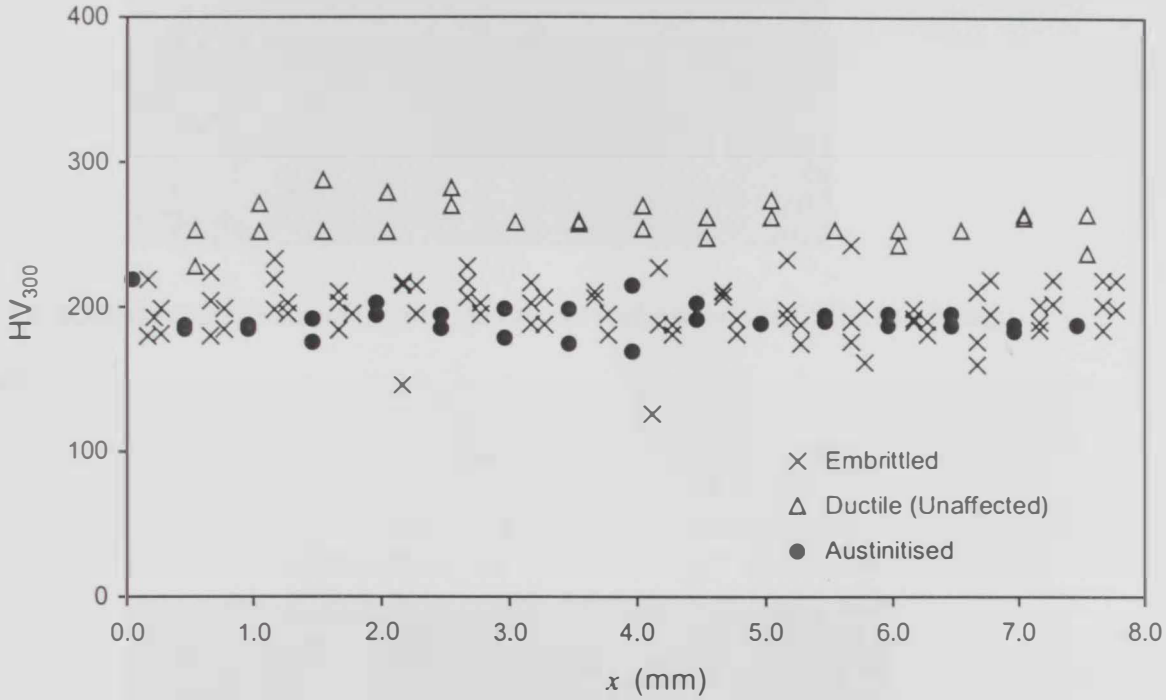

Fig. 5.5: Microhardness profile across section.

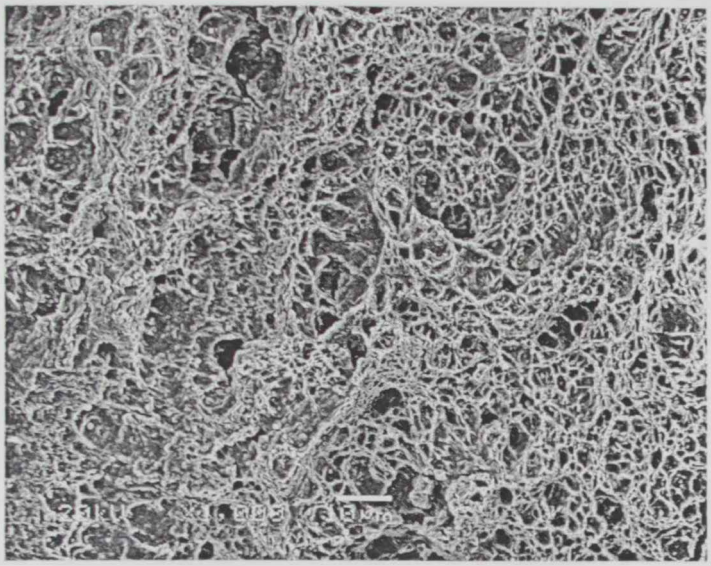

Fig. 5.6: SEM fractograph showing dimpled ruputre surface for unaffected specimens (x1000).

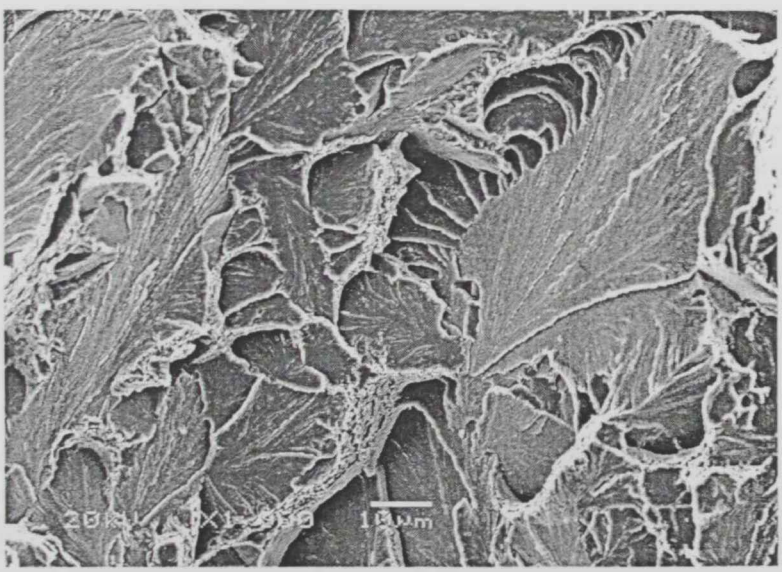

Fig. 5.7: SEM fractograph showing transgranular cleavage for an embrittled specimen (x1000).

CHAPTER 6

CONCLUSION

Fracture tests were conducted on CT specimens made from 34NiCrMo6 low alloy steel. Three a_0/W ratios of 0.45, 0.50 and 0.55 were used with loading angles of 90°, 80°, 70° and 65° for a notch radius of 0.08 mm. Results have shown the P_{max} increases with loading angle. It was found that there exists a linear fit for inverse of $P_{max}/P_{l\text{-}max}$ ratio with loading angle. It was also found that $\Delta_{P\text{-}max}$ and Δa_{core} were scattered within a range of values and therefore taken as constants. Normalisation was done to all P-Δ_{LL} curves, and all curves were represented as a single characteristic curve; where the load was represented as ratio of P_{max}, and Δ_{LL} as a ratio of W. Such normalisation was found to be successful for P-Δa curves too. This indicates that normalised P-Δ_{LL} and P-Δa curves can be characteristic material curves.

Preliminary tests on specimens with notch radii of 0.16 mm showed that the P-Δ_{LL} behaviour was similar to notch radius of 0.08 mm. This prompted tests into larger notch radii and results have shown that despite of more than ten times increase in notch radii (1.00 mm), P_{max} only changed by just below 15% and $\Delta_{P\text{-}max}$ by under 10%. A linear fit was obtained for P_{max} values against notch radii, though slope was shallow. This was

interesting, as this would suggest that notch behaviour is very similar to pre-cracked specimens.

Investigations on anomalous behaviour of unexpected embrittlement in 4340 CT specimens were attribute to tempered martensite embrittlement. It was found that material exhibited ductile stable crack growth when austinitised.

FUTURE WORK

Outcomes of this thesis are by no means decisive. Even though comparisons have been presented with results of other materials and specimen configurations, more testing is needed. Comparison with results of fatigue-precracked specimens is warranted too. There has been an indication regarding non-suitability of normalisation when more constraint is involved. This would be confirmed through testing thicker specimens. Moreover, no methods have been suggested for prediction of P_{max}, which can only be possible through characterising the stress fields, possible by FE analyses. Loading angles also need be correlated with mode-mixity values. Work on initiation load of cracks from notches is also warranted.

REFERENCES

1- Anderson TL. *Fracture Mechanics: Fundamentals and Applications*, 2nd Ed., CRC Press LLC, 1995.

2- Broek D. *Elementary Engineering Fracture Mechanics*, 4th Ed., Kluwer Academic Publishers, Dordrecht 1986.

3- Hertzberg RW. *Deformation and Fracture Mechanics of Engineering Materials*, * ed., Wiley NY 1976.

4- Parker AP. *The Mechanics of Fracture and Fatigue: An Introduction*, E & F Spon Ltd. London 1981.

5- Murakami. *Stress Intensity Factors Handbook*, Vol. I, II and III, Pergamon Press, Oxford 1993.

6- Neimitz A. A Study Of Stable Crack Growth Using Experimental Methods, Finite Elements, And Fractography. *Engineering Fracture Mechanics 71*, pp 1325-1355, 2004.

7- Thaulow C, Østby E, Nyhus B, Olden V, Zhang Z. The Philosophy Of Constraint Correction. *2nd International Symposium on High Strength Steel*, April 2002, Stiklestad, Norway.

8- E399, Standard Test for Plane-Strain Fracture Toughness of Metallic Materials. *Annual Book of ASTM Standards*, American Society for Testing and Materials, Philadelphia 1997.

9- Dowling NE. Mechanical Behaviour of Materials. 2nd Ed. Prentice & Hall 1999.

10- E 561, Standard Practice for R-curve Determination. *Annual Book of ASTM Standards*, American Society for Testing and Materials, Philadelphia 1997.

11- Schwalbe K-H, Newman Jr. J, Shannon Jr. J.Fracture Mechanics Testing on Specimens with Low Constraint – Standardisation activities within ISO and

12- Sumpter JDG. An Alternative View of R-curve Testing. *Engineering Fracture Mechanics 64*, pp. 161-176, 1999.

13- E 1737-96, Standard Method for *J*-Integral Characterisation of Fracture Toughness. *Annual Book of ASTM Standards*, American Society for Testing and Materials, Philadelphia 1997.

14- Brocks W, Yuan H. Numerical Investigation on the Significance of J for Large Stable Crack Growth. *Engineering Fracture Mechanics 32*, pp. 459-468, 1989.

15- Neimitz A, Dzioba I, Molasy R, Lis Z. An Experimental Analysis of Stable Crack Growth. *Archiwum Budowy Maszyn XLIII*, pp. 213-226, 1996.

16- Neimitz A, Dzioba I, Galkiewics J, Molasy R. A Study of Stable Crack Growth Using Experimental Methods, Finite Elements and Fractography. *Engineering Fracture Mechanics 71*, pp. 1325-1355, 2004.

17- Kolednik O. A Simple Model to Explain the Geometry Dependence of J-Δa Curves. *International Journal of Fracture 63*, pp. 263-274, 1993.

18- Shan GX, Kolednik O, Fischer FD. A Numerical Investigation on the Geometry Dependence of the Crack Growth Resistance in CT Specimens. *International Journal of Fracture 66*, pp. 173-187, 1994.

19- Sumpter JDG. The Energy Dissipation Rate Approach to Tearing Instability. *Engineering Fracture Mechanics 71*, pp. 17-37, 2004.

20- Brocks W, Anuschewski P. Parameterising Ductile Tearing Resistance by Four Parameters. *Engineering Fracture Mechanics 71*, pp. 127-146, 2004.

21- Li Q, Shi D, Wei J, Zhong B. A Study of the *J*-COD Relationship. *Engineering Fracture Mechanics 42*, pp. 401-404, 1992.

22- E 1290, Standard Test Method for CTOD Testing. *Annual Book of ASTM Standards*, American Society for Testing and Materials, Philadelphia 1997.

23- Schwalbe K-H, Zerbst U, Brocks W, Cornec A, Heerens J, Amstutz H. The ETM Method for Assessing the Significance of Crack-Like Defects in Engineering Structures. *Fatigue & Fracture of Engineering Materials & Structures 21*, pp. 1215-1231, 1998.

24- Laukkanen A. The Engineering Treatment Model and Comparison to R6-3, *Engineering Fracture Mechanics 67*, pp. 367-380, 2000.

25- Newman J, James MA, Zerbst U. A Review on the CTOA/CTOD Fracture Criterion. *Engineering Fracture Mechanics 70*, pp. 371-385, 2003.

26- Mahmoud S, Lease K. The Effect of Specimen Thickness on the Experimental Characterisation of Critical CTOA in 2024-T351 Aluminium Alloy. *Engineering Fracture Mechanics 70*, pp. 443-456, 2003.

27- James MA, Newman Jr. J. The Effect of Crack Tunnelling on Crack Growth: Experiments and CTOA Analyses. *Engineering Fracture Mechanics 70*, pp.457-468, 2003.

28- Dawicke DS, Sutton MA, Newman Jr. JC, Bigelow CA. Measurement and Analysis of Critical CTOA for an Aluminium Alloy Sheet, *NASA Technical Memorandum 109024 (TM – 109024)*, Langley Research Centre, 1993.

29- Mahmoud S, Lease K. Two-dimensional and Three-Dimensional Finite Element Analysis of CTOA in 2024-T351 Aluminium Alloy at Four Thicknesses. *Engineering Fracture Mechanics 71*, pp. 1379-1391, 2004.

30- Shan GX, Kolednik O, Fischer FD, Stüwe HP.A 2D Numerical Investigations of Stable Crack Growth in Thick Smooth Fracture Mechanics Specimens. *Engineering Fracture Mechanics 45*, pp. 99-106, 1993.

31- Hampton R, Nelson D. Stable Crack Growth and Instability Prediction in Thin Plates and Cylinders. *Engineering Fracture Mechanics 70*, pp. 469-491, 2003.

32- Lam PS, Kim Y, Chao YJ. The Non-Constant CTOD/CTOA in Crack Propagation. WSRC-MS-2004-00532, Office of Scientific and Technical Information (OSTI) US Dept. of Energy, 2004.

33- Ainsworth RA, Bannister AC, Zerbst U. An overview of the European flaw assessment procedure SINTAP and its validation. *International Journal of Pressure Vessels and Piping 77*, pp. 869-876, 2000.

34- Wang X. Elastic T-Stress for Cracks in Test Specimens Subjected to Non-Uniform Stress Distribution. Engineering Fracture Mechanics 69, pp. 1339-1352, 2002.

35- Thaulow C, Østby E, Nyhus B, Zhang Z, Skallerud B. Constraint Correction of High Strength Steel: Selection of Test Specimens and Application of Direct Calculations. *Engineering Fracture Mechanics 71*, pp. 2417-2433, 2004.

36- Nyhus B, Zhang ZL, Thaulow C. Normalisation of Material Crack Resistance Curves by the T Stress. *2nd International Symposium on High Strength Steel*, Verdal, Norway. 23-24 April, 2002.

37- Ma L, Lam PW, Kokaly MT and Kobayashi AS. CTOA of a Stable Crack in a Thin Aluminium Fracture Specimen. *Engineering Fracture Mechanics 70*, pp 427-442, 2003.

38- Zhu XK, Jang SK. J-R Curves Corrected By Load-Independent Constraint Parameter in Ductile Crack Growth. *Engineering Fracture Mechanics 68*, pp. 285-301, 2001.

39- Chao YJ, Lam PS. On the Use of Constraint Parameter A2 Determined from Displacement in Predicting Fracture Event. *Engineering Fracture Mechanics 61*, pp. 487-502, 1998.

40- Nikishkov GP. Introduction J-A Fracture Concept. http://www.u-aizu.ac.jp/~niki/javaappl/epas/epas.htm.

41- Nègre P, Steglich D, Brocks W, Koçak M. Numerical Simulation of Crack Extension in Aluminium Welds. *Computational Materials Science 28*, pp. 723-731, 2003.

42- Cornec A, Scheider I, Schwalbe KH. On the practical application of the cohesive model. *Engineering Fracture Mechanics 70*, pp. 1963-1987, 2003.

43- Gullerud AS, Gao X, Dodds Jr. RH, Haj-Ali R. Simulation of ductile crack growth using computational cells: numerical aspects. *Engineering Fracture Mechanics 66*, pp. 65-92, 2000.

44- Chabanet O, Steglich D, Besson J, Heitmann V, Hellmann D, Brocks W. Predicting Crack Growth Resistance of Aluminum Sheets. *Computational Materials Science 26*, pp. 1-12, 2003.

45- Li H, Chandra N. Analysis of crack growth and crack-tip plasticity in ductile materials using cohesive zone models. *International Journal of Plasticity 19*, pp. 849-882, 2003.

46- Zhang ZL, Thaulow C, Ødegård J. A complete Gurson model approach for ductile fracture. *Engineering Fracture Mechanics 67*, pp. 155-168, 2000.

47- Bernauer G, Brocks W. Micro-mechanical modelling of ductile damage and tearing –results of a European numerical round robin. *Fatigue & Fracture of Engineering Materials & Structures 25*, pp. 363-384. 2002.

48- Rivalin F,Besson J, Pineau A, Di Fant M. Ductile tearing of pipeline-steel wide plates -II: Modeling of in-plane crack propagation. *Engineering Fracture Mechanics 68*, pp. 347-364, 2000.

49- Roy YA, Narasimhan R. *J*-Dominance in Mixed-Mode Ductile Fracture Specimens. *International Journal of Fracture 88*, pp. 259-279, 1997.

50- Laukkanen A. Analysis of Experimental Factors in Elastic-Plastic Small Specimen Mixed-Mode I/II Fracture Mechanical Testing. *Fatigue and Fracture of Engineering Materials and Structures 24*, pp. 193-206, 2001.

51- Mahanty DK, Savant GY. Experimental Investigations on Stable Crack Growth in 3PB Specimens under Mode-I and Mixed-Mode (I/II) Loading. *Engineering Fracture Mechanics 43*, pp. 41-53, 1992.

52- Maiti SK, Mourad A-H.I. Criterion for Mixed-Mode Stable Crack Growth – I: 3PB Geometry. *Engineering Fracture Mechanics 52*, pp. 321-347, 1995.

53- Li J, Zhang X-B, Recho N. *J-M*$_P$ based criteria for Bifurcation Assessment of a Crack in Elastic-Plastic Materials under Mixed-Mode (I/II) Loading, *Engineering Fracture Mechanics 71*, pp. 329-343, 2004.

54- Sutton MA, Boone ML, Ma F, Helm JD. A Combined Modelling-Experimental Study Of The Crack Opening Displacement Fracture Criterion For Characterization Of Stable Crack Growth Under Mixed Mode I/II Loading In Thin Sheet Materials. *Engineering Fracture Mechanics 66*, pp. 171-185, 2000.

55- Sutton MA, Reynolds AP, Yang B, Taylor R. Mixed mode I/II Fracture Of 2024-T3 Friction Stir Welds. *Engineering Fracture Mechanics 70*, pp. 2215-2234, 2003.

56- Aoki S, Kishimoto K, Yoshida T, Sakata M, Richard HA. Elastic-Plastic Fracture Behaviour of an Aluminium Alloy under Mixed-Mode Loading. *Journal of Mechanics and Physics of Solids 38*, pp. 195-213, 1990.

57- Roy YA, Narasimhan R, Arora PR. An Experimental Investigation of Constraint Effects on Mixed-Mode Fracture Initiation in Ductile Aluminium Alloy. *Acta Materialia 47*, pp. 1587-1596, 1999.

58- Pirondi A, Dalle-Donne CD. Characterisation of Ductile Mixed-Mode Fracture with Crack-Tip Displacement Vector. *Engineering Fracture Mechanics 68*, pp. 1385-1402, 2001.

59- Mahanty DK, Maiti SK. Experimental and Finite Element Studies on Mode-I and Mixed-Mode (I/II) Stable Crack Growth –I: Experimental. *Engineering Fracture Mechanics 37*, pp. 1237-1250, 1990.

51- Mahanty DK, Savant GY. Experimental Investigations on Stable Crack Growth in 3PB Specimens under Mode-I and Mixed-Mode (I/II) Loading. *Engineering Fracture Mechanics 43*, pp. 41-53, 1992.

52- Maiti SK, Mourad A-H.I. Criterion for Mixed-Mode Stable Crack Growth – I: 3PB Geometry. *Engineering Fracture Mechanics 52*, pp. 321-347, 1995.

53- Li J, Zhang X-B, Recho N. *J-M*$_P$ based criteria for Bifurcation Assessment of a Crack in Elastic-Plastic Materials under Mixed-Mode (I/II) Loading, *Engineering Fracture Mechanics 71*, pp. 329-343, 2004.

54- Sutton MA, Boone ML, Ma F, Helm JD. A Combined Modelling-Experimental Study Of The Crack Opening Displacement Fracture Criterion For Characterization Of Stable Crack Growth Under Mixed Mode I/II Loading In Thin Sheet Materials. *Engineering Fracture Mechanics 66*, pp. 171-185, 2000.

55- Sutton MA, Reynolds AP, Yang B, Taylor R. Mixed mode I/II Fracture Of 2024-T3 Friction Stir Welds. *Engineering Fracture Mechanics 70*, pp. 2215-2234, 2003.

56- Aoki S, Kishimoto K, Yoshida T, Sakata M, Richard HA. Elastic-Plastic Fracture Behaviour of an Aluminium Alloy under Mixed-Mode Loading. *Journal of Mechanics and Physics of Solids 38*, pp. 195-213, 1990.

57- Roy YA, Narasimhan R, Arora PR. An Experimental Investigation of Constraint Effects on Mixed-Mode Fracture Initiation in Ductile Aluminium Alloy. *Acta Materialia 47*, pp. 1587-1596, 1999.

58- Pirondi A, Dalle-Donne CD. Characterisation of Ductile Mixed-Mode Fracture with Crack-Tip Displacement Vector. *Engineering Fracture Mechanics 68*, pp. 1385-1402, 2001.

59- Mahanty DK., Maiti SK. Experimental and Finite Element Studies on Mode-I and Mixed-Mode (I/II) Stable Crack Growth –I: Experimental. *Engineering Fracture Mechanics 37*, pp. 1237-1250, 1990.

51- Mahanty DK, Savant GY. Experimental Investigations on Stable Crack Growth in 3PB Specimens under Mode-I and Mixed-Mode (I/II) Loading. *Engineering Fracture Mechanics 43*, pp. 41-53, 1992.

52- Maiti SK, Mourad A-H.I. Criterion for Mixed-Mode Stable Crack Growth – I: 3PB Geometry. *Engineering Fracture Mechanics 52*, pp. 321-347, 1995.

53- Li J, Zhang X-B, Recho N. *J-M*$_P$ based criteria for Bifurcation Assessment of a Crack in Elastic-Plastic Materials under Mixed-Mode (I/II) Loading, *Engineering Fracture Mechanics 71*, pp. 329-343, 2004.

54- Sutton MA, Boone ML, Ma F, Helm JD. A Combined Modelling-Experimental Study Of The Crack Opening Displacement Fracture Criterion For Characterization Of Stable Crack Growth Under Mixed Mode I/II Loading In Thin Sheet Materials. *Engineering Fracture Mechanics 66*, pp. 171-185, 2000.

55- Sutton MA, Reynolds AP, Yang B, Taylor R. Mixed mode I/II Fracture Of 2024-T3 Friction Stir Welds. *Engineering Fracture Mechanics 70*, pp. 2215-2234, 2003.

56- Aoki S, Kishimoto K, Yoshida T, Sakata M, Richard HA. Elastic-Plastic Fracture Behaviour of an Aluminium Alloy under Mixed-Mode Loading. *Journal of Mechanics and Physics of Solids 38*, pp. 195-213, 1990.

57- Roy YA, Narasimhan R, Arora PR. An Experimental Investigation of Constraint Effects on Mixed-Mode Fracture Initiation in Ductile Aluminium Alloy. *Acta Materialia 47*, pp. 1587-1596, 1999.

58- Pirondi A, Dalle-Donne CD. Characterisation of Ductile Mixed-Mode Fracture with Crack-Tip Displacement Vector. *Engineering Fracture Mechanics 68*, pp. 1385-1402, 2001.

59- Mahanty DK, Maiti SK. Experimental and Finite Element Studies on Mode-I and Mixed-Mode (I/II) Stable Crack Growth –I: Experimental. *Engineering Fracture Mechanics 37*, pp. 1237-1250, 1990.

60- Maiti SK, Mourad A-H.I. Criterion for Mixed-Mode Stable Crack Growth-II: Compact Tension Geometry with and without Stiffener. *Engineering Fracture Mechanics 52*, pp. 349-378, 1995.

61- Mourad A-H.I, Al-Ghafri MJ, Abu-Zeid OA, Maiti SK. Experimental Investigation on Ductile Stable Crack Growth Emanating From Wire-Cut Notch in AISI 4340 Steel. *Nuclear Engineering and Design (Article In Press).*

62- Bose K, Castañeda P. Stable Crack Growth under Mixed-Mode Conditions, *Journal of Mechanics and Physics of Solids 40*, pp. 1053-1103, 1992.

63- Ma F, Deng X, Sutton MA, Newman Jr. JC. A CTOD Based Mixed-Mode Fracture Criterion. *Mixed Mode Crack Behaviour, ASTM STP 1359*, pp. 86-110, 1999.

64- Dhirendra VK, Narasimhan R. Mixed-Mode Steady-State Crack Growth in Elastic-Plastic Solids. *Engineering Fracture Mechanics 59*, pp. 543-559, 1998.

65- Sutton MA, Deng X, Ma F, Newman Jr. JC, James MA. Development and Application of a CTOD based Mixed-Mode Fracture Criterion. *International Journal of Solids and Structures 37*, pp. 3591-3618, 2000.

66- Sutton MA, Zhao W, Boone ML, Reynolds AP, Dawicke DS. Prediction of Crack Growth Direction for Mode I/II Loading Using Small Scale Yielding and Void Initiation/Growth Concepts. *International Journal of Fracture 83*, pp. 275-290, 1997.

67- Giovanola JH, Kirkpatrick SW and Crocker JE. Fracture of Geometrically Scaled, Notched Three-Point-Bend Bars of High Strength Steel. *Engineering Fracture Mechanics 62*, pp. 291-310, 1999.

68- Krompholz K, Kalkhof D. Fracture Initiation Of Geometrically Scaled, Notched Three-Point-Bend Bars Of A Low-Alloy Ferritic Steel. *Engineering Fracture Mechanics 70*, pp. 2459-2472, 2003.

69- Lee W-S, Su TT. Mechanical Properties And Microstructural Features Of AISI 4340 High-Strength Alloy Steel Under Quenched And Tempered Conditions. *Journal of Materials Processing Technology* 87, pp. 198-206, 1999.

70- Zia-Ebrahimi F, Krauss G. Mechanisms Of Temprered Martensite Embrittlement In Medium Carbon Steels. *Acta Metallurgica 32*, pp.1767-1777, 1984.

71- Lee KB, Yoon SH, Kwon H. On The Transgranular Type Of Tempered Martensite Embrittlement. *Scripta Metallurgica et Materialia* 30, pp. 1111-1115, 1994.

72- Lee KB, Yoon SH, Hong SI, Kwon H. On Intergranular Tempered Martensite Embrittlement. *Scripta Metallurgica et Materialia* 32, pp. 1197-1201, 1995.

73- J. A. Peters, J. V. Bee, B. Kolk and G. G. Garrett, On The Mechanisms Of Tempered Martensite Embrittlement, *Acta Metallurgica 37*, pp. 675-686, 1989.

الخلاصة

تدرس هذه الرسالة تجريبيا نمو الصدع المستقر(stable crack growth) المنبثق من النقرات الحادة (sharp notches) خلال سبيكة من سبائك الصلب و المصنفة برقم EN 34NiCrMo6 - حسب التصنيف الأوروبي. و قد أجريت اختبارات على عينات الشد المدمج (CT) بزوايا تحميل و أطوال صدوع مختلفة. و تم تحليل بيانات الاختبار و تم التوصل الى طريقة للتطبيع النتائج (normalisation) و توحيد كل المنحنايات في منحنى نسقي واحد شامل. و قد تم تطبيق طريقة التطبيع هذه على منحنايات لاختبارات أخرى سابقة و تظهر الطريقة الجديدة نتائج مشجعة في حل مشكلة التنسيب لبيانات التجارب المعملية (transferability). و قد تم ايضا معاينة سطوح الصدوع المختلفة كما تمت معاينة التنقيب الصدعي و مدى نمو الصدع المستقر باستخدام صبغة خاصة. و أجريت أيضا تجارب على نقرات ذات مقاسات مختلفة و قد أظهرت النتائج أنه بالرغم من زيادة مقاس مقدمة النقرة أكثر من عشر مرات فإن الحمولة القصوى للعينة لم تزد عن 15%.

جامعة الإمارات العربية المتحدة
عمادة الدراسات العليا
برنامج ماجستير علوم المواد

نمو الصدع اللدن من النقرات الحادة خلال سبيكة صلب

إعداد

علاء الدين إحسان عطاالله أبوعاصي

رسالة مقدمة لعمادة الدراسات العليا بجامعة الإمارات العربية المتحدة
ضمن متطلبات الحصول على درجة الماجستير في علوم و هندسة المواد

إشراف
د. عبد الحميد اسماعيل مراد
قسم الهندسة الميكانيكية
جامعة الإمارات العربية المتحدة

2004 - 2005